

UNIVERSITÀ DEGLI STUDI DI CATANIA

Ph.D. in Materials Science XXXIII Cycle

Ph.D. Thesis

***Engineering of Alkali Metalorganic Precursors:
Synthesis to Mechanistic Aspects***



Nishant Peddagopu

Advisor:
Prof. Graziella Malandrino

Coordinator:
Prof. Giuseppe Compagnini

2018-2021

श्रद्धा और सबुरी

(Faith & Patience)

माँ, पापा, अम्मा, अंकिता और मेरे साईं

(Mom, dad, grandma, Ankita, and my Sai)

Acknowledgments

To put three years of doctoral research work into perspective, one can imagine, it is not a one-person job. Firstly, and foremostly the person who has had the single most significant influence on me while at the University of Catania has been my advisor, Prof. Graziella Malandrino. I have acquired so much during my time in her lab that it would be impossible to summarize it all. I recognize her for giving me the freedom to explore my ideas/point of view and ever so politely guiding me through my mistakes with a patience of a saint that too humbly and kindly. She has undoubtedly made me a better scientist. My gratitude goes out to her for pushing me to keep improving and for caring about her students and their work. I would also like to thank Dr. Anna Pellegrino for her invaluable suggestions throughout my Ph.D. studies.

Thanks, are also owed to European Union for providing an excellent fellowship program for budding scientists to expand their horizons not only professionally but personally as well by training the researchers to develop inter-personal skills as well. MSCA-ITN ENHANCE Project has helped me to integrate with the scientific community in ways beyond perception. In, this regard I would also like to thank my employer INSTM (National Interuniversity Consortium of Materials Science and Technology) and the University of Catania for giving me the opportunity as a Junior Researcher and a doctoral candidate and also for taking care of any/every logistic issue in terms of resources and its availability. Furthermore, I would like to take this opportunity to thank my collaborators, Dr. Simon Rushworth, EpiValence, Prof. Ausrine Bartasyte, University of Franche Comte, Project leader for ENHANCE Project, and Prof. Sanjay Mathur, University of Cologne. I cannot imagine the success of my work without their due support and supervision.

I am grateful to several academic staff; without their guidance, this thesis would not have been possible: Prof. Patrizia Rossi for collecting single-crystal data, Dr. Carmela Bonaccorso for solid-state NMR work, and Prof. Samuel Margueron for training me with Raman Spectroscopy. Thanks, are also due to my colleagues and friends, especially Quentin Micard, Gabriel Barrientos, and Vanessa Jungbluth; they have been a trustworthy source of inspiration and support for me through the last three years.

On a personal note, I would like to thank my parents for helping and supporting me throughout the years of my study and my lovely wife, who has been a rock for me. All my brothers and sisters have also been invaluable for helping me continue with my studies and all of my friends in and out of chemistry for their support, friendship, and guidance. Finally, I would like to acknowledge the ENHANCE project, Grant Agreement N.722496, to fund this research work.

Table of Contents

Introduction	1
Chapter 1: Alkali Metal Complexes	6
1.1 Coordination Chemistry: State of the Art.....	6
1.1.1 Historical Background.....	6
1.2 Conventional ligands.....	8
1.2.1 Solvents as ligands.....	8
1.2.2 Anionic ligands.....	11
1.2.3 Electrically Neutral Ligands.....	13
1.2.4 Coordinated Ligands.....	14
1.3 Macromolecular Ligands.....	14
1.4 Conclusions.....	14
References.....	15
Chapter 2: Lithium β-diketonate glymes: Synthesis and Characterization	22
2.1 Experimental Section.....	23
2.2 Results and Discussions	26
2.3 Conclusions	42
References.....	43
Chapter 3: Potassium β-diketonate glymes: Synthesis and Characterization	48
3.1 Experimental Section.....	49
3.2 Results and Discussions.....	52
3.3 Conclusions.....	68
References.....	68

Chapter 4: Sodium β-diketonate glyme adducts: Synthesis and Characterization.....	72
4.1 Experimental Section	74
4.2 Results and Discussions	76
4.3 Conclusions	94
References.....	94
Chapter 5: Validation of “Li(hfa)•glyme” through applications in PI-MOCVD processes of Lithium Niobate films.....	98
5.1 Experimental Section	100
5.2 Results and Discussions.....	101
5.3 Conclusions	114
References	115
Chapter 6: Functional validation of the Na and K β-diketonate glyme adducts: fabrication of Potassium Sodium Niobate nanostructures.....	118
6.1 Experimental Section.....	120
6.2 Results and Discussions	101
6.3 Conclusions	135
References.....	135
Conclusions & Future Work.....	138
Appendix A: Selected Bond lengths and Bond Angles.....	142
Author’s Biography.....	148

INTRODUCTION

There has been a growing need for sustainability in the present generation and a greener energy source to combat the ever-increasing problems caused by pollution. The automobile sector is one of those areas where the human population has been overly dependent. With the advancement of technology and novel materials, we must find much more efficient ways of utilizing energy. ENHANCE Project (Piezoelectric Energy Harvesters for Self-Powered Automotive Sensors: from Advanced Lead-Free Materials to Smart Systems) is devoted to creating a convergence of multidisciplinary joint research activity, implying chemistry, materials science, physics, mechanics, engineering, and electronics to synthesize, develop, optimize, and fabricate novel piezoelectric materials to be utilized as energy harvesters. The project aims to convert vibrations, heat, and light sources of energy into electricity. The project's global outlook also focuses on developing this energy to power the car's sensors through wireless technology, thereby eliminating obsolete technology like wires, which increases the car's weight by around 100 kgs. This way, we can reduce the car's weight, reducing fuel consumption and the carbon footprint.

In this aspect, arguably the best commercially exploited material that shows piezoelectric, pyroelectric, and photovoltaic properties is the PZT (Lead Zirconate Titanate) so the ENHANCE project aims to find alternative materials to PZT, i.e., materials that are devoid of lead and possess less toxicity to the environment. Thus, we focus on three significant materials: lithium niobate LiNbO_3 , bismuth ferrite BiFeO_3 , and potassium sodium niobate $\text{K}_{(1-x)}\text{Na}_x\text{NbO}_3$.

Synthesis and fabrication of the previously mentioned materials in thin-film form require alkali metal precursors to provide the respective metal center and a favorable thermal property for a successful deposition. These precursors are nothing but a complex of (metal)(ligand), which binds together to provide specific properties to the materials required.

Lately, the pursuit for the fabrication of high-quality oxide thin films by MOCVD has led researchers to investigate β -diketonate complexes as a prospective molecular precursor.

They have been widely studied in the context of coordination compounds. Also, their chemistry has been explored for most of the metals in the periodic table. Accordingly, the ever-increasing demand for various thin-film materials for new industrial applications is also a significant reason for the rapid development of Metal-Organic Chemical Vapor Deposition (MOCVD). Nevertheless, in the case of alkali metal compounds, there are several underlying problems. The first one is the precursors' inability to be stable enough to be stored for a long time. The second is developing alkali-deficient phases due to alkali oxide evaporation during film evolution at elevated temperatures (700-900°C). The fact is that alkali cations with larger ionic radius have higher coordination numbers. Thus, in the conventional metal β -diketonates, commonly employed as volatile precursors for MOCVD deposition of thin films of materials containing p- and d-elements, the central ion's coordination sphere is not saturated in the case of s-elements. This, in turn, may give rise to the growth of polymeric or oligomeric structures with low volatility. In hindsight, typically, such precursors must be volatile, have adequate stability to be transported to the deposition site, and decompose efficiently to give the preferred material. In this regard, the metal β -diketonate complexes often exhibit more excellent hydrolytic stability than the alkoxides. A wide variety of β -diketonate complexes of both main and transition metals have been employed to fabricate thin films of metals, metal oxides, metal sulfides, and metal fluorides.

Metal β -diketonates $M(\text{RCOCHCOR})_n$ (where R = alkyl, aryl, and others while the R groups are not necessarily equivalent) can form chelates with the metal and delocalize the negative charge, while changing the R groups, influences the properties of developed compounds. The bonding and structural aspects associated with these complexes and the nature of these ligands to cover various metals have presented inorganic chemists with examples of compounds of electropositive metal ions that represent covalent characteristics, i.e., property to dissolve in organic solvents and high volatilities. These unique attributes have been comprehensively exploited in the past for solvent extraction and gas-liquid chromatographic techniques. Curiosity in metal β -diketonate complexes grows from their application as contact shift reagents for the enhanced resolution of nuclear magnetic resonance (NMR) spectra, laser technology, and the polymer industry. The occurrence of trace quantities of β -diketonate complexes in fuels has also been responsible for this growing interest.

In this context, the present thesis's work emphasizes the [(alkali-metal)-(β -diketonate)-(glyme)] systems for the synthesis of novel precursor complexes. β -diketonate is used as the anionic ligand to counter-balance the charge of the cation, and glyme is used as the neutral ligand to complete the coordination sphere and hold the complex together because of its chelating property. Also, the insertion of fluorine substituents in the β -diketonate core is used to fine-tune the metal-organic structure's properties. Partially fluorinated ligands are specifically utilized to improve precursor volatility and enhance complexes' solubility providing superior crystallization. Furthermore, because of the additional coordination of fluorine atoms with metal ions in heterometallic structures, the solvent co-ligands can be transferred from the coordination sphere. The primary aim of these precursors' synthesis is to have distinct characteristics that include volatility, stability at room temperature, clean disproportionation at low temperatures, facile synthesis, and nontoxic decomposition by-products.

In brief, the thermal properties characterization has been carried out through thermogravimetric (TGA) experiments under atmospheric pressures and differential scanning calorimetry (DSC). The complex structures were determined in collaboration with Prof. Patrizia Rossi, Department of Industrial Engineering, University of Florence, using single-crystal X-ray diffraction. Additional information regarding the complex's coordination is gathered by Fourier transform Spectroscopy FT-IR. The complexes are also characterized by $^1\text{H-NMR}$ and $^{13}\text{C-NMR}$. Finally, to validate the synthesized complexes' functional property as precursors and deposit the oxides of interest for the project, several application routes have been utilized, viz. sol-gel and pulse injection MOCVD (PI-MOCVD). Film morphology was investigated by field-emission scanning electron microscopy (FE-SEM), while the phase composition was analyzed by energy dispersive X-ray analysis (EDX). The structure of films was studied by X-ray diffraction (XRD) and Raman spectroscopy.

Reiterating, the research activity has been carried out to synthesize novel alkali metal precursors that can be utilized to deposit the desired materials, facilitating the present industry standards compared to the commercially available precursors. The work is done at the University of Catania in close collaboration with multiple local academic and industrial partners.

The work is encapsulated in the following points:

- Synthesis of the precursor complexes
- Engineering of the complex system for crystallization of the complexes.
- Characterization by Single-crystal XRD, FTIR, TGA, DSC, and NMR
- Application of the synthesized precursors for the deposition of the functional perovskite of interest.

Summarizing the Ph.D. work, the thesis is organized in the following chapters:

- Chapter 1: The present study's aim and the development of the alkali metal complexes have been described. A base to the significance and role of different components of the complexes has been laid down. The particular focus is on the different kinds of alkali metal coordination compounds from the past and the recent trends.
- Chapter 2: Lithium forms the focal point of this chapter. Emphasis is on Li-complexes, specifically for MOCVD applications. Novel synthetic routes for Li- β -diketonate complexes have been studied in detail. The precursor is studied in particular from a structural point of view regarding interesting coordination moieties observed and the presence of H₂O in the coordination sphere. Thermal analysis is also done to assert the importance of its physical property.
- Chapter 3: The significance of K-complexes focusing on the recent trends in complex development has been discussed. The synthesis of novel precursor complexes forms the core of this chapter. The complexes are investigated in detail from their structural and thermal property point of view.
- Chapter 4: Sodium complexes and the recent trend in Na complex chemistry is discussed in this chapter. A unique one-pot, open-air synthetic route has been taken for the synthesis of these complexes. Structural studies have been carried out to understand the physical nature of the complex. Thermal analysis is done to further substantiate and exploit the functional property for the fabrication of desired materials.

- Chapter 5: Novel Li- β -diketonate complexes are utilized to fabricate LiNbO₃ thin films by pulse injection, i.e., PI-MOCVD. An inference is drawn from the structural property observed and the importance of the pulse injection technique of MOCVD. Thin films are thoroughly investigated in view of the morphology and secondary phases.
- Chapter 6: Novel potassium- β -diketonate complexes and sodium- β -diketonate complexes have been utilized to fabricate K_{1-x}Na_xNbO₃ thin-film and nanofibers. The sol-gel technique has been employed for the formation of these nanostructures. Unique properties of thin films and fibers form the focal point of this study.

CHAPTER 1

Alkali metal Complexes

1.1 Coordination Chemistry: State of the art

Coordination complexes consist of one or multiple metal centers bonded to ligands (ions or molecules that donate electrons to the metal). These complexes, as observed, can be neutral or charged. In charged complexes, the neighboring counter-ions help in stabilizing the compound. The ligands may be attached to the central ion by coordinate (dative covalent) bonds, and in some cases, the bonding is more complicated.^[1]

1.1.1 Historical Background:

Alkali and alkaline earth cations started developing in the 1970s, "Metal-ammonia" were the first derivatives of M^{z+} with electrically neutral ligating molecules to be known and reported in 1830^[2] and later.^[3] Alfred Werner further influenced the study on M^{z+} -ammonia products in the field of coordination chemistry,^[4] reasonably to discover auxiliary valency for M^{z+} . Around the same period, Ettling^[5] in 1840 worked on some organic derivatives of M^{z+} [$ML(HL)_n$, ($n = 1$ or 2) where HL is an organic acid and L its anion] for the first time. He reported a somewhat vague understanding of the formation and structure of $Na(\text{salicylaldehyde})(\text{salicylaldehyde})(H_2O)_{1/2}$. Later, around 1906, Hantzsch^[6] synthesized its monohydrated analog and similar compounds calling it "acid salts." Bennett's report^[7] further elaborated it on $K(p\text{-hydroxybenzoate})-(p\text{-hydroxybenzoic acid})(H_2O)$ in 1915, and by the report of Sidgwick and Plant^[8] on M-indoxylspirocyclopentane ($M = Li, Na, \text{ and } K$) derivatives, viz., $M(C_{12}H_{12}ON)(C_{12}H_{13}ON)$.

With the sudden fascination in the alkali metal complexes, an interesting work started developing at the same time on the stable solid solvates of M^{z+} with various organic solvents. These solvates of the type $M(\text{anion})-(\text{solvent})_n$ were obtained by crystallizing the salts from the respective solvent. Most of these discoveries were rather unintentional and could only be observed during solubility studies of the salts. Solvates of this kind are: $M^+(\text{anion})(ROH)_n$ ^[9-13], and $M^{2+}(\text{anion})(ROH)_n$ ^{[10-12], [14, 15]} ($M^+ = Li, Na, \text{ or } K$; $M^{2+} = Mg, Ca, \text{ or } Sr$).

Sr; ROH is generally MeOH or EtOH or occasionally a higher alcohol), $M^+(\text{anion})(\text{Me}_2\text{CO})_n$,^[16,17] and $M^{2+}(\text{anion})(\text{Me}_2\text{CO})_n$,^[14, 17] ($M^+ = \text{Li}^+$ or Na^+ ; $M^{2+} = \text{Mg}^{++}$, Ca^{++} , or Sr^{++}), $\text{Mg}(\text{anion})(\text{PhCHO})_n$,^[14] $\text{Mg}(\text{I})_2(\text{RCO}_2\text{R}')_6$,^[14] ($\text{R} = \text{H}$ or Me , and $\text{R}' = \text{Me}$ or a higher alkyl group), $\text{Mg}(\text{halide})_2(\text{Et}_2\text{O})_2$,^[14,18] $\text{Mg}(\text{I})_2(\text{MeCN})_6$,^[14] $\text{Li}(\text{Cl})(\text{pyridine})_2$,^[19] $\text{Mg}(\text{halide})_2(\text{aniline})_6$,^[14] and $\text{Li}(\text{Cl})(\text{quinoline})_2$.^[20] The stable $M(\text{anion})(\text{DX})_n$, ($\text{DX} = \text{dioxane}$) complexes^[21, 22] could even be synthesized by solvent exchange with DX from the solutions of the salts in EtOH or Et₂O.

Notably, the status of β -diketonates as anionic ligands for M^{Z+} was also explored and recognized^[23] quite early. Sidgwick and Brewer's^[24] work carries historical importance concerning the solubility characteristics of the metal β -diketonates. They observed that the anhydrous $\text{Na}(1\text{-phenylbutane-1,3-dionato})$ salt was toluene-insoluble, whereas its dihydrated form was found toluene-soluble. The solubility of the dihydrated product in such a nonpolar solvent could only be explained if there was proper coordination of the water molecules with Na and if Na-OH_2 formed a covalent bond. This could only happen if the anion and water molecules acted as true ligands.

The organic reactions involving the use of alkali and alkaline earth hydroxides or salts have been frequently hypothesized with the formation of M^{Z+} -derivative intermediates along with electrically neutral reactants and the reaction intermediates.^[25] Nevertheless, such observations were abandoned since neither the organic synthetic chemist attempted to deliberate improvements on synthetic procedures by incorporating appropriate coordinative reactants of M^{Z+} nor the coordination chemist tempted to investigate many newer organic ligating species to study the coordination chemistry of M^{Z+} .^[26]

Important observations, which illustrate the coordination of a neutral molecule with an s-block cation can be summarized as: (i) the synthesis of $\text{NaBr}(\text{acetamide})_2$ (1901)^[27] (ii) synthesis of defined M^+ -PHEN (PHEN = 1,10-phenanthroline) complexes (1938)^[28] (iii) synthesis of stable $\text{MX}(\text{EN})_n$, ($M^+ = \text{Li}$ or Na ; $X^- = \text{I}$, Br , Cl , or ClO_4 ; and $\text{EN} = \text{ethylenediamine}$). Marullo and Lloyd (1966)^[29] found out that p,p'-diamino-2,3-diphenylbutane (DDB), a seemingly monodentate amine, could precipitate salts like NaCl from water.

1.2. Conventional Ligands

The ligands that have generally been researched in the coordination chemistry of transition cations are called conventional ligands. A complex can be organized based on the nature of the ligands, and thus a complex of the type $M(\text{anion})(\text{ligand})(\text{solvent})$ could be treated at three different places, i.e., the anion, the ligand, or the solvent.^[30]

1.2.1 Solvents as Ligands

Numerous empirical methodologies have been utilized for communicating M^{Z+} -solvent interaction. The solvent polarity concept^[31] based on dielectric constant (ϵ) values is one such approach. Gutmann's donor number theory^[32-38] related to the thermodynamic studies on solvating abilities of solvents has received rising considerations. Appropriately, a meaningful and straightforward classification was laid down by Kay et al.,^[39] according to which there are four major divisions of the polar solvents: i) acidic solvents, for example, fluorinated alcohols, which do not coordinate a cation but bond to an anion; ii) neutral solvents, for example, acetone, which weakly coordinates a cation; iii) basic solvents, for example, *N,N'*-dimethylformamide (DMF), which strongly coordinate a cation; and iv) hydrogen bonding solvents, for example, water, which strongly coordinates a cation and also bond to an anion.^[40] We will hence, discuss few parts of these classifications for our educational and understanding needs.

A. M^{Z+} -Solvent Coordination in Solution

During the dissolution of the ionic salt MX , the solvents act as ligands, as electron donors for M^{Z+} , and possibly as proton donors for X^{Z-} . Since the hard^[41], i.e., cations that are comparatively rigid and non-deformable with low polarizability, prefer to form ionic bonds in complex formation as they hold their electron firmly. M^{Z+} exhibits a pronounced attraction towards the hard X^{Z-} , ion-ion involvements play a significant role during M^{Z+} -solvent interactions than is typically understood for transition cations. Thus, in solution, the existence of contact ion pairs, in addition to solvent-separated ion pairs,^[34,42] is a more

common phenomenon. The position of ion-ion involvements is, however, greatly influenced by the nature of the solvent so that, in general, ion-ion involvements decrease and ion-solvent interactions increase when for a given ion pair a neutral solvent is substituted by a basic one and the latter by a hydrogen bonding one; neutral solvents usually frequently fail to cause charge separation of an ion pair even at a reasonably high solvent/salt ratio,^[43] whereas in the case of the hydrogen bonding solvents, the formation of the solvent-separated ion pairs usually is possible even at low solvent/salt ratios. It has been observed that M^{Z+} -anion and M^{Z+} -solvent competition leads to relatively difficult results to predict. This is so since ion solvation is at least a function of charge density of M^{Z+} , the solvating capability of the solvent, the nucleophilicity of the anion, and (in the case of the tight ion-pairs) the solvent/salt ratio.

B. M^{Z+} -Solvent Coordination in Solid State

Salts of particularly small cations possess the capacity to spring various types of solvents in the crystal lattice to yield what may be called solid solvates. The formation of a solid solvate can be determined by the solvent's nature and the nature of the salt's lattice packing. The hydrogen-bonding solvents have chemical reasons to appear in the lattice under most conditions that can be interrelated with each ion of a crystallizing salt, as evidenced by various salts' hydration. The basic solvents may be visualized to form solid solvates that also possess a distinct coordinating ability. Such as the transition cations generate coordination compounds like the metal ammines. In the case of M^{Z+} -solvent systems, the charge neutralizing anion may often remain in the cation's first sphere of attraction. It behaves fairly-stable in the lattice once "crystallization" with hydrogen-bonding, or a basic solvent becomes possible. Incorporating a neutral solvent in the lattice is also possible, at least in part, because of a definite M^{Z+} -solvent interaction. However, such results are usually unpredictable due to a facilitated solvent/water exchange.^[44]

The nature of the counter anion is vital in defining the nature of the solid solvate, that is, whether the cation is entirely within the environment of the solvent molecules (solvent complex) or is within that of the counter anion(s) and the solvent molecule(s) (solvated ion

pair).^[45] The counter anion also impacts the solvent/ M^{Z+} ratio in the solid product; the arrangement of the LiBr and LiI solvates with DX is ^[46] LiBr(DX) and LiI(DX)₂, for example, which may be credited to the nucleophilicity difference between the halide ions.

(i) Solvent Complexes

There are some closely hydrated salts, especially the inorganic salts of small M^{Z+} , which are charge separated and comprise the cation coordinated only with the solvent molecules; the anion in the protic case solvent derivatives is usually carried on the polarized hydrogen of the solvent. Na₂SO₄·10H₂O is one of the commonly known solvent complexes wherein the cation is within the Na(OH₂)₆ octahedron (Na-O, 2.37-2.47 Å).^[47]

(ii) Solvated Ion Pairs

The weakly coordinating solvents can bond with a cation but fail to stabilize the anion. These solvents are usually aprotic. Thus, their solid solvates are anticipated to be ion-paired under most conditions. The solid solvates LiCl(DX)^[48] (Li-Cl, 2.39 and 2.42 Å), and LiCl(pyridine)^[49], and LiCl(pyridine)₂(H₂O)^[50] (Li-Cl, 2.33 Å), for example, are solvated ion pairs.

(iii) Solvated Complexes

There are various compounds of the type M(anion)(ligand)(solvent) where “ligand” is the core ligand, and “solvent” acts as a co-ligand. There are occurrences during which the solvent molecule may get into the composition to fill up the unoccupied regions of the complexed cation. For example, MeCN in Li(antamanide)Br•MeCN^[51] or EtOH in Na(antamanide)Br•EtOH.^[52] In some cases, however, the solvent's role is crucial in triggering charge separation/ion-pair slackening of the salt, followed by complexation with the core ligand. This is projected for the complexes NaX(benzo-15-crown-5)(H₂O) (X⁻ = Br⁻ or I⁻), which cannot be crystallized in the anhydrous state from a dehydrated reaction mixture but rather are obtained in a hydrated form only from reaction mixtures including some water.^[53]

C. M^{Z+} -Solvent Coordination at Solid-Solvent interface

In an effort^[54] to explain the solubilization process, it was reasoned that lattice energy of the salt and dielectric constant of the solvent is not of elementary importance and only influences the rate magnitude of solubilization concerning alkali and alkaline earth halides in water. This is because solubility in water and lattice energy of the salt both rise toward fluoride. Since salts like $BaSO_4$ and $KClO_4$, which are primarily ionic, are practically insoluble in water, it was also discussed^[54] that the ions do not instigate the ion-solvation process due to their formal (or partial) charge.

1.2.2 Anionic Ligands

The contribution of the charge neutralizing anion as one of the ligands in the complexes of M^{Z+} is much more traditional than that in the coordination compounds of transition cations. For example, the solution of metallic Na in liquid ammonia ($[Na(NH_3)_n]^+ + e^{0-1}$) on reacting with NO gas results in the formation of $[Na(NH_3)_n]^+NO^-$ from which only Na^+NO^- is crystallized.^[55] This alkali cation action contrasts with the transition cations' general behavior, which produces ammine complexes from ammonia. The situation is in concurrence with the Hard and Soft Acids and Bases concept.^[56] Some publications^[57-60] have shown that the synthesis of M^{Z+} complexes with electrically neutral ligands is influenced by the nature of the charge neutralizing anion; the anion's impact becomes progressively significant as donicity of the solvent medium falls.^[61] The upsurge in charge density of M^{Z+} influences the cation-anion interaction. It increases in the order Cs^+ to Li^+ , i.e., M^+ to similar-sized M^{2+} .

The ability to ligate the M^{Z+} with an anion depends fundamentally on electrostatic attractions. Still, there can be a degree of covalency in the bond subject to whether one of the ions polarizes the counterion. The cation's polarizing capability for the neutral co-ligand (if any) is reduced when an anion participates in coordination; in other words, the anion strongly bonds the cation to the extent that the latter fails to be solvated. Various salts are insoluble even in donor organic solvents. Anion universally is anticipated to exercise a strong influence on the cation under conditions hindering the cation's solvation, and in the essence of this explanation may be considered a ligand of significant importance.

Additionally, suppose the anion carries a neutral donor site, then as a ligand, in this case, it becomes more effective and acts as a charge neutralizer and serves to fulfill the coordinative requirements of M^{z+} . For example, the EDTA anions belong to this group, and it rationalizes why they act as active isolating agents.

An interesting relationship between ion-pair formation and stereochemistry of the anion was found during the study of metal - β -diketonates. Although the forced chelation of the smaller cations on the anion arrest carbonyl functions in the cis form (Z, Z form), the larger cations allow the coulombic repulsions between the carbonyls to rotate one (E, Z form) or both (E, E form) carbonyls along with C-C bond(s)^[62, 63] due to the formation of weak ion pairs. X-ray diffraction solid-state studies carried out on 2,4-pentanedionatolithium^[64] show that the complex consists of endless chains of $[\text{Li}(\text{acac})_2]^-$ anions, connected by Li-ions. The anion constitutes a square plane (Li-O^- , 1.93 Å), while each bridging Li-ion is within an approximately tetrahedral environment (Li-O^- , 1.95 Å) of two pairs of oxygens belonging to neighboring $[\text{Li}(\text{acac})_2]^-$ ions. In the (1-phenylbutane-1,3-dionato)(ethylene glycol)sodium^[65] complex, only one β -diketonate chelate the cation, and on the other hand, ethylene glycol acts as a monodentate and connects the adjacent Na ions to form a polymeric structure. The classical parallel complex (1-phenylbutane-1,3 dionato)sodium dihydrate^[24] is stable in the solid-state and appears to carry water molecules covalently bonded to the cation, being toluene-soluble. One of the other observed things was that the anionic ligand's nucleophilicity is reduced, as of hexafluoroacetylacetate (hfac). The presence of highly electronegative fluorine atoms then favored the conditions for the formation of the anionic complexes. The complexes obtained from this anion are of the types^[66, 67] $(M^+)_m[M^+(\text{hfac})_n]^-$ ($m = 1$ or 2 , and $n = 2$ or 3) and $[\text{TMNDH}^+][M^{z+}(\text{hfac})_n]^-$ (TMND = 1,8-bis(dimethylamino)naphthalene) wherein, as previously observed the higher charge density cation gets into the anionic complex; few other notable complexes of the former group are: $M' [M(\text{hfac})_2]$ ($M' = \text{Cs}$ when M is K or Rb , or is Rb when M is K), $M'_2[M(\text{hfac})_3]$ ($M' = \text{Rb}$ or Cs , and $M = \text{Na}$), and $M'[M(\text{hfac})_2(\text{H}_2\text{O})]$ ($M' = \text{K}$, Rb , or Cs when $M = \text{Li}$, or is K when $M = \text{Na}$).^[66] The latter group complexes are: $[\text{TMNDH}^+][\text{Li}(\text{hfac})_2]^-$, $[\text{TMNDH}^+][\text{Na}(\text{hfac})_2(\text{H}_2\text{O})]^-$, $[\text{TMNDH}^+][\text{Mg}(\text{hfac})_3]^-$, $[\text{TMNDH}^+]_2[\text{Ca}(\text{hfac})_4]^{2-}$ and $[\text{TMNDH}^+][\text{Ca}(\text{hfac})_3(\text{H}_2\text{O})_2]^-$.^[66,67] In the first group complexes, the crystal structure of $\text{Rb}_2[\text{Na}(\text{hfac})_3]$, which is isomorphous with $\text{Cs}_2[\text{Na}(\text{hfac})_3]$, is known.^[66] The lattice consists of $\text{Na}(\text{hfac})_3^{2-}$ anionic units wherein Na is six-

coordinated by all the three hfac anions with Na-O-bonds ranging from 2.20 Å to 2.47 Å. The property of formation of the anionic complexes is mainly due to the high charge density cations.

1.2.3 Electrically Neutral Ligands

In the context of alkali metal complexes, coordination of a neutral molecule with an s-block cation was also observed. These include: (i) the synthesis of NaBr(acetamide)₂ (1901),^[68] (ii) synthesis of the crystalline CaCl₂(β-D-mannofuranose) (1929),^[69] (iii) synthesis of defined M⁺-PHEN (PHEN = 1, 10-phenanthroline) complexes (1938),^[70] and (iv) synthesis of stable MX(EN)_n, (M⁺ = Li or Na; X = I, Br, Cl, or ClO₄; and EN = ethylenediamine). Later in (1966),^[71] Marullo and Lloyd made a rather surprising observation in that the p,p'-diamino-2,3-diphenylbutane, a seemingly monodentate amine, could precipitate salts like NaCl from water. The most important advancement in the subject took place in 1967 when Pedersen at Du Pont (Delaware) discovered^[72] the property of electrically neutral macrocyclic polyethers, acting as efficient Ligands of M²⁺.

Electrically neutral ligands, whether O-donor or N-donor, can be divided into two categories: (i) ligands that lack polar or polarizable hydrogen, such as a glyme or 1, 10-phenanthroline. Such ligands generally produce ion-paired complexes and stabilize only the cation and not its counter anion. The ligand: M²⁺ ratio (usually low) in the product is a function of the anion's nucleophilicity and decreases as the anion's nucleophilicity increases.^[73] The charge separation of the complexing salt may become a consequence of complexation even though these ligands do not complex a cation via its charge separation. M²⁺ is effectively complexed by the ligands of this group when electron density of the donor atom is enhanced (a) by a delocalized electronic arrangement of the molecule holding the donor atom as in 1, 10-phenanthroline,^[74] (b) by the inclusion of electronic effects, e.g., by substitution of +I group(s) (positive Inductive effect) on the donor atom as Me in a glyme or TMED, or (c) by assisting the donor atom through direct linkage with an electronegative atom such as oxygen in pyridine oxides, arsine oxides, and phosphine oxides. Ligands corresponding to condition (c) may be labelled "reinforced ligands." Small cations exhibit a self-complexing property due to their high charge density. These ligands can influence a charge separation of the complexing salt on steric and electronic reasons to yield charge-

separated results of a high ligand: M^{2+} ratio. (ii) Ligands, such as hydroxyl compounds or amines that carry a polar proton or polarizable hydrogen atom, can also stabilize the complexing cation's counter anion by bonding it at the polar hydrogen and acting as "double-action ligands," which are exemplified by sugars and amides. Charge separation of the complexing salt during complexation with these ligands is aided by the complexation of the anion's cation and bonding.^[19] The charge-separated products so obtained are usually marked by a high coordination number for the complexed cation. Complexation occurs when the complexing salt and a highly acidic M^{2+} are composed of a highly basic anion; only under these conditions are M^{2+} complexation, and anion stabilization both enabled.^[75] This contrasts with the group's behavior as the efficiency of ligands, which for a given cation enhances with the decrease in the counter anion's nucleophilicity. These group ligands' complexes show the counter anion's ultimate behavior during pairing with the complexed cation, bonding with polar protons of the ligand, and its presence in the system disordered ion depending on availability of the space around the cation and compactness of the resulting lattice.

1.2.4 Coordinated Ligands

Structural studies show that in complexes that comprise a transition cation M^{n+} and M^{2+} , the latter captures a good coordination position concerning those ligands coordinated with the former. Such ligands may be studied as "coordinated ligands" or "metal complexes as ligands."

Studies on compounds like K-bis(tri-p-tolylphosphine)- Cu^+ -bis(dithiooxalato-O,O')stannate• $2Me_2CO$ ^[76] and also a large complex system such as Li-ethylenediamine-N,N'-diacetato-N,N'-di-3-propionatochromate(III)• $5H_2O$ ^[77] has also shown coordination of M^{2+} through the metal complex moieties.

1.3 Macromolecular Ligands

Natural antibiotics and synthetic compounds like crowns and cryptands form the core of the multidentate macromolecules (MMM) and are studied as ligands for M^{2+} . The antibiotics can be cyclic or acyclic, whereas the synthetic ligands can be acyclic, monocyclic, or polycyclic. The macromolecular ligands have grown in importance due to the chemistry of M^{2+} than the conventional ligands, which can be attributed to the fact that they bind M^{2+} effectively and

render the latter soluble in nonpolar solvents^[78] and because they are more applicable to the chemistry of M^{Z+} in biological systems which therein include the macro biomolecules principally. The strong M^{Z+} -MMM interaction is due to the multichelate effect (for acyclic MMM) or the superchelate effect^[79] (multichelate effect plus macrocyclic effect^[80-83] for closed-chain MMM). The solution and solid-state studies on M^{Z+} -MMM systems have been conducted significantly, and the interest is persistent.^[79, 80-106]

1.4 Conclusions

The historical development of the coordination complexes helped us to navigate through the precursor chemistry and understand the different mechanisms at play to successfully synthesize an alkali metalorganic precursor. Notably, the use of β -diketonates as anionic ligand, which can counterbalance the charge of the central metal ion and the pivotal role it plays, especially the fluorinated derivatives of the β -diketonates to impart appropriate mass transport properties and solubility, forms the essential part of this research work. Also, the use of neutral ligands such as glymes, to complete the coordination sphere and act as a chelating agent, has been the corner stone for the synthesis of the novel precursors developed during the course of this PhD work.

REFERENCES

- [1] G. A. Lawrance, Wiley, 2010.
- [2] H. Rose, Pogg. Ann., 20, 154 (1830).
- [3] C. F. Rammelsberg, Pogg. Ann., 55, 239 (1842).
- [4] F. Ephraim, Ber., 45, 1322 (1912).
- [5] H. Ettlting, Justus Liebigs Ann. Chem., 35, 252 (1840).
- [6] A. Hantzsch, Ber., 39, 3089 (1906).
- [7] G. M. Bennett, Trans. Chem. Soc., 107, 351 (1915).
- [8] N. V. Sidgwick and S. G. P. Plant, J. Chem. Soc., 209 (1925).

- [9] W. E. S. Turner and C. C. Bissett, *J. Chem. SOC.*, 1904 (1913)
- [10] D. G. R. Bonnell and W. J. Jones, *J. Chem. SOC.*, 318 (1926).
- [11] E. Lloyd, C. B. Brown, D. Glynwyn, R. Bonnell. and W. J. Jones, *J. Chem. SOC.*, 658 (1928).
- [12] H. Henstock, *J. Chem. SOC.*, 1340 (1934).
- [13] (a) H. Oosaka and T. Sawaya, *J. Chem. SOC. Jpn., Pure Chem. Sect.*, 71, 159 (1950);
(b) T. Pavlopoulos and H. Strehlow, *Z. Phys. Chem.*, 202, 474 (1954).
- [14] B. N. Menshutkin, *Z. Anorg. Allg. Chem.*, 52, 9, 155 (1907); 53, 26 (1907).
- [15] L. Quinet, *Bull. SOC. Chim. Fr.*, 2, 1201 (1935).
- [16] R. Macy and E. W. Thomas, *J. Am. Chem. SOC.*, 48, 1547 (1926).
- [17] W. R. G. Bell, C. B. Rowlands, I. J. Bamford, W. G. Thomas, and W. J. Jones, *J. Chem. SOC.*, 1927 (1930).
- [18] H. H. Rowiey, *J. Am. Chem. SOC.*, 58, 1337 (1936).
- [19] L. Kahlenberg and F. C. Krunskopf, *J. Am. Chem. SOC.*, 30, 1104 (1908).
- [20] J. H. Walton and C. R. Wise, *J. Am. Chem. SOC.*, 44, 103 (1922).
- [21] H. Rheinboldt, A. Luyken, and H. Schmittmann, *J. Prakt. Chem.*, 148,81 (1937).
- [22] H. Rheinboldt, A. Luyken, and H. Schmittmann, *J. Prakt. Chem.*, 149,30 (1937).
- [23] G. A. Guter and G. S. Hammond, *J. Am. Chem. SOC.*, 78, 5166 (1956).
- [24] N. V. Sidgwick and F. M. Brewer, *J. Chem. Soc.*, 2379 (1925).
- [25] F. W. Bergstrom & J. F. Carson, *J. Am. Chem. Soc.*, 63(11), 2934–2936 (1941).
- [26] P.N. Kapoor; R.C. Mehrotra (1974). *Coord. Chem. Rev.*, 14(1), 0–27 (1974)
- [27] A. W. Titherley. *J. Chem. SOC.*, 79, 413 (1901).
- [28] P. Pfeiffer and W. Christeleit, *Z. Anorg. Allg. Chem.*, 239, 133 (1938).
- [29] N. P. Marullo and R. A. Lloyd, *J. Am. Chem. SOC.*, 88, 1076 (1966).

- [30] K. L. Haas and K. J. Franz, *Chem. Rev.* 2009, 109, 4921–4960.
- [31] L. M. Jackman and B. C. Lange, *Tetrahedron*, 33, 2737 (1977).
- [32] (a) V. Gutmann and E. Wychera, *Inorg. Nucl. Chem. Lett.*, 2,257 (1966); (b) V. Gutmann, "Coordination Chemistry in Nonaqueous Solvents," Springer-Verlaa Vienna, 1968: (c) V. Gutmann. *Coord. Chem. Rev.*, 18, 225 (1976). -
- [33] J. F. Coetzee and C. D. Ritchie, Eds., "Solute-Solvent Interactions," Marcel Dekker, New York: (a) Vol. 1, 1969; (b) Vol. 2, 1976.
- [34] "Ions and ion Pairs in Organic Reactions," Vol. 1, M. Szwarc, Ed., Wiley-Interscience, New York, 1972.
- [35] E. S. Amis and J. F. Hinton, "Solvent Effects on Chemical Phenomena," Vol. 1, Academic Press, New York, 1973.
- [36] "Solutions and Solubilities," M. R. J. Dack, Ed., Vol. 8 of the series "Techniques of Chemistry," A. Weissberger, Ed., Wiley-Interscience, New York, 1975.
- [37] (a) J. O'M. Bockris and P. P. S. Saluja, *J. Phys. Chem.*, 76, 2298 (1972); (b) P. P. S. Saluja, *MTPInt. Rev. Sci., Phys. Chem., Ser. Two*, 6, 1-51 (1976).
- [38] L. M. Jackman and B. C. Lange, *Tetrahedron*, 33, 2737 (1977).
- [39] R. L. Kay, D. F. Evans, and M. A. Matesich, in ref 35, Chapter 10.
- [40] S. Alvarez, *Chem. - Eur. J.*, (2020)
- [41] "Hard and Soft Acids and Bases" (Benchmark Papers in Inorganic Chemistry), R. G. Pearson, Ed., Dowden, Hutchinson, and Ross, Inc., Stroudsburg, Pa., 1973.
- [42] (a) S. Winstein, E. Clippinger, A. H. Fainberg, and G. C. Robinson, *J. Am. Chem. SOC.*, 76, 2597 (1954); (b) H. Sadek and R. M. Fuoss, *ibid.*, 78, 5897. 5905 (1954).
- [43] N. Ahmad and M. C. Day, *J. Am. Chem. SOC.*, 99,941 (1977).
- [44] M. Den Heijer and W. L. Driessen, *Inorg. Chim. Acta*, 26, 227 (1979)
- [45] C. Näther, H. Bock, Z. Havlas, and T. Hauck, *Organometallics* 1998 17 (21), 4707-4715
- [46] J. C. Barnes and C. S. Duncan, *J. Chem. SOC., Dalton Trans.*, 1732 (1972)

- [47] H. W. Ruben, D. H. Templeton, R. D. Rosenstein, and I. Olovsson, *J. Am. Chem. Soc.*, **83**, 820 (1961). Redetermination: H. A. Levy and G. C. Lisensky, *Acta Crystallogr., Sect. B*, **34**, 3502 (1978).
- [48] F. Durant, Y. Gobillon, P. Piret, and M. van Meerssche, *Bull. SOC. Chim. Belg*, **75**, 52 (1966).
- [49] F. Durant, J. Verbist, and M. van Meerssche, *Bull. SOC. Chim. Belg.*, **75**, 806 (1966).
- [50] F. Durant, P. Piret, and M. van Meerssche, *Acta Crystallogr.*, **22**, 52 (1967).
- [51] (a) I. L. Karle, J. Karle, W. Burgermeister, H. Faulstich, and B. Witkop, *Proc. Natl. Acad. Sci. U.S.A.*, **70**, 1836 (1973); (b) I. L. Karle, *J. Am. Chem. Soc.*, **96**, 4000 (1974).
- [52] I. L. Karle, *Biochemistry*, **13**, 2155 (1974).
- [53] N. S. Poonia, *J. Am. Chem. Soc.*, **96**, 1012 (1974).
- [54] N. S. Poonia, *Univ. Indore Res. J.*, **4**, 1 (1977).
- [55] E. Zintl and A. Harder, *Ber.*, **66B**, 760 (1933).
- [56] Richard M. LoPachin, Terrence Gavin, Anthony DeCaprio, and David S. Barber, *Chem. Res. Toxicol.*, **2012** **25** (2), 239-251
- [57] N. S. Poonia, Abstracts, 17th International Conference on Coordination Chemistry, Hamburg, Sept 1976, p 343.
- [58] N. S. Poonia, *Inorg. Chim. Acta*, **23**, 5 (1977).
- [59] N. S. Poonia, B. P. Yadav, V. W. Bhagwat, V. Naik, and H. Manohar, *Inorg. Nucl. Chem. Lett.*, **13**, 119 (1977); correction: **15**, in press.
- [60] N. S. Poonia, V. W. Bhagwat, and S. K. Sarad, *Inorg. Nucl. Chem. Lett.*, **13**, 227 (1977).
- [61] (a) W. J. DeWitte, R. C. Schoenig, and A. I. Popov, *Inorg. Nucl. Chem. Lett.*, **12**, 251 (1976); (b) W. J. DeWitte, L. Liu, E. Mei, J. L. Dve, and A. I. PODOV, *J. Solution Chem.*, **6**, 337 (1977).
- [62] L. M. Jackman and B. C. Lange, *Tetrahedron*, **33**, 2737 (1977).
- [63] M. Raban, E. A. Noe, and G. Yamamoto, *J. Am. Chem. Soc.*, **99**, 6527 (1977).

- [64] F. A. Schroder and H. P. Weber, *Acta Crystallogr., Sect. 8*, 31, 1745 (1975).
- [65] D. Bright, A. J. Kolombos, G. H. W. Milburn, R. S. Nyholm, and M. R. Truter, *Chem. Commun.*, 49 (1970); D. Bright, G. H. W. Milburn, and M. R. Truter, *J. Chem. Soc. A*, 1582 119711
- [66] (a) D. E. Fenton and C. Nave, *Chem. Commun.*, 662 (1971); (b) D. E. Fenton, C. Nave, and M. R. Truter, *J. Chem. Soc., Dalton Trans.*, 2188 (1973).
- [67] D. E. Fenton and R. Newman, *J. Chem. Soc., Dalton Trans.*, 655 (1974).
- [68] A. W. Titherley, *J. Chem. Soc.*, 79, 413 (1901).
- [69] J. K. Dale, *J. Am. Chem. Soc.*, 51, 2788 (1929).
- [70] P. Pfeiffer and W. Christeleit, *Z. Anorg. Allg. Chem.*, 239, 133 (1938).
- [71] N. P. Marullo and R. A. Lloyd, *J. Am. Chem. Soc.*, 88, 1076 (1966).
- [72] C. J. Pedersen, *J. Am. Chem. Soc.*, 89, 2495, 7017 (1967).
- [73] N. S. Poonia, *Inorg. Chim. Acta*, 23, 5 (1977).
- [74] C. Longuet-Higgins and C. A. Coulson, *J. Chem. Soc.*, 971 (1949).
- [75] N. S. Poonia, *J. Sci. Ind. Res.*, 36, 268 (1977).
- [76] F. J. Hollander, M. Leitheiser, and D. Coucouvanis, *Inorg. Chem.*, 16, 1615 (1977).
- [77] F. T. Helm, W. H. Watson, D. J. Radanovic, and B. E. Douglas, *Inorg. Chem.*, 16, 2351 (1977).
- [78] C. L. Liotta in "Synthetic Multidentate Macrocyclic Compounds," R. M. Izatt and J. J. Christensen, Eds., Academic Press, New York, 1978, Chapter 3.
- [79] N. S. Poonia, in "Progress in Macrocyclic Chemistry," Vol. 1, R. M. Izatt and J. J. Christensen, Eds., Wiley-Interscience, New York, 1979, Chapter 3.
- [80] D. K. Cabbiness and D. W. Margerum, *J. Am. Chem. Soc.*, 91, 6540
- [81] F. P. Hinz and D. W. Margerum, *J. Am. Chem. Soc.*, 96, 4993 (1974).
- [82] J.-M. Lehn and J. P. Sauvage, *J. Am. Chem. Soc.*, 97, 6700 (1975).

- [83] R. D. Hancock and G. J. McDougall, paper presented at the 1st Symposium on Macrocyclic Compounds, Aug 1977, Brigham Young University, Provo, Utah.
- [84] J. J. Christensen, J. O. Hill, and R. M. Izatt, *Science*, 174, 459 (1971).
- [85] M. R. Truter and C. J. Pedersen, *Endeavour*, 30, 142 (1971).
- [86] M. R. Truter. *Chem. Brit.*, 7, 203 (1971).
- [87] C. J. Pedersen and H. K. Frensdorff, *Angew. Chem., Int. Ed. Engl.*, 11, 16 (1972)
- [88] W. E. Morf, D. Ammann, E. Pretsch, and W. Simon, *Pure Appl. Chem.*,
- [89] J. Smid, *Pure Appl. Chem.*, 48, 343 (1976) 13) J.-M. Lehn, *Pure Appl. Chem.*, 49, 857 (1977).
- [90] D. E. Fenton, *Chem. Soc. Rev.*, 6, 325 (1977).
- [91] M. R. Truter in "Metal-Ligand Interactions in Organic Chemistry and Biochemistry" (Proceedings of the Ninth Jerusalem Symposium on Quantum Chemistry and Biochemistry held in Jerusalem, March 29-April 2, 1976), Part 1, B. Pullman and N. Goldblum, Eds., D. Reidel, Dordrecht, Holland, 1977. DD 317-335.
- [92] R. M. Izatt, L. D. Hansen, D. J. Eatough, J. S. Bradshaw, and J. J. Christensen. in ref 15. DD 337-361.
- [93] J.-M. Lehn, *Acc. Chem. Res.*, 11, 49 (1978).
- [94] J. Smid in "Ions and Ion Pairs in Organic Reactions," Vol. 1, M. Szwarc, Ed., Wiley-Interscience, New York, 1972
- [95] J. J. Christensen, D. J. Eatough, and R. M. Izatt, *Chem. Rev.*, 74, 351, 1974
- [96] Yu. A. Ovchinnikov, V. T. Ivanov, and A. M. Shkrob, "Membrane-Active Complexones," BBA Library Vol. 12, Elsevier, Amsterdam, 1974.
- [97] G. Eisenman and S. J. Krasne in *MTP Int. Rev. Sci., Biochem., Ser. One*, 2, 27-50 (1975).
- [98] A. I. Popov in "Solute-Solvent Interactions," Vol. 2, J. F. Coetzee and C. D. Ritchie, Eds., Marcel Dekker, New York, 1976, Chapter 13.

- [99] R. H. Kretsinger and D. J. Nelson, *Coord. Chem. Rev.*, 18, 29 (1976).
- [100] W. Burgermeister and R. Winkler-Oswatitsch, *Top. Curr. Chem.*, 69, 91 (1977).
- [101] C. J. Pedersen in "Synthetic Multidentate Macrocyclic Compounds," R. M. Izatt and J. J. Christensen, Eds., Academic Press, New York, 1978, Chapter 1.
- [102] N. K. Dalley, in ref 39, Chapter 4.
- [103] G. W. Liesegang and E. M. Eyring, in ref 39, Chapter 5.
- [104] I. M. Kolthoff, *Anal. Chem.*, 51, 1R (1979).
- [105] S. Lindenbaum, J. H. Rytting, and Sternson, in "Progress in Macrocyclic Chemistry," Vol. 1, R. M. Izatt and J. J. Christensen, Eds., Wiley-Interscience, New York, 1979, Chapter 5.
- [106] R. Bissig, D. Ammann, W. E. Morf, E. Pretsch, and W. Simon, in ref 79, Chapter 1

CHAPTER 2

Lithium β -diketonate glyme adducts: Synthesis and Characterization

Lithium niobate (LiNbO_3) nanomaterials have been a significant source of interest due to their broad range of functions in the areas of ferroelectrics,^[1,2] piezoelectric,^[3] and nonlinear optics.^[4] This material has been described as the “silicon of photonics” due to its exceptional optical properties.^[5,6] Also, LiNbO_3 based materials, due to its nonlinear optical (NLO) response, are vital components of ultrafast laser writers,^[7] electro-optical modulators,^[8] optical switches,^[9] optical parametric oscillators,^[10] and holographic devices.^[11] The interest in LiNbO_3 has also been boosted by the need to look for lead-free piezoelectric materials due to the European community's restriction on the use of PZT [$(\text{PbZr})\text{TiO}_3$].

Nevertheless, applications for quantum photonics, surface acoustic wave devices, ferroelectric-based devices, etc., require the availability of LiNbO_3 in thin-film form. To this aim, various techniques have been applied, such as capillary liquid epitaxial technique,^[12] RF-magnetron sputtering,^[13] spin-coating^[14], and metal-organic chemical vapor deposition (MOCVD).^[15-17] MOCVD represents one of the most appealing processes because of its easy scalability, but its application requires the use of precursors with appropriate mass transport properties.

Further substantial advantages of MOCVD over physical processes are a capability for large-scale production, easier automation, good conformal coverage, selectivity, and the ability to produce metastable materials.^[18] Despite these promising advantages, industrial applications of an MOCVD process are still limited, likely because starting molecular compounds' commercial availability is insufficient. Very few lithium precursors are known for vapor phase processes, either MOCVD or atomic layer deposition.^[19,20]

Our previous studies have shown that glymes play a pivotal role in stabilizing complexes with the desired thermal properties for MOCVD applications.^[21,22] Glymes often behave like

crown ethers in terms of coordinating/solvating ions of the alkaline-earth,^[23,24] the transition^[25,26] and the rare-earth metals^[22,27] through oxygen-ion complexation, i.e., chelating properties, which leads to thermally stable, and volatile adducts. Additionally, glymes have many other favorable properties, including being liquid at various temperatures (typically >200 °C), low viscosity, high chemical, thermal stability, relatively low vapor pressure, and low toxicity.^[28] Owing to these excellent solvent properties, glymes have been extensively used as solvents in liquid-assisted MOCVD processes, either liquid injection or aerosol assisted.^[29,30]

Glymes have also been widely used to coordinate Li salts, proposed for lithium battery electrolyte applications, to produce crystalline solvate structures that are analyzable through single-crystal X-ray diffraction.^[31] Specifically, monoglyme (dimethoxyethane), diglyme (bis(2-methoxyethyl)ether), and triglyme (2,5,8,11-tetraoxa-dodecane) have been used to coordinate lithium in Li salts, yielding crystalline structures. Nevertheless, for some anions and glymes, liquid systems are observed. Henderson group has reported detailed studies on phase diagrams for glyme mixtures with simple lithium salts^[32] and crystallization kinetics of glymes with a wide range of lithium salts.^[33]

As a merging point from all the considerations mentioned earlier, we decided to synthesize novel lithium precursors using a β -diketone as anion and glyme as coordinating molecules. Here, we give details on the synthesis of novel lithium complexes of the type “Li(hfa)•glyme”, Hhfa= 1,1,1,5,5,5-hexafluoro-2,4-pentanedione, glyme= monoglyme (1,2-Dimethoxyethane), diglyme bis(2-methoxyethyl)ether), triglyme (2,5,8,11-tetraoxadodecane) and tetraglyme (2,5,8,11,14-pentaoxapenta-decane). The mass transport properties, investigated through thermogravimetric analysis and differential scanning calorimetry, are highly affected by the glyme nature, which plays a key role in thermal stability and volatility. They have also been characterized by FT-IR spectroscopy, ¹H, and ¹³C NMR. Single crystal X-ray diffraction studies provide evidence of interesting coordination moieties.

2.1 Experimental section.

Materials. The monohydrate lithium hydroxide [Li(OH)•H₂O, >98%] and 1,1,1,5,5,5-hexafluoro-2,4-pentanedione (H-hfa, >98%), were purchased from Strem Chemicals and

used as received. Monoglyme (1,2-Dimethoxyethane, 99.5%), diglyme (bis(2-methoxyethyl)ether, 99.5%), triglyme (2,5,8,11-tetraoxadodecane, >98%), tetraglyme (2,5,8,11,14-pentaoxapentadecane, >99%), dichloromethane (CH_2Cl_2 , >99.5%) and n-pentane were purchased from Sigma Aldrich.

General procedures. Elemental microanalysis was performed using a Carlo Erba 1106 elemental analyzer. Fourier Transform Infrared (FT-IR) spectra were recorded using a Jasco FT/IR-430 spectrometer with nujol mull between NaCl plates. Melting points were taken on tiny single crystals using a Kofler hot-stage microscope. Thermogravimetric analyses were made using a Mettler Toledo TGA2 and the STAR^e software. Dynamic thermal studies were carried out under purified nitrogen flow (50 sccm) at atmospheric pressure with a $5\text{ }^\circ\text{C min}^{-1}$ heating rate. The weights of the samples were between 7–10 mg. Differential scanning calorimetry analyses were carried out using a Mettler Toledo Star System DSC 3 under purified nitrogen flow (30 sccm) at atmospheric pressure with a $5\text{ }^\circ\text{C/min}$ heating rate. The weights of the samples were between 5-8 mg. NMR experiments were carried out at $27\text{ }^\circ\text{C}$ using a 500 MHz spectrometer (^1H at 499.88 MHz, ^{13}C NMR at 125.7 MHz) equipped with a pulse-field gradient module (Z-axis) and a tunable 5mm Varian inverse detection probe (ID-PFG); chemical shifts (δ) are expressed in ppm and are referenced to residual deuterated solvent. NMR data were processed using the MestReC software.

Synthesis of $[\text{Li}_{12}(\text{hfa})_{12}\bullet\text{monoglyme}\bullet 4\text{H}_2\text{O}]$ (1). The $\text{Li}(\text{OH})\bullet\text{H}_2\text{O}$ (0.385 g, 9.18 mmol) 30% excess was first suspended in dichloromethane (40 mL) followed by monoglyme (0.636 g, 7.06 mmol), and finally, Hhfa (1.47 g, 7.06 mmol) was added after 10 min, and the mixture was refluxed under stirring for one hour. The excess of LiOH was filtered off. The colorless crystals precipitated after partial evaporation of the solvent. The crystals were collected, washed with pentane, filtered, and dried under vacuum. The reaction yield was 70%. The crude product did not melt up to $220\text{ }^\circ\text{C}$ using the Kofler hot-stage microscope (760 Torr). NMR analysis reports: δ_{H} (500 MHz, CD_3CN , $27\text{ }^\circ\text{C}$) 5.88 (s, 12H, CH_{HFA}) 3.49 (s, 4H, CH_2), 3.32 (s, 6H, OCH_3) ppm; δ_{C} (125 MHz, CD_3CN , $27\text{ }^\circ\text{C}$) 176.02 (q, CO_{HFA} , $^2J(\text{C},\text{F})=32.4\text{ Hz}$), 118.08 (q, CF_3_{HFA} , $^1J(\text{C},\text{F})=287.5\text{ Hz}$), 86.59 (CH_2), 71.38 (CH_2), 57.89 (CH_3) ppm. Elemental analysis for **1** ($\text{Li}_{12}\text{C}_{64}\text{H}_{30}\text{F}_{72}\text{O}_{30}$): Calc: C, 28.36; H, 1.11. Found: C, 28.21; H, 1.09.

Synthesis of [Li₂(hfa)₂•diglyme•H₂O] (2). The Li(OH)•H₂O (0.385 g, 9.18 mmol) 30% excess was first suspended in dichloromethane (40 mL) followed by diglyme (0.473 g, 3.53 mmol), and finally, Hhfa (1.47 g, 7.06 mmol) was added after 10 min, and the mixture was refluxed under stirring for one hour. The excess of LiOH was filtered off. The colorless crystals precipitated after partial evaporation of the solvent. The crystals were collected, washed with pentane, filtered, and dried under vacuum. The reaction yield was 86%. The melting point of the crude product was 80-82°C (760 Torr). NMR analysis reports: δ_{H} (500 MHz, CD₃CN, 27 °C) 5.88 (s, 2H, CH_{HFA}), 3.61 (m, 4H, CH₂), 3.52 (m, 4H, CH₂), 3.32 (s, 6H, OCH₃) ppm; δ_{C} (125 MHz, CD₃CN, 27 °C) 176.01 (q, CO_{HFA}, ²J(C,F)=32.5 Hz), 118.10 (q, CF₃ HFA, ¹J(C,F)=287.5 Hz), 86.54 (CH₂), 71.09 (CH₂), 69.53 (CH₂), 57.92 (CH₃) ppm. Elemental analysis for **2** (Li₂C₁₆H₁₈F₁₂O₈): Calc: C, 33.13; H, 3.10. Found: C, 33.24; H, 3.14.

Synthesis of Li(hfa)•triglyme•H₂O (3). The Li(OH)•H₂O (0.385 g, 9.18 mmol) 30% excess was first suspended in dichloromethane (40 mL) followed by triglyme (1.25 g, 7.06 mmol), and finally, Hhfa (1.47 g, 7.06 mmol) was added after 10 min, and the mixture was refluxed under stirring for one hour. The excess of LiOH was filtered off. The obtained product did not crystallize and is liquid. NMR analysis reports: δ_{H} (500 MHz, CDCl₃, 27 °C) 5.92 (s, 1H, CH_{HFA}), 3.734 (s, 4H, CH₂), 3.66 (m, 4H, CH₂), 3.54 (m, 4H, CH₂), 3.32 (s, 6H, CH₃) ppm; δ_{C} (125 MHz, CDCl₃, 27 °C) 176.55 (q, CO_{HFA}, ²J(C,F)=32.6 Hz), 117.98 (q, CF₃ HFA, ¹J(C,F)=287.8 Hz), 87.53 (CH₂), 71.05 (CH₂), 69.85 (CH₂), 69.56 (CH₂), 58.78 (CH₃) ppm. Elemental analysis for **3** (LiC₁₃H₁₉F₆O₆): Calc: C, 39.80; H, 4.88. Found: C, 39.61; H, 4.99.

Synthesis of Li(hfa)•tetraglyme•H₂O (4). The Li(OH)•H₂O (0.385 g, 9.18 mmol) 30% excess was first suspended in dichloromethane (40 mL) followed by tetraglyme (1.57 g, 7.06 mmol), and finally, Hhfa (1.47 g, 7.06 mmol) was added after 10 min, and the mixture was refluxed under stirring for one hour. The excess of LiOH was filtered off. The product obtained does not crystallize and is liquid. NMR: δ_{H} (500 MHz, CDCl₃, 27 °C) 5.91 (s, 1H, CH_{HFA}), 3.68 (m, 8H, CH₂), 3.64 (m, 4H, CH₂), 3.54 (m, 4H, CH₂), 3.33 (s, 6H, CH₃) ppm; δ_{C} (125 MHz, CDCl₃, 27 °C) 176.52 (q, CO_{HFA}, ²J(C,F)=32.9 Hz), 117.98 (q, CF₃ HFA, ¹J(C,F)=287.4 Hz), 87.45(CH₂), 71.18 (CH₂), 69.85 (CH₂), 69.83(CH₂), 69.80 (CH₂), 58.80 (CH₃) ppm. Elemental analysis for **4** (LiC₁₅H₂₃F₆O₇): Calc: C, 45.93; H, 5.31 Found: C, 45.72; H, 5.14

Single crystal X-ray structure. The molecular and crystal structure of the two complexes $[\text{Li}_{12}(\text{hfa})_{12} \cdot \text{monoglyme} \cdot 4\text{H}_2\text{O}]$ (**1**) and $[\text{Li}_2(\text{hfa})_2 \cdot \text{diglyme} \cdot \text{H}_2\text{O}]$ (**2**), was investigated employing single-crystal X-ray diffraction at 100 K. Measurements for **1** were carried out with a Bruker APEX-II CCD diffractometer. In contrast, for **2**, an Oxford Diffraction Excalibur diffractometer was used. In the two measurements, the Cu-K α radiation ($\lambda = 1.54184 \text{ \AA}$) was used. Data collections were performed with the program CrysAlis CCD^[34] for **2** and with the Bruker APEX2 program for **1**.^[35] Data reductions were carried out with the program CrysAlisPRO^[36] for **2** and Bruker SAINT^[37] for **1**. Finally, absorption corrections were performed with the program ABSPACK in CrysAlis RED for **2** and SADABS for **1**.^[38] Structures were solved using the SIR-2004 package^[39] and subsequently refined on the F^2 values by the full-matrix least-squares program SHELXL-2013.^[40]

Geometrical calculations were performed by PARST97^[41], and molecular plots were produced by the program Mercury (v3.7).^[42]

2.2 Results & Discussions

The complexes are synthesized in a single-step reaction from the lithium hydroxide monohydrate, Hhfa, and glyme ligands in dichloromethane. A $\text{LiOH} \cdot \text{H}_2\text{O} : \text{Hhfa} : \text{glyme}$ stoichiometry of 1:1:1 was used for all the reactions, except for adduct **2**, when a 1:1:0.5 stoichiometry was used. The combination was refluxed under stirring for **1** hour (Eq. (2.1)). Adducts **1** and **2** are solid, while **3** and **4** are colorless liquids at room temperature.



1. $[\text{Li}_{12}(\text{hfa})_{12} \cdot \text{monoglyme} \cdot 4\text{H}_2\text{O}]_n$
2. $[\text{Li}_2(\text{hfa})_2 \cdot \text{diglyme} \cdot \text{H}_2\text{O}]$
3. $\text{Li}(\text{hfa}) \cdot \text{triglyme} \cdot \text{H}_2\text{O}$
4. $\text{Li}(\text{hfa}) \cdot \text{tetraglyme} \cdot \text{H}_2\text{O}$

In Table 2.1., crystal data and refinement parameters of the investigated structures are reported. The fluorine atoms bonded to the carbon atom C(4) of the hfa anion in **2** and all the fluorine atoms attached to C(9) in **1** are disordered. Such a disorder was modelled, in the two crystals, by introducing three positions for each fluorine atom (occupancy factors: 0.34, 0.33, 0.33 in **1** and 0.45, 0.30, 0.25 in **2**).

Table 2.1. Crystallographic data and refinement parameters for **1** and **2**.

	[Li ₁₂ (hfa) ₁₂ •monoglyme•4H ₂ O] _n (1)	[Li ₂ (hfa) ₂ (diglyme)•H ₂ O] (2)
Empirical formula	C ₆₄ H ₃₀ O ₃₀ F ₇₂ Li ₁₂	C ₁₆ H ₁₈ O ₈ F ₁₂ Li ₂
Formula weight	2730.16	580.18
Temperature (K)	100	100
Wavelength (Å)	1.54184	1.54184
Crystal system, space group	Monoclinic, P2 ₁ /n	Triclinic, P-1
Unit cell dimensions (Å, °)	a = 17.930(1) b = 9.2458(5); β = 103.158(3) c = 30.375(2)	a = 9.427(1); α = 112.482(9) b = 11.433(1); β = 95.14(1) c = 12.245(1); γ = 92.239(9)
Volume (Å ³)	4903.3(5)	1210.6(2)
Z, D _c (mg/cm ³)	2, 1.849	2, 1.592
μ (mm ⁻¹)	2.073	1.631
F(000)	2676	584
Crystal size (mm)	0.25x0.20x0.18	0.35x0.30x0.28
θ range (°)	2.63 to 60.23	3.93 to 74.18
Reflections collected / unique	50824 / 7307	11683 / 4594
Data / parameters	7307 / 820	4594 / 359
Goodness-of-fit on F ²	1.040	1.085
Final R indices [I > 2σ(I)]	R1 = 0.0605, wR2 = 0.1418	R1 = 0.0972, wR2 = 0.2580
R indices (all data)	R1 = 0.0722, wR2 = 0.1561	R1 = 0.1448, wR2 = 0.3398

For the non-hydrogen atoms, anisotropic thermal parameters were used. In all the two structures, the water molecules' hydrogen atoms were found in the Fourier difference map, and their positions were freely refined. In contrast, their thermal parameters were refined accordingly to the bonded atoms.

In the crystal structure of $[\text{Li}_6(\text{hfa})_6 \cdot 0.5(\text{monoglyme}) \cdot 2\text{H}_2\text{O}]_\infty$ (**1**) [with monoglyme=1,2-dimethoxyetane] there are six independent $\text{Li}(\text{hfa})$ moieties, two water molecules and half of a monoglyme ligand (fig. 2.1).

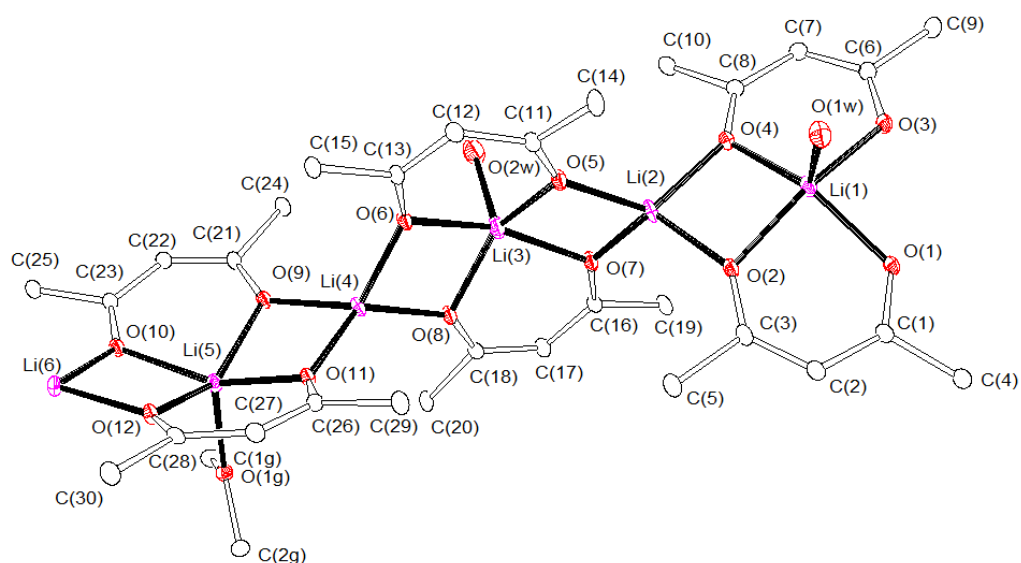


Fig. 2.1. Ortep view of the $[\text{Li}_6(\text{hfa})_6 \cdot 0.5(\text{monoglyme}) \cdot 2\text{H}_2\text{O}]_\infty$ asymmetric unit (the monoglyme ligand possesses a center of symmetry). Hydrogen atoms and fluorine atoms have been omitted for sake of clarity. Ellipsoids are at 20% probability.

The hfa ligands act as bridges, linking the lithium ions through the oxygen atoms into one-dimensional polymeric chains made up by Li-O_{hfa} moieties, which adopt a wave-like overall shape (fig. 2.2a). Within the chain, lithium 4- and 5-coordinated alternate, with the tetra-coordinated ion acting as a bridge between two mutually perpendicular $\text{Li}(\text{hfa})_2$ moieties. The fifth position in the 5-coordinated lithium ions (Li(1), Li(3), and Li(5)) is occupied by the oxygen atom provided by a water molecule (O(1W) and O(2W)) or the monoglyme molecule (O(1G)). The resulting coordination sphere can be described as square pyramidal ($\tau=0.21$ for Li(1) and Li(3), 0.16 for Li(5)), with the metal ion shifted toward the oxygen atom at the apex of the sp. In the 4-coordinated lithium-ion, the oxygen atoms describe a quite distorted

tetrahedron. The Li-O bond distances (table A.1.) appear a little bit shorter than those found in (1). The shortest Li-Li distance within the polymeric chain is 2.871(9) Å.

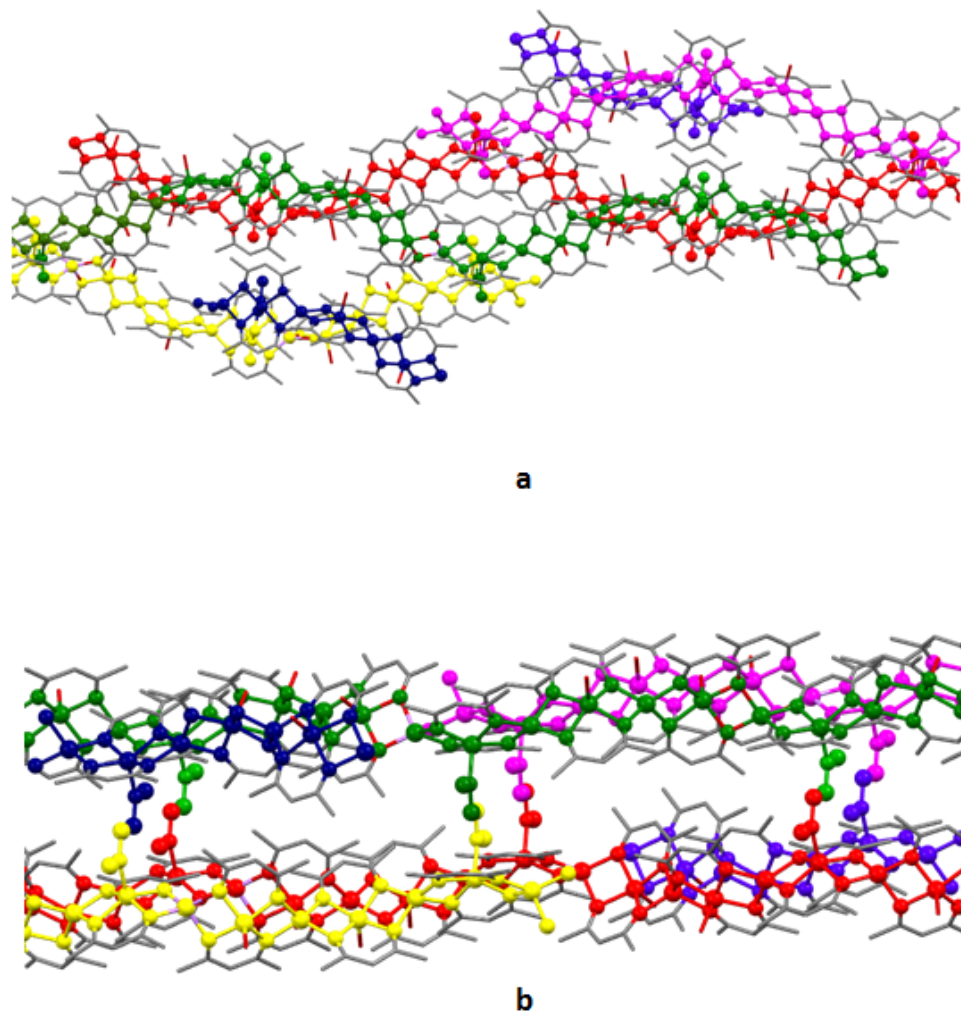


Fig. 2.2. Ball and stick view of the $[\text{Li}_6(\text{hfa})_6 \cdot 0.5(\text{monoglyme}) \cdot 2\text{H}_2\text{O}]_\infty$ polymeric chains. **a)** View along the a-axis direction (different colors have been used to highlight the wave-like motif described by the Li- O_{hfa} moieties). **b)** View highlighting the Li-monoglyme-Li bonds, which assemble the Li- O_{hfa} polymeric chains.

The Li(5) metal ions of different chains have linked each other (they are 6.434(9)Å apart) through the oxygen donors of the monoglyme molecules that are located around a center of symmetry. These latter act as bidentate bridges linking together the Li- O_{hfa} polymeric chains. In particular, each Li- O_{hfa} chain is bonded to two symmetry-related chains (fig. 2.2b); thus, a double layer of polymeric chains is formed and held together by the Li-monoglyme-Li

unit (fig. 2.3). A survey in the CSD shows that only one-dimensional polymeric chains based on LiO_4 units are present (EJUZIT,^[48] EUZUZ,^[49] HEYVIR^[50], and REGQAW^[51]).

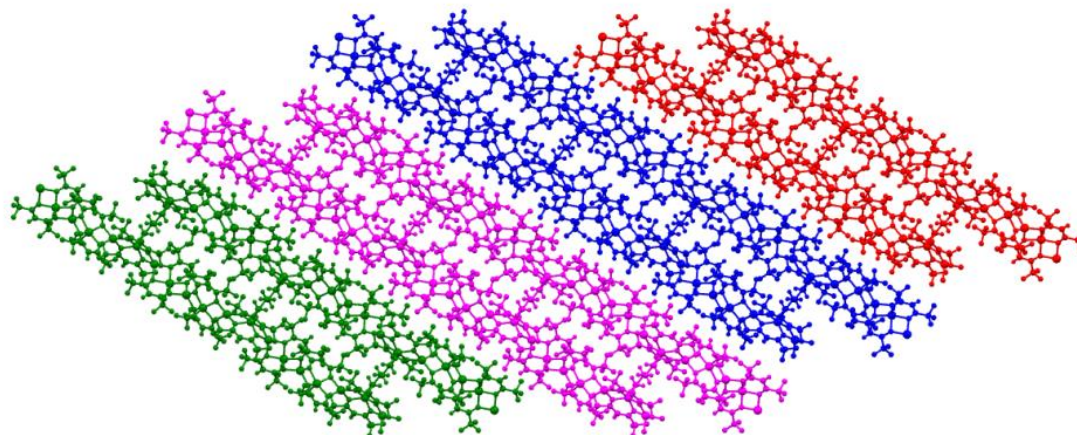


Fig. 2.3. Ball and stick view of the crystal packing of $[\text{Li}_6(\text{hfa})_6 \cdot 0.5(\text{monoglyme}) \cdot 2\text{H}_2\text{O}]_\infty$ view along the b axis direction highlighting the monoglyme bridges between polymeric chains).

The crystal structure of $[\text{Li}_2(\text{hfa})_2 \cdot (\text{diglyme}) \cdot \text{H}_2\text{O}]$ (**2**) [with Hhfa = 1,1,1,5,5,5-hexafluoro-2,4-pentandione and diglyme=1-methoxy-2-(2-methoxyethoxy)ethane] consists of binuclear lithium complexes (fig. 2.4). Each metal ion is penta coordinated, and in both cases, the polyhedron surrounding the lithium-ion can be described as a square pyramid (sp , as revealed by the value of the trigonal index^[43] τ ($\tau=0.21$ and 0.00 for Li(1) and Li(2), respectively). All the Li-O bond distances (table B.2.) are within the expected range, as provided by a search in the Cambridge Structural Database for crystal structure featuring the molecular fragment shown in figure 2.5a (CSD 5.39, November 2017+updates)^[44] for analogous chemical species. As for Li(1), the donor atoms are provided by the oxygen atoms of the two hfa anions and a water molecule in the axial position. The metal ion is displaced by $0.457(9)\text{\AA}$ from the mean plane described by the four hfa oxygen atoms and shifted toward the oxygen atom of the water molecule that occupies the sp 's apex.

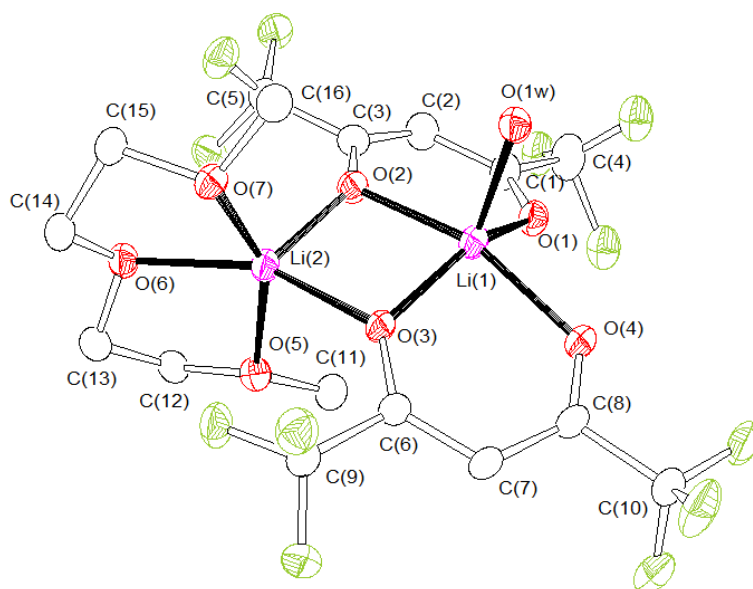


Fig. 2.4. Ortep view of the binuclear complex $[\text{Li}_2(\text{hfa})_2(\text{diglyme})\cdot\text{H}_2\text{O}]$. Hydrogen atoms have been omitted for the sake of clarity; just one model for the fluorine atoms bonded to C(5) has been reported. Ellipsoids are at 20% probability.

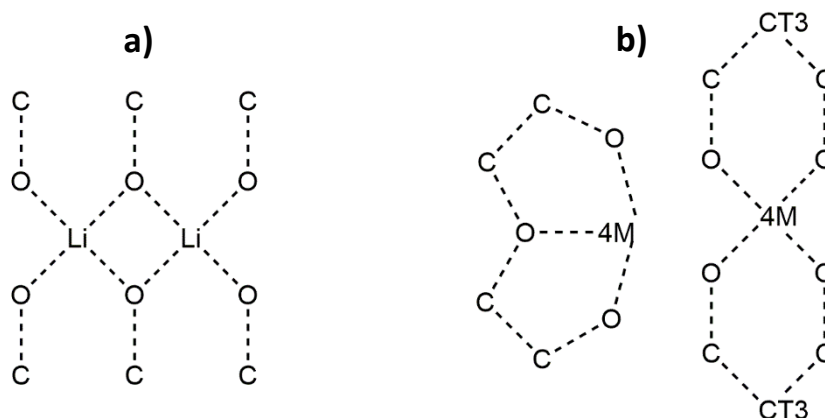


Figure 2.5. Fragments searched in the CSD.

Finally, Li(1) is 2.92(1) Å apart from Li(2) thanks to the hfa oxygen atoms O(2) and O(3) that work as bridging donors between the two metal ions. The Li-O-Li angles are 91.8(4) and 94.2(4)°, with the four atoms of the Li_2O_2 moiety well in a plane (all the geometrical parameters related to this moiety well compare with those found for the fragment sketched in figure 2.5a). The coordination sphere of Li(2) is completed by the oxygen atoms provided

by the diglyme molecule, whose oxygen atoms define, together with O(3), the base of the sp, being the other hfa oxygen atom O(2) at the apex. In this case, also the metal ion is shifted toward O(2) (0.44(1)Å). The two square pyramids' bases are almost perpendicular to each other (as provided by the angle between the corresponding mean planes, 74.5(1)°). A search in the CSD for structures featuring the fragment sketched in figure 2.5b reveals 35 hits; in 3 of them, the hfa bridges the metal ions structures (QADFIL,^[45] SATCOI^[46] and SUDYOF^[47] ref codes). In QADFIL, the Tl(hfa)·diglyme moieties give rise to a polymeric chain. As for the binuclear species, at variance with (1), in all cases, the two metal ions have an identical coordination environment: in SATCOI, there are centrosymmetric binuclear [Ba(hfa)₂(trigmo)]₂ molecules, while in [Ag(hfa)(diglyme)]₂ (SUDYOF) the two moieties are related by a two-fold axis.

In the crystal lattice, centrosymmetric dimers are formed through two identical pairs of strong H-bonds involving the water molecule working as H-bond donor and the hfa oxygen atoms O(1) and O(4) that act as acceptors (fig. 2.6, table A.2.). Within each dimer, adjacent lithium ions [Li(1)] are 4.39 Å apart.

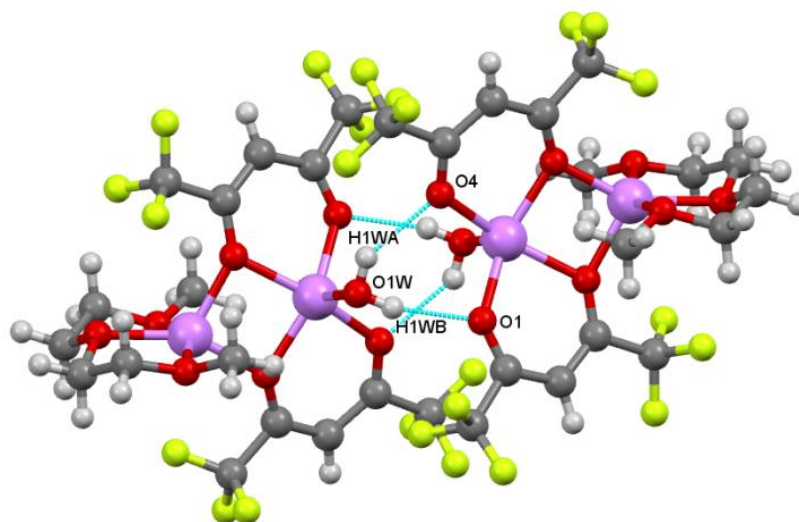


Fig. 2.6. Ball and stick view of the [Li₂(hfa)₂·(diglyme)·H₂O] dimer.

FTIR – Spectroscopy. The Fourier transform infrared (FT-IR) spectra, recorded in the range 4000-500 cm^{-1} (Fig. 2.7), has allowed us to confirm the formation of the adducts, and specifically also of the liquid adducts **3** and **4**.

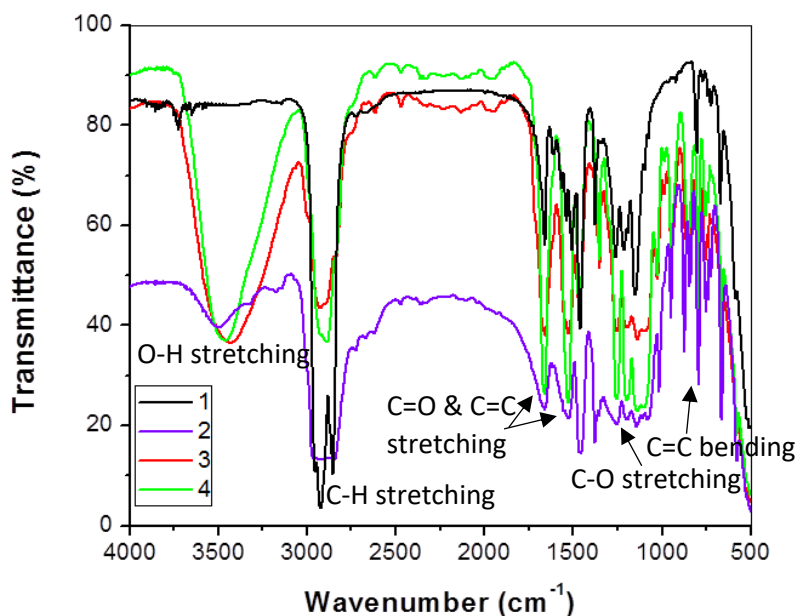


Fig. 2.7. FT-IR spectra of adducts **1**, **2**, **3** and **4**

In the spectra of the adducts **2**, **3**, and **4**, we observe broadband around 3600 cm^{-1} due to the OH stretching modes of coordinated water. Comparing the FT-IR spectra of all the four adducts and that of the H-hfa ligand in the carbonyl range, it is possible to observe that the two peaks at about 1660 cm^{-1} and 1530 cm^{-1} , associated respectively with the C=O and C=C stretching, are indicative of the hfa ligand coordination. The shifting of these peaks also observed in the “Li(hfa)•glyme” **3** and **4** adducts (an enlarged region in the range 1800-1400 cm^{-1} is reported in Fig. 2.8) compared to those of the free ligand, suggests that the hfa ligand coordinates the lithium-ion and the liquid compounds are not a mixture of ligands. The IR spectra recorded in the function of temperature (Fig. 2.9) allow confirming that diglyme is partially lost after heating up to 160°C.

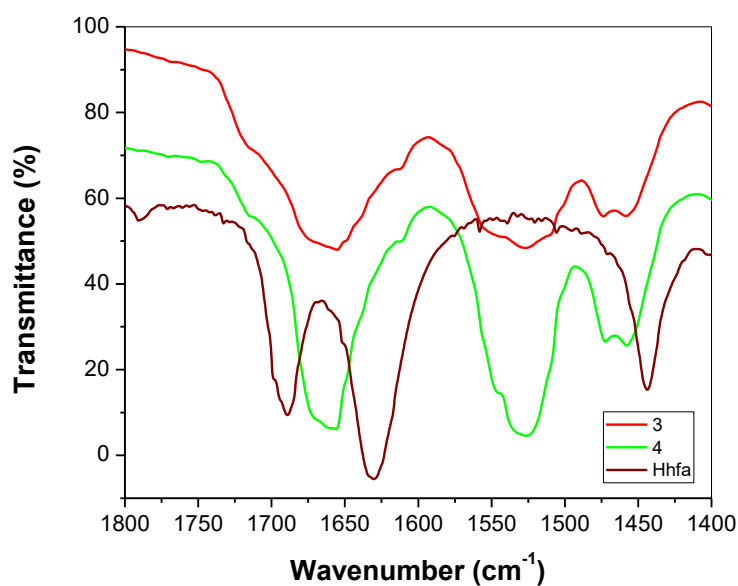


Fig. 2.8. FT-IR spectra of **3** and **4** vs. the free Hhfa ligand in the carbonyl range.

It is completely lost at 250 °C, since the peaks at 1004 cm⁻¹, 946 cm⁻¹, and 874 cm⁻¹, due to the glyme coordination,^[52] are missing on heating the sample.

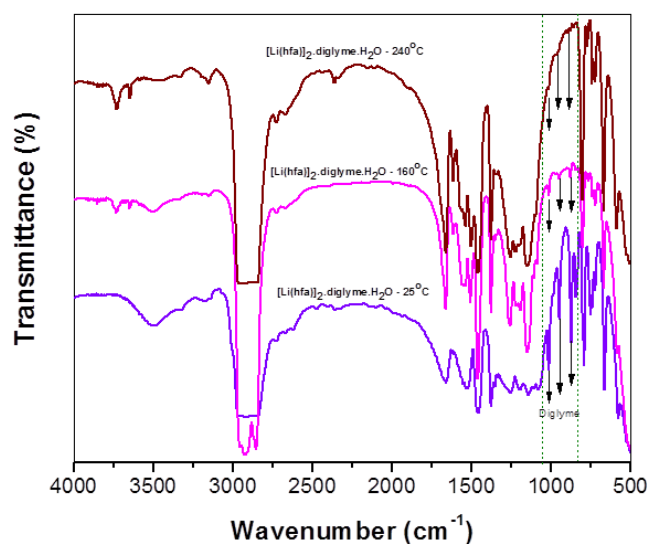


Fig. 2.9. FT-IR spectra of **2** were recorded at 25°C, 160°C, and 240°C.

NMR Spectroscopy. The ^1H -NMR and ^{13}C -NMR spectra of the Li(hfa)-glyme adducts have been carried out dissolving **1** & **2** in CD_3CN while **3** & **4** in CDCl_3 . All ^1H -NMR spectra (Fig. 2.10 – Fig. 2.13) show at $\delta \approx 3.3$ -3.4 ppm a singlet consistent with the protons of the terminal methyl groups of the glyme ligand, while multiplets at $\delta = 3.6$ -3.7 represent resonances of methylenic protons of the same ligand.

^1H -NMR measurement was conducted by dissolving the adduct **1** in deuterated acetonitrile as it is insoluble in chloroform. The obtained spectrum (Fig. 2.10a) shows a singlet at $\delta \approx 3.3$ ppm consistent with the protons of the terminal methyl groups of the glyme ligand. At around 3.5 ppm, the signals can be traced back to the CH_2 of monoglyme. At 5.9 ppm, the peak for the only proton of the hfa binder appears. Spectrum ^{13}C -NMR is recorded under decoupling conditions (Fig. 2.10b). At the chemical shift value of 86 ppm, the carbon signal falls into the two ketonic groups of the hfa. Finally, the two quartets at about 119 ppm and 176 ppm can be traced back to the C of the CF_3 and C-O groups of the binder. The quartets are due to coupling with the fluoride atoms of the CF_3 groups.

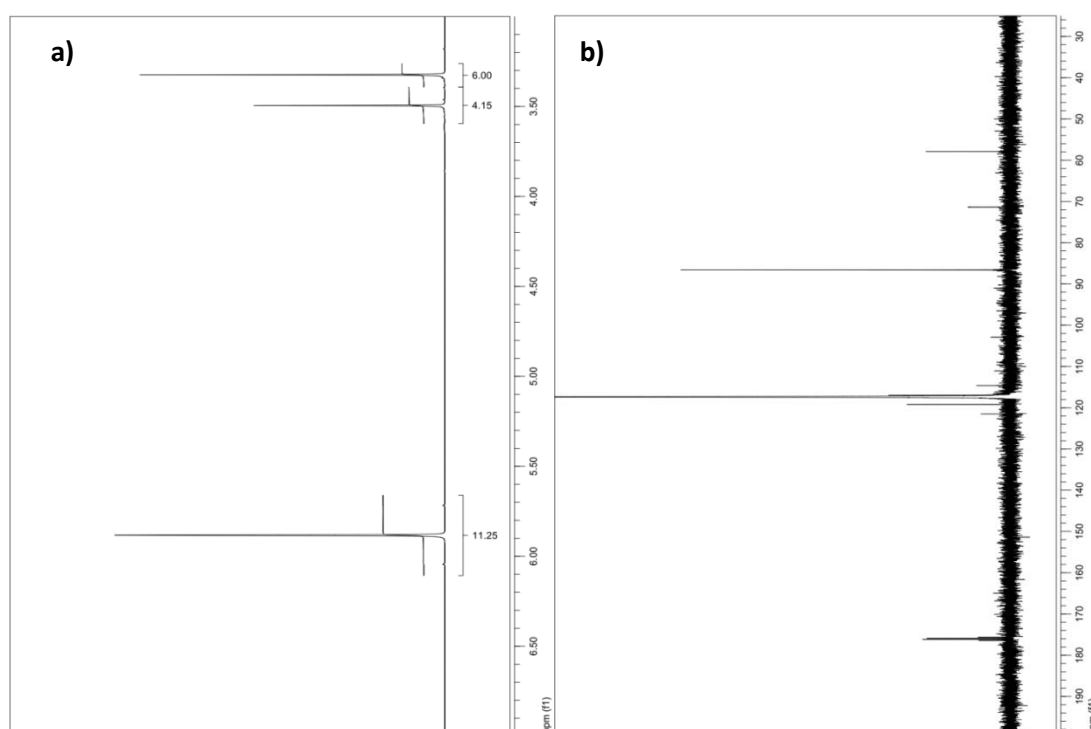


Fig. 2.10. a) ^1H -NMR spectrum of **1** (CD_3CN , 500 MHz, 27 °C) b) ^{13}C -NMR spectrum of **1** (CD_3CN , 125 MHz, 27 °C)

The ^1H -NMR spectrum of the adduct **2** was carried out in deuterated acetonitrile (Fig. 2.11 a). For adduct **2** in the ppm range of 3.5 ppm to 3.7 ppm, we find signals for the polyether's eight methylenic hydrogens. At the chemical shift value of 5.9 ppm, the singlet signal of the only hydrogen of the "diketonate" binder appears. Spectrum ^{13}C -NMR is recorded under decoupling conditions (Fig. 2.11 b). At the chemical shift value of 86 ppm, the carbon signal falls into the two ketonic groups of the hfa. Finally, the two quartets at about 119 ppm and 176 ppm can be traced back to the C of the CF_3 and C-O groups of the binder. The quartets are due to coupling with the fluoride atoms of the CF_3 groups.

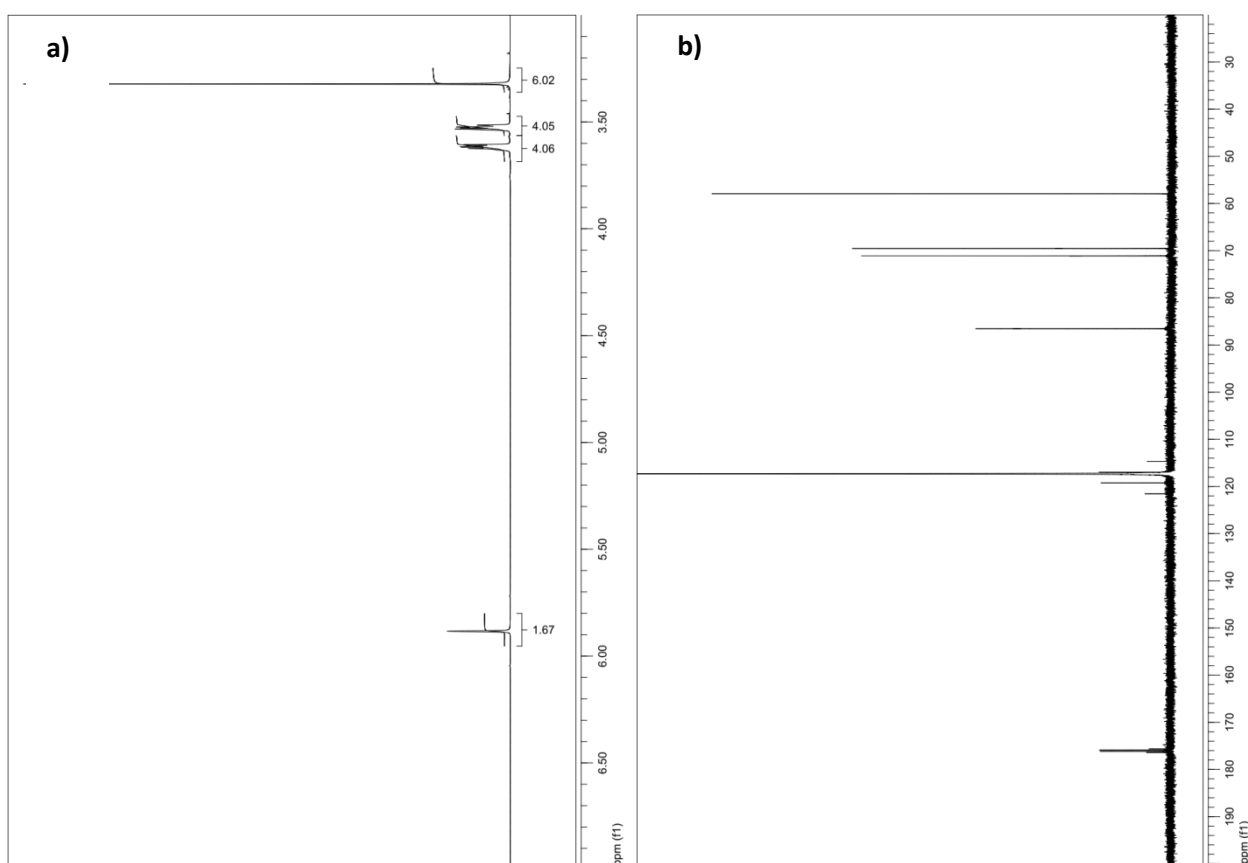


Fig. 2.11. a) ^1H -NMR spectrum of **2** (CD_3CN , 500 MHz, 27 °C) b) ^{13}C -NMR spectrum of **2** (CD_3CN , 125 MHz, 27 °C)

The ^1H -NMR spectrum of the adduct **3** was carried out in deuterated chloroform (Fig. 2.12a) and presented all the signals related to the resonant protons of the complex in question. The integration of the intense 3.3 ppm singlet indicates the six equivalent protons of the two terminal methyl groups of the triglyme. In the chemical shift from 3.5 ppm to 3.7 ppm, two multiplets and one singlet can be seen from the polyether's twelve methylinic hydrogens. At 5.9 ppm, we find the singlet relative to the proton compared to the diketone's two carbonyl groups. Spectrum ^{13}C -NMR (Fig. 2.12b) is recorded in decoupling conditions. For a chemical shift value of 58 ppm, the signal for the two methyl carbons of the polyether is observed. Between 68 ppm and 72 ppm, the methylinic C of the triglyme resonates. At 77 ppm, the signal for the deuterated chloroform used as a solvent is observed. Finally, at the value of 85 ppm, the carbon resonates in the two ketonic groups. The two quartets at about 118 ppm and 176 ppm can be traced back to the C of the CF_3 and $\text{C}=\text{O}$ groups, respectively of the β -diketone. The quartets are due to coupling with the fluoride atoms of the CF_3 groups.

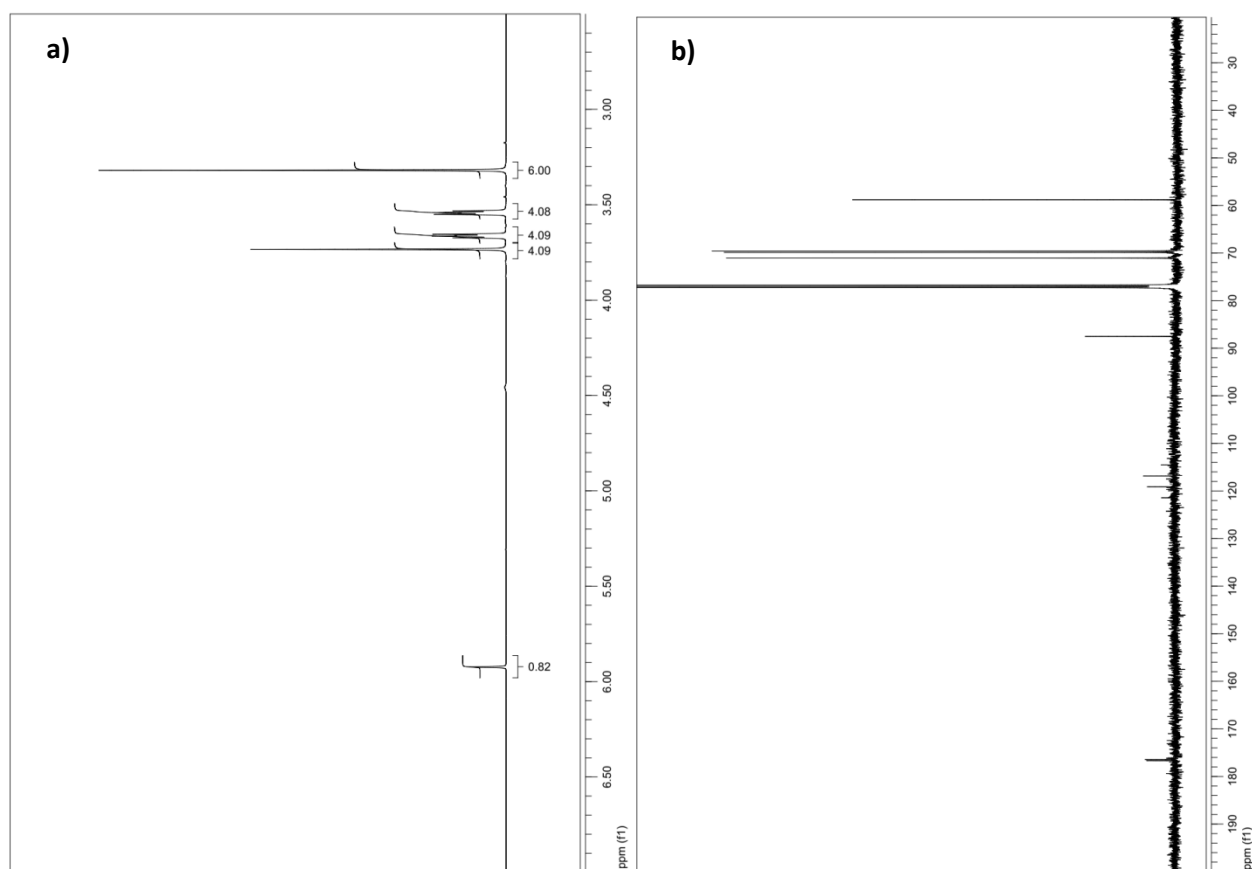


Fig. 2.12. a) ^1H -NMR spectrum of **3** (CDCl_3 , 500 MHz, 27 °C) b) ^{13}C -NMR spectrum of **3** (CDCl_3 , 125 MHz, 27 °C)

The ^1H -NMR spectrum of adduct **4** was carried out in deuterated chloroform (Fig. 2.13a) and showed an intense 3.3 ppm singlet, which relates to the resonance of the six equivalent protons of the two terminal methyl groups of the polyether. Signals ranging from 3.5 ppm to 3.7 ppm can be traced back to the sixteen methylenic protons of tetraglyme. The 5.9 ppm singlet is related to the proton linked to carbon dioxide in the two carbonyl groups of the hfa. Spectrum ^{13}C -NMR (Fig. 3.13b) shows an intense 59 ppm signal, typical of the two methyl C of the tetraglyme. Between 69 ppm and 71 ppm, signals are seen for the eight methylenic C of the polyether. At 77 ppm, the signal from the deuterated chloroform used as a solvent is observed. At the chemical shift value of 86 ppm, the carbon signal falls in the two ketonic groups of the hfa. Finally, the two quartets at about 118 ppm and 174 ppm can be traced back to the C of the CF_3 and $\text{C}=\text{O}$ groups of the binder. The quartets are due to coupling with the fluoride atoms of the CF_3 groups.

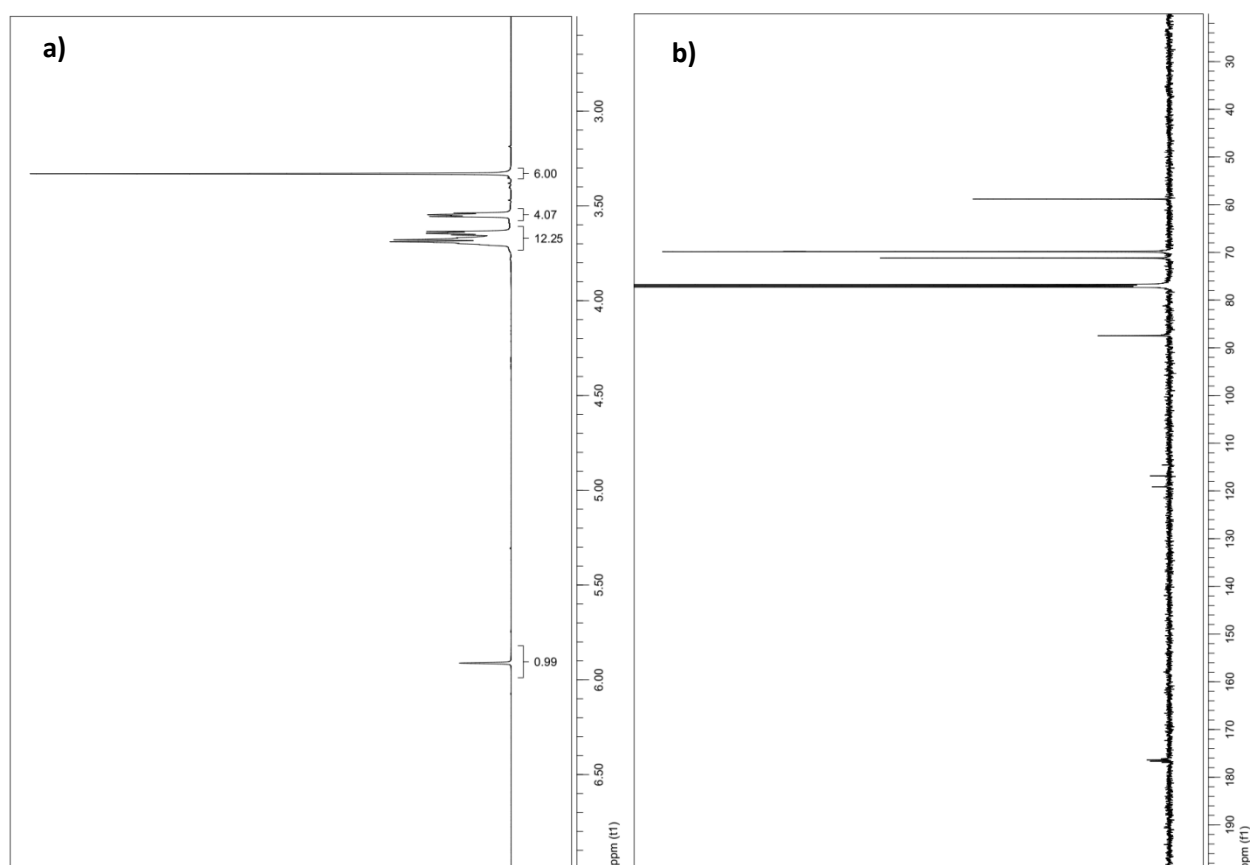


Fig. 2.13. a) ^1H -NMR spectrum of **4** (CDCl_3 , 500 MHz, 27 °C) b) ^{13}C -NMR spectrum of **4** (CDCl_3 , 125 MHz, 27 °C)

Confirmation of the formation of the liquid adducts has been obtained through recording the ^1H -NMR spectra. The metal cation binding affects the signals of the ^1H NMR spectra of the triglyme (Fig. 2.14) and tetraglyme (Fig. 2.15) ligands.

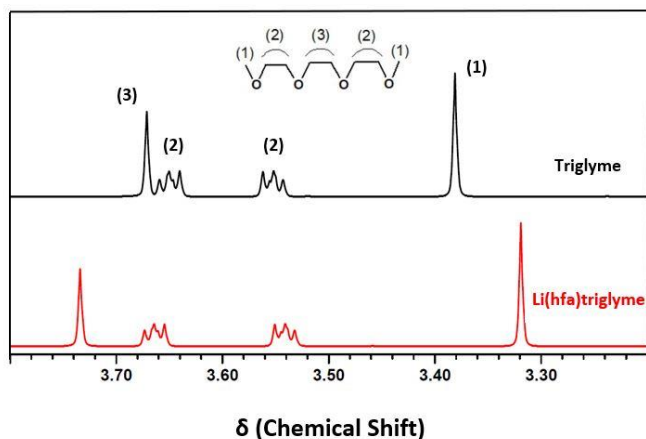


Fig. 2.14. Comparison of ^1H -NMR spectra (polyether region) of Triglyme (—) and $\text{Li}(\text{hfa})\cdot\text{triglyme}$ (—).

Also, the integrations of the ^1H -NMR peaks of **3** (Fig. 2.12a) and **4** (Fig. 2.13a) confirm a 1:1 hfa: glyme ratio in adducts **3** and **4**, thus pointing to the formation of complexes with formula $\text{Li}(\text{hfa})\cdot\text{triglyme}$ and $\text{Li}(\text{hfa})\cdot\text{tetraglyme}$.

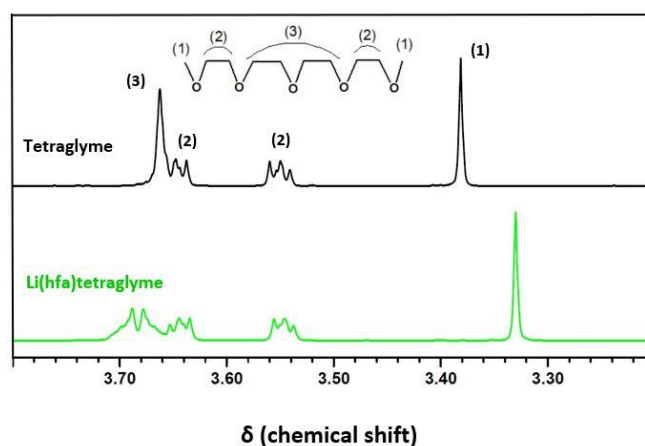


Fig. 2.15. Comparison of ^1H -NMR spectra (polyether region) of tetraglyme (—) and $\text{Li}(\text{hfa})\cdot\text{tetraglyme}$ (—).

Changes are observed for almost all the triglyme ligand protons in the adduct **3**: the methylene protons of the innermost portion undergo an upfield shift while the external methyl groups experience a downfield shift. These observations provide further evidence that the metal ion is coordinated through the oxygen atoms and that the ligands rearrange upon complexation. A similar trend is observed for the tetraglyme adduct **4** (Fig. 2.15).

The findings mentioned above may be interestingly compared with the Watanabe group's data ^[53-55] for Li complexes prepared by mixing lithium bis(trifluoromethyl- sulfonyl)-amide and triglyme or tetraglyme in a 1:1 molar ratio. Clear liquids were also obtained in those cases, and their behavior as room temperature ionic liquid was discussed.^[53-55]

For other anions ($X = \text{CF}_3\text{SO}_3^-$, BF_4^- , ClO_4^- , AsF_6^- , and PF_6^-) solid crystalline structures have been observed for the (triglyme) $1:\text{LiX}$ with the Li-ion in a four- to five- coordinated environment,^[56, 57] while for AsF_6^- , BF_4^- , CF_3CO_2^- anions tetraglyme gives crystalline structures with a six-coordination sphere for Li^+ .^[58]

Similar four- or five-coordination moieties have been observed through the Lindgren group's ab-initio studies for Li-triglyme and Li-tetraglyme systems.^[59, 60] They suggested that the high chain flexibility of glymes enables many stable structures within a narrow energy range with very different geometrical arrangements of the ether oxygens.^[59, 60] Coordination numbers ranging from four to six have also been found for Li in alkoxides and β -diketonates complexes, see ref. [61] and references therein.

Thermal analysis. The thermal behaviors of the as-synthesized precursors have been investigated by thermogravimetric (TG) measurements (Fig. 2.16a) and differential scanning calorimetry (DSC) (Fig. 2.16b), which are thereby compared with the behavior of the commercial precursor, i.e., $\text{Li}(\text{tmhd})(\text{H}_2\text{O})_2$, (2,2,6,6-tetramethyl-3,5-heptanedionato lithium dihydrate). TG curves of the “Li(hfa)•glyme” **1**, **3**, and **4** show a two-step mass loss associated with the H_2O molecule loss around 100°C and vaporization of the adducts. Specifically, adduct **1** shows a weight loss of about 5.6% in the range 25-140°C, which accounts for the loss of the four water molecules and the monoglyme of the $[\text{Li}_{12}(\text{hfa})_{12}\bullet\text{monoglyme}\bullet 4\text{H}_2\text{O}]_n$ polymeric structure, the theoretical weight loss being equal to 5.9%. The primary mass loss due to the adduct vaporization occurs in the range 230-

340°C, with a residue of 6.2%. The vaporization of $\text{Li}(\text{tmhd})(\text{H}_2\text{O})_2$ occurs in two steps as well, the first one (10.5% at 100°C) is associated with the loss of two water molecules, and the second one related to the complex vaporization with a residue at 300°C of 3.3%. Depending on the synthetic procedures, tetrameric units of $[\text{Li}(\text{tmhd})]_4$ ($[\text{Li}(\text{dpm})]_4$ following the previously used nomenclature of dipivaloylmethane for the Htmhd) have been found without water molecules in the coordination sphere, showing a higher residue in the TG analysis.^[62, 63] The range temperature of vaporization of **1** is higher than the commercial $\text{Li}(\text{tmhd})(\text{H}_2\text{O})_2$ precursor, but this is not a drawback for its applications in liquid-assisted MOCVD processes given its solubility in common organic solvents.

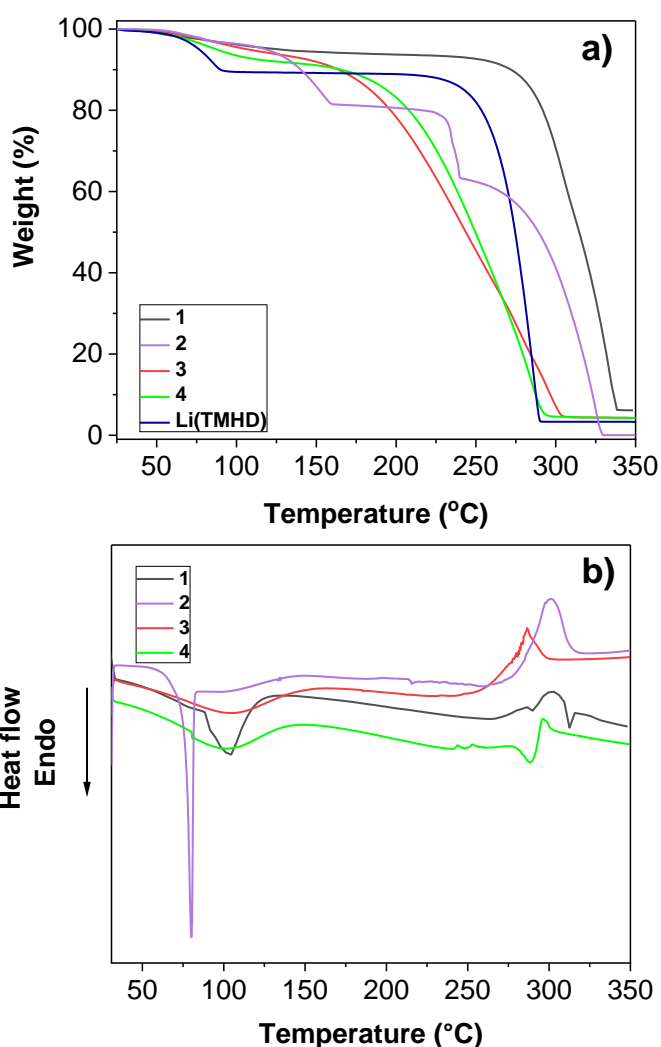


Fig. 2.16. TG curves (a) of the four "Li(hfa)•glyme" adducts vs. Li(tmhd). DSC curves (b) of the four "Li(hfa)•glyme" adducts.

The TG curves of adducts **3** and **4** (Fig. 2.16a) show a nearly single step weight loss with a residue of 4.3% at 300 °C and 4.4% at 300 °C, respectively. The TG curve of the $[\text{Li}_2(\text{hfa})_2 \cdot \text{diglyme} \cdot \text{H}_2\text{O}]$ adduct shows a three-step weight loss, with a residue of 1% at 330 °C. Interpretation of the individual steps is not straightforward. It is worthy to note that the presence of H_2O molecules in the coordination sphere of Li-ion is not a drawback for the thermal properties of present complexes. An excellent thermal behavior for MOCVD applications has been previously observed for the $\text{Mg}(\text{hfa})_2 \cdot 2\text{H}_2\text{O} \cdot 2\text{diglyme}$ ^[24] and $\text{Co}(\text{hfa})_2 \cdot 2\text{H}_2\text{O} \cdot \text{tetraglyme}$ ^[26] adducts, despite the presence of H_2O molecules in the coordination sphere.

The DSC curves (fig. 2.16b) of adduct **1** show a broad endothermic peak around 100°C, likely associated with the loss of H_2O molecules and a small, sharp endothermic peak at 312.6°C, which may be related to the melting of the polymeric structure. The DSC curve of adduct **2** presents a sharp endothermic peak at 80.3°C due to the adduct melting and a broad exothermic peak at 300°C, which can be associated with its partial vaporization decomposition. In adducts **3** and **4**, very broad peaks around 100°C are observed due to the H_2O molecule loss. In contrast, the exothermic peaks around 290°C may be associated with vaporization overlapped with a partial decomposition of the products.

2.3 Conclusions

The major constraints with alkali metal precursors are, due to their reactivity, the storage, which is very difficult for longer periods of time and also the alkali metal losses at elevated temperatures when subjected to CVD. In conclusion, to counter the above problems, the reported research provides a detailed study on the syntheses of four novel lithium's adducts. The straightforward one-pot nature of the presently reported synthetic route envisages the possibility to efficiently synthesize and produce these precursors on a large scale for industrial applications and to store for longer time as the precursors are stable in air. Various glymes have been used to complete the Li ion's coordination sphere, giving rise to volatile compounds by changing the coordination moieties. TG data and the excellent solubility of the adduct **1** in common organic solvents, even though it is a polymeric structure, make this precursor suited for MOCVD applications. Besides, it is evident from the

TG analyses that the adducts **3** and **4** represent viable options compared to $\text{Li}(\text{tmhd})(\text{H}_2\text{O})_2$, owing to their single step mass loss, low residue, and comparable vaporization temperatures. Functional validation of these precursors has been assessed through their application to liquid-assisted MOCVD processes of LiNbO_3 films to counter the issue of higher alkali metal losses at elevated temperatures.

REFERENCES

- [1] M. Schröder, A. Haußmann, A. Thiessen, E. Soergel and T. Woike, *Adv. Funct. Mater.*, 2012, 22, 3936–3944.
- [2] D. Xue and K. Kitamura, *Ferroelectrics*, 2003, 297, 19–27.
- [3] Z. Chen, J. Huang, Y. Yang, Y. Wang, Y. Wu, H. He, X. Wei, Z. Ye, H. Zeng, H. Cong and Z. Jiang, *RSC Adv.*, 2012, 2, 7380–7383.
- [4] R. Grange, J. W. Choi, C. L. Hsieh, Y. Pu, A. Magrez, R. Smajda, L. Forro and D. Psaltis, *Appl. Phys. Lett.*, 2009, 95, 143105.
- [5] R. Bhatt, I. Bhaumik, S. Ganesamoorthy, R. Bright, M. Soharab, A. K. Karnal, and P. K. Gupta, *Crystals*, 2017, 7, 23.
- [6] D. Kwei, C. Wang, H. Wang, X. Hu, D. Wei, X. Fang, Y. Zhang, D. Wu, Y. Hu, J. Li, S. Zhu and M. Xiao, *Nat. Photonics*, 2018, 12, 596-600.
- [7] W. Yang, P. G. Kazansky, and Y. P. Svirko, *Nat. Photonics*, 2008, 2, 99-104.
- [8] C. Wang, M. Zhang, X. Chen, M. Bertrand, A. Shams-Ansari, S. Chandrasekhar, P. Winzer and M. Loncar, *Nature*, 2018, 562, 101-104.
- [9] A. Guarino, G. Poberaj, D. Rezzonico, R. Degl’Innocenti and P. Günter, *Nat. Photonics*, 2007, 1, 407–410.
- [10] M. H. Dunn and M. Ebrahimzadeh, *Science*, 1999, 286, 1513–1517.
- [11] K. Buse, A. Adibi and D. Psaltis, *Nature*, 1998, 393, 665–668.

- [12] T. Fukuda and H. Hirano, *J. Cryst. Growth*, 1980, 50, 291-298.
- [13] J. Ye, X. Sun, Z. Wu, J. Liu, and Y. An, *J. Alloys Comp.*, 2018, 768, 750-755.
- [14] M. A. Fakhri, E. T. Salim, A. W. Abdulwahhab, U. Hashim and Z. T. Salim, *Optics & Laser Technol.*, 2018, 103, 226-232.
- [15] A. Bartasyte, S. Margueron, T. Baron, S. Oliveri and P. Boulet, *Adv. Mater. Interfaces*, 2017, 4, 1600998.
- [16] A. Dabirian, Y. Kuzminykh, S. Cosmin Sandu, S. Harada, E. Wagner, P. Brodard, G. Benvenuti, S. Rushworth, P. Mural, and P. Hoffmann, *Cryst. Growth Des.*, 2011, 11, 203-209.
- [17] M. Iwai, M. Ohmori, T. Yoshino, S. Yamaguchi, and M. Imaeda, *Jpn. J. Appl. Phys.*, 2004, 43, 8195–8198.
- [18] A. C. Jones and M. L. Hitchman, *Chemical Vapour Deposition: Precursors, Processes, Applications*, Royal Society of Chemistry, Cambridge UK, 2009.
- [19] J. A. Ocón, J. G. Murillo, M. Miki-Yoshida, M. N. Cardoza, and O. E. Contreras-López, *J. Cryst. Growth*, 2014, 408, 64–70.
- [20] M. Nisula, Y. Shindo, H. Koga and M. Karppinen, *Chem. Mater.*, 2015, 27, 6987–6993.
- [21] G. G. Condorelli, G. Malandrino and I. L. Fragalà, *Coord. Chem. Rev.*, 2007, 251, 1931-1950.
- [22] G. Malandrino and I. L. Fragala, *Coord. Chem. Rev.* 2006, 250, 1605-1620.
- [23] G. Malandrino, I. L. Fragala, D. A., Neumayer, C. L. Stern, B. J. Hinds and T. J. Marks, *J. Mater. Chem.*, 1994, 4, 1061-1066.
- [24] M. E. Fragalà, R. G. Toro, P. Rossi, P. Dapporto and G. Malandrino, *Chem. Mater.*, 2009, 21, 2062-2069.
- [25] H. Liu, S. Battiato, A. L. Pellegrino, P. Paoli, P. Rossi, C. Jiménez, G. Malandrino and D. Munoz-Rojas, *Dalton Trans.*, 2017, 46, 10986-10995.

- [26] A. Gulino, P. Dapporto, P. Rossi, G. Anastasi and I. Fragalà, *J. Mater. Chem.*, 2004, 14, 2549-2553.
- [27] G. Malandrino, R. Lo Nigro, C. Benelli, F. Castelli and I. L. Fragalà, *Chem. Vap. Deposition*, 2000, 6, 233-238.
- [28] S. Tanga and H. Zhao, *RSC Adv.*, 2014, 4, 11251-11287.
- [29] S. Battiato, J.L. Deschanvres, H. Roussel, L. Rapenne, B. Doisneau, G. G. Condorelli, D. Munoz-Rojas, C. Jiménez and G. Malandrino, *Dalton Trans.*, 2016, 45, 17833-17842
- [30] S.-T. Zhang, M. Modreanu, H. Roussel, C. Jiménez and J.-L. Deschanvres, *Dalton Trans.*, 2018, 47, 2655-2661.
- [31] D. W. McOwen, S. A. Delp, E. Paillard, C. Herriot, S. D. Han, P. D. Boyle, R. D. Sommer, and W. A. Henderson, *J. Phys. Chem. C*, 2014, 118, 7781–7787
- [32] W. A. Henderson, *J. Phys. Chem. B*, 2006, 110, 13177–13183.
- [33] W. A. Henderson, *Macromolecules*, 2007, 40, 4963–4971.
- [34] CrysAlisPro, Agilent Technologies, 2011
- [35] BRUKER APEX2, Bruker AXS Inc., Madison, Wisconsin, USA, 2012
- [36] CrysAlisPro 1.171.39.46, Rigaku OD, 2018
- [37] BRUKER SAINT, Bruker AXS Inc., Madison, Wisconsin, USA, 2012
- [38] L. Krause, R. Herbst-Irmer, G. M. Sheldrick and D. Stalke, *J. Appl. Cryst.*, 2015, 48, 3-10.
- [39] M. C. Burla, R. Caliendo, M. Camalli, B. Carrozzini, G. L. Cascarano, L. Da Caro, C. Giacovazzo and G. Polidori, R. Spagna, *J. Appl. Cryst.*, 2005, 38, 381-388.
- [40] T. Gruene, H. W. M. Hahn, A. V. Luebben, F. Meilleur and G. M. Sheldrick, *J. Appl. Cryst.*, 2014, 47, 462-466.
- [41] M. Nardelli, *J. Appl. Cryst.*, 1995, 28, 659.
- [42] C. F. Macrae, I. J. Bruno, J. A. Chisholm, P. R. Edgington, P. McCabe, E. Pidcock, E. Rodriguez-Monge, R. Taylor, V. De Streek, P. A. J. Wood, *J. Appl. Cryst.*, 2008, 41, 466-470.

- [43] Addison, A. W.; Rao, T. N.; Reedijk, J.; Van Rijn, J.; Verschoor, G.C. *J. Chem. Soc., Dalton Trans.* 1984, 1349-.
- [44] Groom, C. R.; Bruno, I. J.; Lightfoot, M. P.; Ward, S. C. *Acta Crystallogr., Sect. B: Struct. Sci., Cryst. Eng. Mater.* 2016, 72, 171–179.
- [45] Malandrino, G.; Borzì, A.M Castelli, F.;Fragalà, I.L.; Dastrù, W.; Gobetto, R.; Rossi, P.; Dapporto, P. *Dalton Trans.* 2003, 369-364.
- [46] Tsymbarenko, D.M.; Makarevich, A.M.; Shchukin, A.E.; Malkerova, I.P.; Alikhanyan, A.S.; Kuzmina, N.P., *Polyhedron* 2017, 134, 246-356.
- [47] Darr, J.A.; Poliakov, M.; Blake, A.B.; Li, W.-S., *Inorg. Chem.*, 1998, 37, 5491-5496.
- [48] P. A. Slepukhin, N. S. Boltacheva, V. I. Filyakova, V. N. Charushin, *Izv. Akad. Nauk SSSR, Ser. Khim. (Russ.) (Russ. Chem. Bull.)*, 2009, 1195-
- [49] Burla, M.C.; Caliendo, R.; Camalli, M.; Carrozzini, B.; Cascarano, G. L.; Da Caro, L.; Giacovazzo, C.; Polidori, G.; Spagna, R. *J. Appl. Cryst.*, 2005, 38, 381-388.
- [50] E. S. Filatov, I. A. Baidina, I. K. Igumenov, *Zh. Strukt. Khim. (Russ.) (J.Struct.Chem.)*, 2006, 47, 498-
- [51] N. S. Karpenko, V. I. Filyakova, G. G. Aleksandrov, V. N. Charushin, *Zh. Strukt. Khim. (Russ.) (J. Struct. Chem.)*, 2005, 46, 987-
- [52] G. Malandrino, A. M. Borzì, F. Castelli, I. L. Fragalà, W. Dastrù, R. Gobetto, P. Rossi, and Paolo Dapporto, *Dalton Trans.* 2003, 369-374.
- [53] T. Tamura, K. Yoshida, T. Hachida, M. Tsuchiya, M. Nakamura, Y. Kazue, N. Tachikawa, K. Dokko, and M. Watanabe, *Chem. Lett.*, 2010, 39, 753–755.
- [54] K. Yoshida, M. Nakamura, Y. Kazue, N. Tachikawa, S. Tsuzuki, S. Seki, K. Dokko and M. Watanabe, *J. Am. Chem. Soc.*, 2011, 133, 13121–13129.
- [55] N. Tachikawa, K. Yamauchi, E. Takashima, J. W. Park, K. Dokko and M. Watanabe, *Chem. Commun.*, 2011, 47, 8157–8159.
- [56] W. A. Henderson, N. R. Brooks, W. W. Brennessel, and V. G. Young Jr., *Chem. Mater.*, 2003, 15, 4679-4684.

- [57] S. D. Han, S. H. Yun, O. Borodin, D. M. Seo, R. D. Sommer, V. G. Young Jr., and W. A. Henderson *J. Phys. Chem. C*, 2015, 119, 8492–8500.
- [58] W. A. Henderson, N. R. Brooks, and V. G. Young, Jr. *Chem. Mater.*, 2003, 15, 4685-4690.
- [59] P. Johansson, S. P. Gejji, J. Tegenfeldt and J. Lindgren, *Solid State Ionics*, 1996, 86-88, 297–302.
- [60] P. Johansson, J. Tegenfeldt and J. Lindgren, *Polymer*, 1999, 40, 4399–4406.
- [61] S. Mishra and S. Daniele, *Chem. Rev.*, 2015, 115 ,8379-8448.
- [62] E. S. Filatov, P. A. Stabnikov, P.P. Semyannikov, S. V. Trubin and I K. Igumenov, *Russ. J. Coord. Chem.*, 2006, 32, 126-129.
- [63] E. S. Filatov, S. V. Sysoev, L. N. Zelenina, T. P. Chusova, V. A. Logvinenko, P. A. Stabnikov, P. P. Semyannikov and I K. Igumenov, *J. Therm. Anal. Cal.*, 2006, 86, 537-539.

CHAPTER 3

Potassium β -diketonate glyme adducts: Synthesis and Characterization

In the late 1960s, the first report on cyclic polyethers, named crown ethers, was reported by Pedersen.^[1, 2] This pioneering work opened the route to coordination chemistry of alkaline ions to produce salt-polyether complexes relatively stable due to the ion-dipole interaction between the cation and the negatively charged O atoms of the polyether ring.^[3, 4] Being the polyether neutral, an anion is always needed to counterbalance the positive cation charge and produce neutral complexes.^[5, 6]

Among organic ligands, β -diketone is a mono-anion and belongs to the most exploited ligand systems to complex metal ions.^[7, 8, 9] The presence of two oxygen atoms in the diketones offers various metal-organic architectures behaving as bidentate ligands.

Likewise, monoanionic bidentate N,N' of the type β -diketiminates^[10] and aminotroponiminates^[11] and N,O such as azonaphthoxide^[12] are conventionally used ligands in the coordination chemistry of the main group and transition metals.

Another essential issue in the synthesis of an alkali metal complex is the cation's large ionic radius, which requires high coordination numbers. In fact, except for Li^+ , all the alkaline metal ions from Na^+ to Cs^+ have an ionic radius higher than 1 Å, independently from the coordination number.^[13] Thus, the central ion's coordination sphere in the traditional metal β -diketonates is not saturated in the case of s-elements. This results in polymeric or oligomeric structures with low volatility.^[14]

Among alkaline metals, potassium compounds are actively studied for various applications such as precursors for the metal-organic chemical vapor deposition (CVD) processes of the ferroelectric $(\text{K}, \text{Na})\text{NbO}_3$ ^[15], the atomic layer deposition (ALD) of potassium oxide^[16], sol-gel processes to produce hybrid organic-inorganic materials^[17] and in catalytic processes such as the ring-opening polymerization.^[18, 19]

Potassium ion has a large ionic radius ($r_{6\text{-coord}} = 1.51 \text{ \AA}$), [Shannon], which is responsible for interesting coordination moieties giving rise in the coordinating ligands' function to fancy oligomeric or polymeric network.^[20, 21, 22]

The formation of mixed ligand complexes $M^{m+}(\beta\text{-dik})_m Q_n$ (where $\beta\text{-dik}$ = pentane-2,4-dionate (acac⁻), 2,2,6,6-tetramethylpentane-3,5-dionate (thd⁻); Q = 1,10-phenanthroline (phen), 2,2'-bipyridyl (bipy)) with neutral ligands was successfully carried out for alkaline-earth and rare earth elements to saturate the coordination sphere and to attain the volatile compounds with molecular structure.^[10, 11]

Former studies have shown that glymes play a crucial role in stabilizing complexes of alkaline-earth,^[23, 24, 25, 26, 27] transition^[28, 29] and rare-earth metals^[30, 31] through oxygen-ion complexation. We have recently devoted our attention to alkaline metals, namely Li^[32] and Na.^[33] We have thus reported the synthesis and the crystal structures of Lithium β -diketonate complexes with a polymeric, $[\text{Li}(\text{hfa})]_{12} \cdot \text{monoglyme} \cdot 4\text{H}_2\text{O}]_n$, and a dimer, $[\text{Li}(\text{hfa})]_2 \cdot \text{diglyme} \cdot 2\text{H}_2\text{O}$, structure.^[32] Concerning Na, a novel monomeric complex of the type, $\text{Na}(\text{hfa}) \cdot \text{tetraglyme}$,^[33] has been synthesized and applied to the sol-gel processes of the NaYF_4 phase.^[34] An analogous coordination architecture for Na has been observed in the heterobinuclear Na-RE (RE = Y and Gd) complexes of formula $[\text{RE}(\text{hfa})_4][\text{Na} \cdot \text{tetraglyme}]$.^[35]

Here, we report on the synthesis of novel potassium complexes of the type " $\text{K}(\text{hfa}) \cdot \text{glyme}$ ", [$\text{Hhfa} = 1,1,1,5,5,5\text{-hexafluoro-2,4-pentanedione}$, glyme = monoglyme (1,2-Dimethoxyethane), diglyme (bis(2-methoxyethyl)ether), triglyme (2,5,8,11-tetraoxadodecane) and tetraglyme (2,5,8,11,14-pentaoxapentadecane)], with glymes performing like crown ethers in terms of coordinating/solvating ions, i.e. in terms of chelating properties.^[36] Single crystal X-ray diffraction experiments provide evidence of interesting coordination moieties. They have also been characterized by FT-IR spectroscopy, ^1H , and ^{13}C NMR.

3.1 Experimental Section

Materials. The potassium hydroxide [KOH, >98%] and 1,1,1,5,5,5-hexafluoro-2,4-pentanedione (H-hfa, >98%), were purchased from Strem Chemicals and used as received.

Monoglyme (1,2-Dimethoxyethane, 99.5%), diglyme (bis(2-methoxyethyl)ether, 99.5%), triglyme (2,5,8,11-tetraoxadodecane, >98%), tetraglyme (2,5,8,11,14-pentaoxapentadecane, >99%), dichloromethane (CH₂Cl₂, >99.5%) and n-pentane were purchased from Sigma Aldrich.

General procedures. Fourier Transform Infrared (FT-IR) spectra were recorded using a Jasco FT/IR-430 spectrometer with nujol mulls between NaCl plates. Melting points were taken on tiny single crystals using a Kofler hot-stage microscope. Thermogravimetric analyses were made using a Mettler Toledo TGA2 and the STAR^e software. Dynamic thermal analyses were carried out under purified nitrogen flow (50 sccm) at atmospheric pressure with a 5 °C min⁻¹ heating rate. The weights of the samples were between 7–10 mg. Differential scanning calorimetry analyses were carried out using a Mettler Toledo Star System DSC 3 under purified nitrogen flow (30 sccm) at atmospheric pressure with a 5 °C/min heating rate. The weights of the samples were between 5-8 mg. NMR tests were carried out at 27 °C using a 500 MHz spectrometer (¹H at 499.88 MHz, ¹³C NMR at 125.7 MHz) furnished with a pulse-field gradient module (Z-axis) and a tunable 5mm Varian inverse detection probe (ID-PFG); chemical shifts (δ) are stated in ppm and are referenced to residual deuterated solvent. NMR data were administered using the MestReC software.

Synthesis of [K(hfa)]₃•monoglyme] (1). The K(OH) (0.515 g, 9.18 mmol) 30% excess was first suspended in dichloromethane (40 mL) followed by monoglyme (0.636 g, 7.06 mmol), and finally, Hhfa (1.47 g, 7.06 mmol) was added after 10 min, and the mixture was refluxed under stirring for 1 h. The excess of KOH was filtered off. The colorless crystals precipitated after partial evaporation of the solvent. The crystals were collected, washed with pentane, filtered, and dried under vacuum. The reaction yield was 80%. The crude product did not melt up to 220 °C using the Kofler hot-stage microscope (760 Torr).

Synthesis of [K(hfa)]₂•diglyme] (2). The K(OH) (0.515 g, 9.18 mmol) 30% excess was first suspended in dichloromethane (40 mL) followed by diglyme (0.636 g, 7.06 mmol), and finally, Hhfa (1.47 g, 7.06 mmol) was added after 10 min, and the mixture was refluxed under stirring for 1 h. The excess of KOH was filtered off. The colorless crystals precipitated after partial evaporation of the solvent. The crystals were collected, washed with pentane,

filtered, and dried under vacuum. The reaction yield was 86%. The melting point of the crude product was 80-82°C (760 Torr).

Synthesis of K(hfa)•triglyme•H₂O (3). The K(OH) (0.515 g, 9.18 mmol) 30% excess was first suspended in dichloromethane (40 mL) followed by triglyme (1.25 g, 7.06 mmol), and finally, Hhfa (1.47 g, 7.06 mmol) was added after 10 min, and the mixture was refluxed under stirring for 1 h. The excess of KOH was filtered off. The obtained product did not crystallize and is liquid.

Synthesis of [K(hfa)]₄•tetraglyme (4). The K(OH) (0.515 g, 9.18 mmol) 30% excess was first suspended in dichloromethane (40 mL) followed by tetraglyme (1.57 g, 7.06 mmol), and finally, Hhfa (1.47 g, 7.06 mmol) was added after 10 min, and the mixture was refluxed under stirring for 1 h. The excess of KOH was filtered off. The crystals were collected, washed with pentane, filtered, and dried under vacuum. The reaction yield was 91%. The crude product melts at 52°C using the Kofler hot-stage microscope (760 Torr).

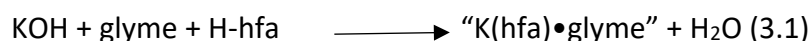
Single crystal X-ray structure. Complexes **1** and **2** intensity data were accumulated at 100 K by using a Bruker Apex-II CCD diffractometer. Information was collected with the Bruker APEX2 program^[37] and integrated and reduced with the Bruker SAINT software^[38]; absorption correction was performed with SADABS-2016/2.^[39] radiations used were Cu-K α ($\lambda = 1.54184 \text{ \AA}$) for [K(hfa)]₃•(monoglyme) (**1**) and Mo-K α radiation ($\lambda = 0.71073 \text{ \AA}$) for [K(hfa)]₂•(diglyme) (**2**). Measurements for [K(hfa)]₄•(tetraglyme) (**4**) were carried out with an Oxford Diffraction Excalibur diffractometer; the temperature was set to 100 K, and the Cu-K α radiation ($\lambda = 1.54184 \text{ \AA}$) was used. Data collection and data reduction were performed with the program CrysAlisPro^[40]; absorption correction was performed with the program ABSPACK implemented in CrysAlisPro. All the crystal structures were solved using the SIR-2004 package^[41] and refined by full-matrix least-squares against F^2 using all data (SHELXL-2018/3^[42]).

In all three structures, all non-hydrogen atoms were refined with anisotropic displacement parameters. All the hydrogen atoms of structures **1** and **4** were found in the Fourier difference map. Their coordinates were freely refined while their thermal parameters were set following one of the atoms to which they are bonded. In structure **2** the hydrogen atoms

were introduced in an idealized position, and their coordinates and thermal parameters were refined in agreement to those of the atom to which they are bonded. Geometrical calculations were performed by PARST97^[43], and molecular plots were produced by the program Mercury (v4.3.1)^[44] and Discovery Studio Visualizer 2019.^[45]

3.2 Results & Discussions

The complexes are synthesized in a single-step reaction from the potassium hydroxide, Hhfa, and glyme ligands in dichloromethane. A KOH:Hhfa: glyme stoichiometry of 1:1:1 was used for all the reactions. The mixture was refluxed under stirring for 1 hour (Eq. (3.1)). Adducts **5**, **6**, and **8** are solid, while **7** is a colorless liquid at room temperature



5. [K(hfa)]₃•monoglyme
6. [K(hfa)]₂•diglyme
7. K(hfa)•triglyme•H₂O
8. [K(hfa)]₄•tetraglyme

The structures of **5**, **6**, and **8** have been defined through single-crystal X-ray diffraction data. In fig. 3.1, ORTEP-3 representations of the asymmetric unit of the three compounds, **5**, **6**, and **8**, are reported. Crystallographic data and refinement parameters are reported in Table 3.1.

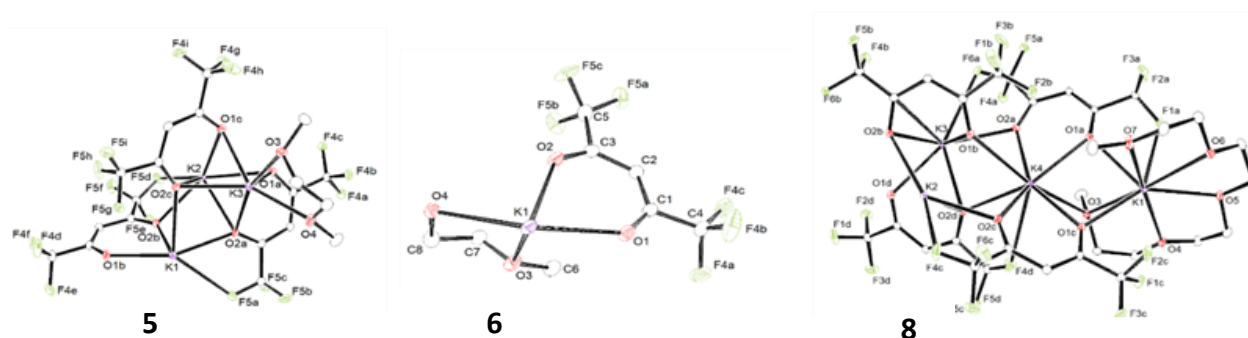


Fig. 3.1. ORTEP view of the asymmetric unit of **5**, **6**, and **8**. For the sake of clarity, hydrogen was not introduced, and labels were added just for non-carbon atoms. (Ellipsoid probability = 20%)

Table 3.1. Crystallographic data and refinement parameters for compounds **5**, **6**, and **8**.

	5	6	8
Formula	C ₁₉ H ₁₃ F ₁₈ K ₃ O ₈	C ₁₆ H ₁₆ F ₁₂ K ₂ O ₇	C ₃₀ H ₂₆ F ₂₄ K ₄ O ₁₃
M	828.59	626.49	1206.91
T (K)	100	100	100
λ (Å)	1.54184	0.71073	1.54184
Crystal system, space group	Monoclinic, P2 ₁ /n	Monoclinic, C2/c	Triclinic, P-1
Unit cell dimensions (Å, °)	a = 11.83(1) b = 13.685(1); β = 99.104(4) c = 19.326(2)	a = 19.3273(9) b = 8.5690(3); β = 94.628(3) c = 15.2927(6)	a = 9.6660(2); α = 81.103(2) b = 12.2845(3); β = 80.523(2) c = 20.2205(5); γ = 82.429(2)
V (Å ³)	3088(3)	2524.5(2)	2301.89(9)
Z, ρ (mg/cm ³)	4, 1.782	4, 1.648	2, 1.723
μ (mm ⁻¹)	5.351	0.497	4.834
F(000)	1640	1256	1204
Crystal size	0.20 X 0.22 X 0.27	0.20 x 0.22 x 0.25	0.24 x 0.27 x 0.33
2 θ range (°)	7.95 – 160.14	4.23 – 53.43	8.06 – 141.86
Reflns collected /	17482 / 6372	10849 / 2679 (0.0893)	32890 / 8621

unique (R_{int})	(0.0456)		(0.0297)
Data / parameters	6372 / 433	2679 / 168	8621 / 640
Final R indices [$I > 2\sigma$]	R1 = 0.497, wR2 = 0.1347	R1 = 0.509, wR2 = 0.1381	R1 = 0.297, wR2 = 0.0743
R indices (all data)	R1 = 0.0600, wR2 = 0.1432	R1 = 0.650, wR2 = 0.1495	R1 = 0.0356, wR2 = 0.0782
GoF	1.097	1.055	1.061

In all the three investigated potassium complexes, due to bridging μ^2 and μ^3 oxygen atoms, 1D polymers are formed. In **5**, they are directed along the b axis, while in **6** and **8**, the propagation directions are along with the c and a axis, respectively (Figures 3.2-3.4). No strong interactions connecting the polymer chains are present (see Fig. 3.5-3.7).

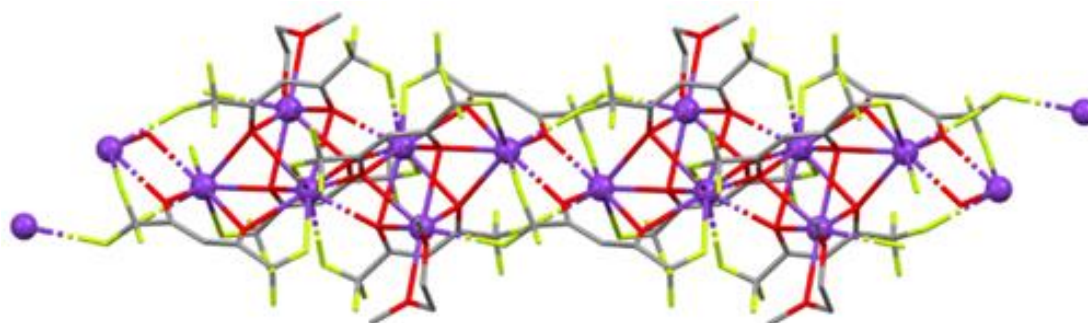


Fig. 3.2. **5** 1D polymer (view along the ac plane diagonal).

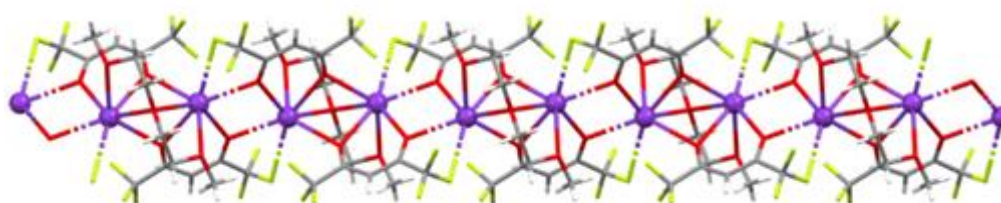


Fig. 3.3. **6** 1D polymer (view along the b axis direction).

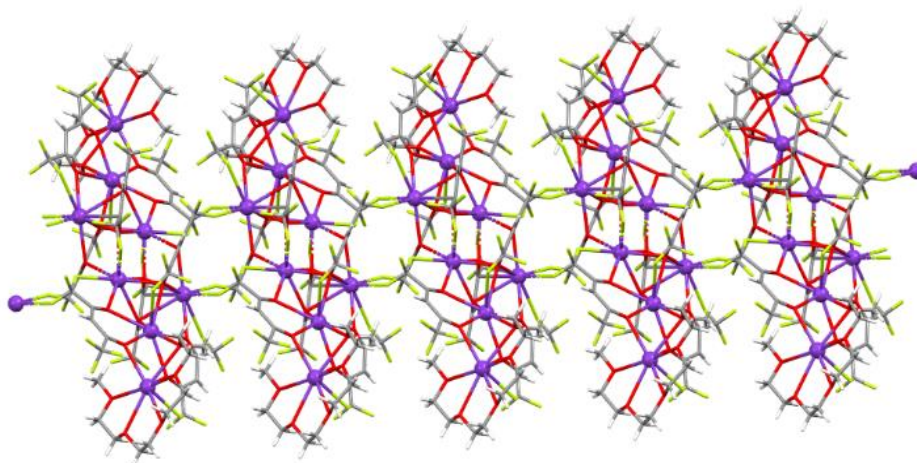


Fig. 3.4. 8 1D polymer (view along the b axis direction).

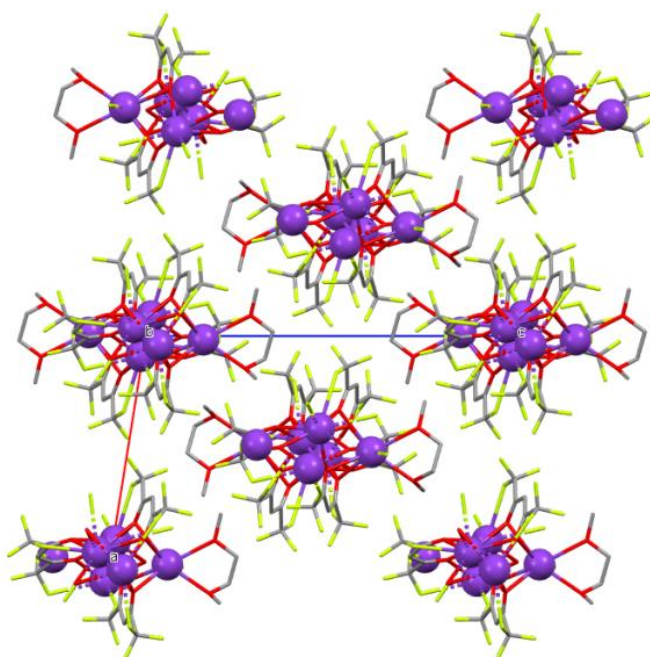


Fig. 3.5. Crystal packing of **5**.

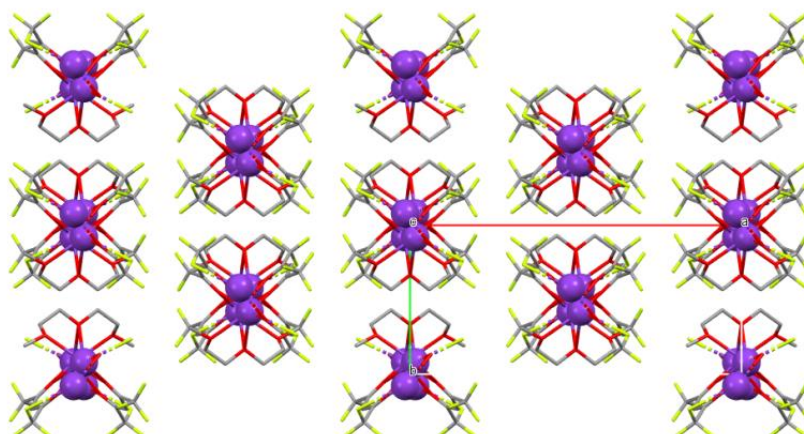


Fig.3.6. Crystal packing of **6**.

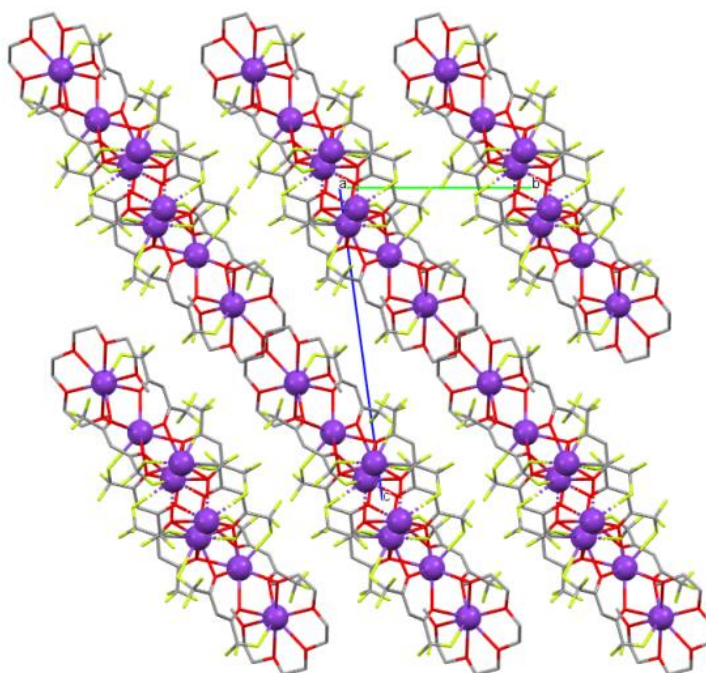


Fig. 3.7. Crystal packing of **8**.

Concerning the disposition of the potassium cation inside the polymer chains, while in **5** and **8** a sort of ladder is present, whose steps are formed by six and eight potassium ions, respectively (see fig. 3.8), in **6**, the metal cations take a more linear disposition (see fig. 3.8).

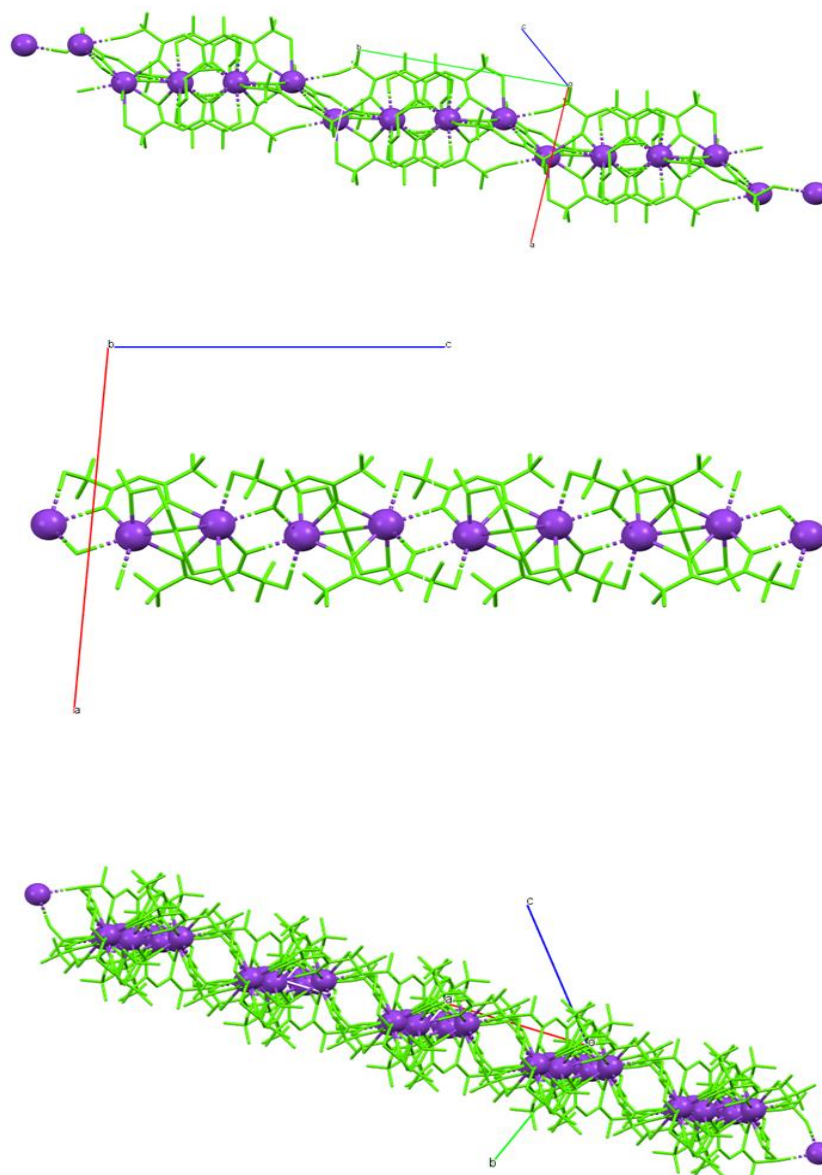


Fig. 3.8. Potassium cations disposition inside the 1D polymer chain in **5** (top), **6** (middle) and **8** (bottom).

In particular, **5** crystallizes in the monoclinic crystal system, P21/n space group, in its asymmetric unit, the $[K(hfa)]_3 \cdot (\text{monoglyme})$ unit is present (see fig. 3.1).

The three potassium cations, K1, K2, and K3, show a different coordination number. In all cases, their coordination spheres are completed by fluorine atoms of a CF_3 moiety (see

Table A.3). More in detail, K1 and K2 are coordinated by five hfa anions giving rise to a octa- and deca-coordinated environment (see fig. 3.9).

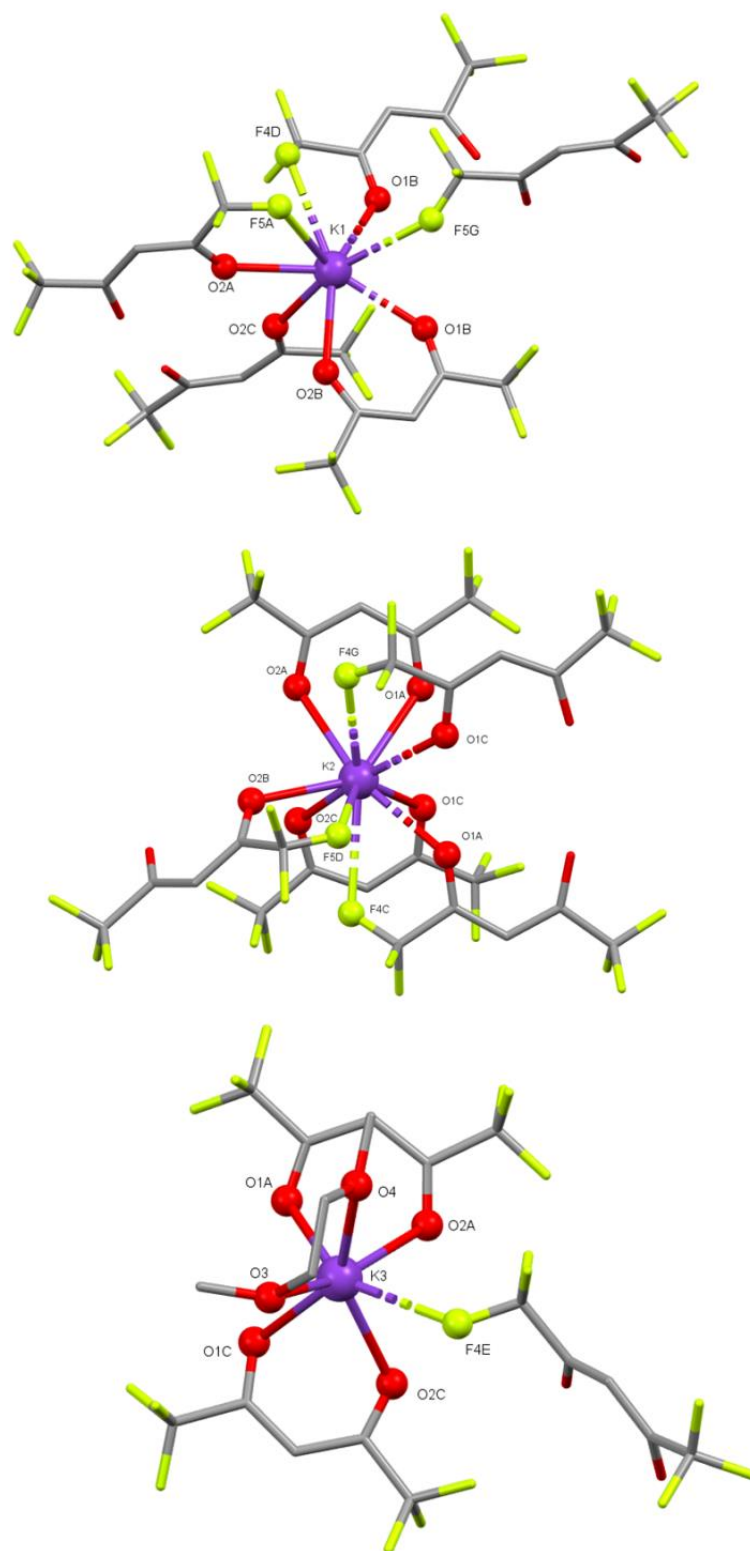


Fig. 3.9. Coordination sphere around K1, K2, and K3 in **5**.

Finally, K3 is coordinated by three hfa anions and one monoglyme molecule; the resulting coordination is the hepta one. All the hfa anions' oxygen atoms act as bridging donor atoms, while the monoglyme oxygen atoms bind just one potassium cation (K3).

Also, **6** crystallizes in the monoclinic crystal system, but this time the space group is C2/c. In this case, the asymmetric unit is more straightforward than that observed in **5**, and just one $[K(hfa)]_{0.5}(\text{diglyme})$ unit is present. The potassium cation K1 is hepta-coordinated by three hfa anion and one diglyme molecule (see fig 3.10, Table A.4.)

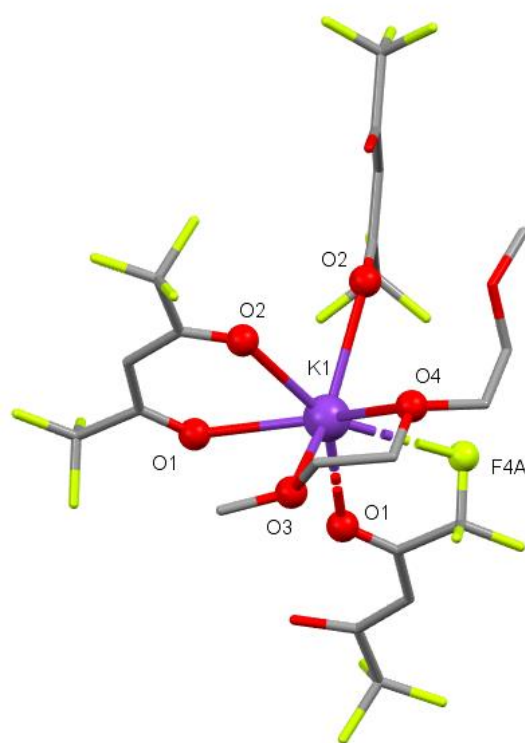


Fig. 3.10. Coordination sphere around K1 in **6**.

The asymmetric unit of **8** (crystal system triclinic, space group P-1) contains the $[K(hfa)]_4(\text{tetraglyme})$ unit. The four potassium cations show different coordination spheres. While K1, K3, and K4 are octa-coordinated (K1 by two oxygen atoms and one fluorine atom of two hfa anion and by five oxygen atoms of a tetraglyme molecule, K3 by five oxygen and three fluorine atoms of four different hfa anions, and K4 by six oxygen and one fluorine atoms of four hfa anions and one oxygen atom of one tetraglyme molecule), K2 is hepta-coordinated by six oxygen and one fluorine atoms of five hfa anion (see fig 3.11, Table A.5.).

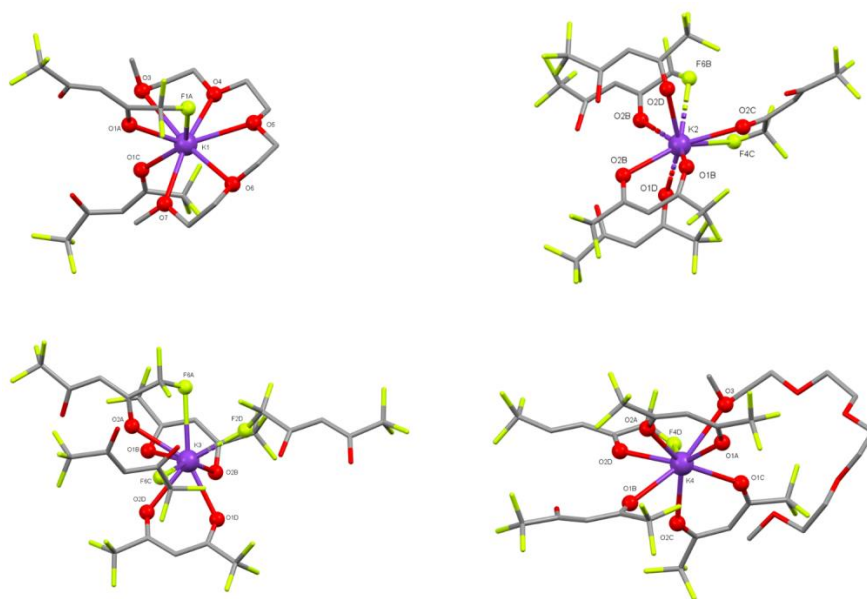


Fig. 3.11. Coordination sphere around K1, K2, K3, and K4 in **8**.

Finally, the Cambridge structural database (CSD, v 5.41, update 2 May 2020)^[46] was used to retrieve potassium similar complexes; just one structure was found containing a related CF₃-β-diketonate ligand (L in the following).^[47] Also, in the KL complex (CSD Refcode = COYPUE), a 1D polymer is formed (see fig. 3.12). The K...K distances observed in **5**, **6**, and **8** are comparable with those published for COYPUE (K...K distances range = 3.552-4.246 Å).

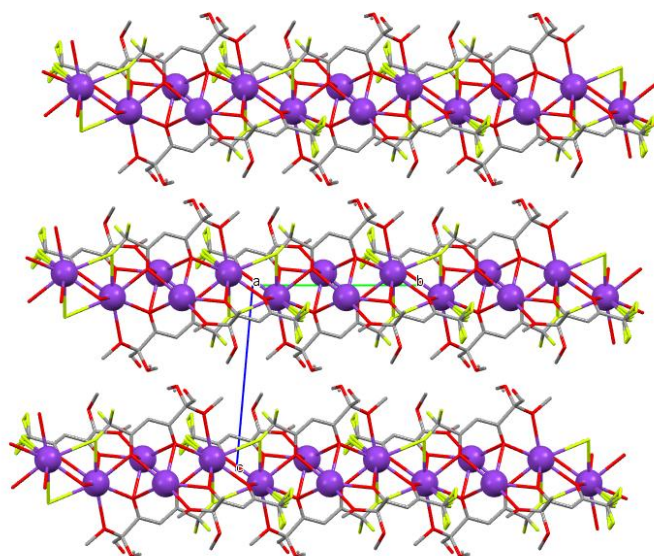


Fig. 3.12. Crystal packing of COYPUE (view along the a-axis).

FTIR – Spectroscopy: The FT-IR spectra of all the adducts **5-8** are reported in Fig. 3.13. The absence of bands around 3500-3600 cm^{-1} in the spectra of **5**, **6**, and **8**, related to O-H's stretching, indicates the lack of water molecules in the metal coordination sphere of **5**, **6**, and **8**. Comparing the FT-IR spectra of all the four adducts and that of the free H-hfa ligand in the carbonyl range, it is possible to observe that the two peaks at about 1660 cm^{-1} and 1530 cm^{-1} , associated respectively with the C=O and C=C stretching, are indicative of the hfa ligand coordination.

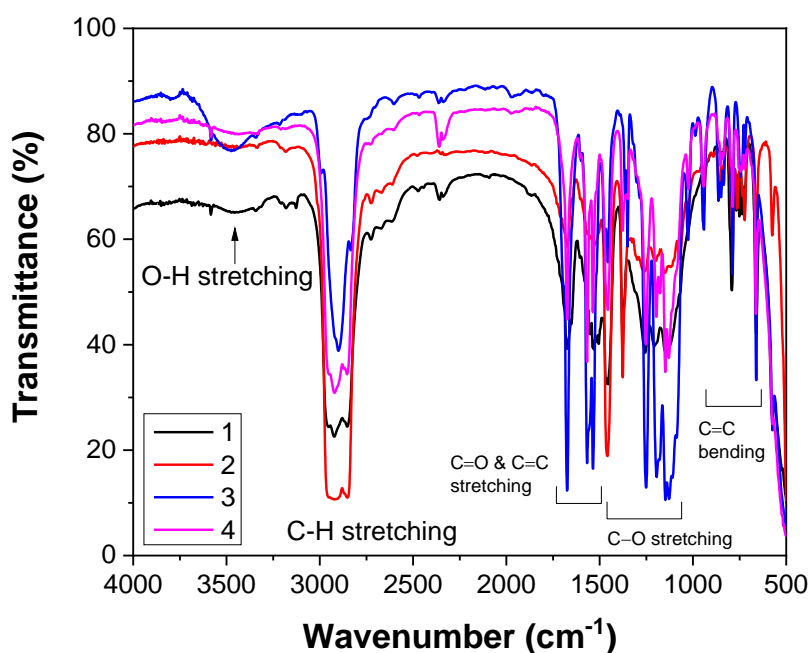


Fig. 3.13. FT-IR spectra of adducts **5**, **6**, **7** and **8**

The bands around 1350-1250 cm^{-1} are due to the overlap of the vibration of stretching and/or bending of the C-O bond with the stretching of the C-F bond. The spectrum shows, around 863 cm^{-1} and 1017 cm^{-1} , signals that can be considered fingerprints of the glyme coordinated to the hexafluoroacetylacetonate potassium system. Adduct **7**, carried out on the neat liquid sample, shows bands around 3500 cm^{-1} which is indicative of the presence of water molecules due to metal coordination or impurities not eliminated as being in the liquid state at room temperature. The shift of the signals related to the stretching of the C=O and C=C at 1675 cm^{-1} and 1565 cm^{-1} , and those characteristics of the free ligand were observed at 1690 cm^{-1} and 1630 cm^{-1} dispels any doubts about the liquid nature of the

obtained product. The coordination of triglyme (fig. 3.14) is confirmed by the presence of the band at 2900 cm^{-1} , due to the C-H stretching of the polyether, and of the peaks at 855 cm^{-1} and 1026 cm^{-1} , signals that can be considered as fingerprints of triglyme coordination to the hexafluoroacetylacetonate potassium system.

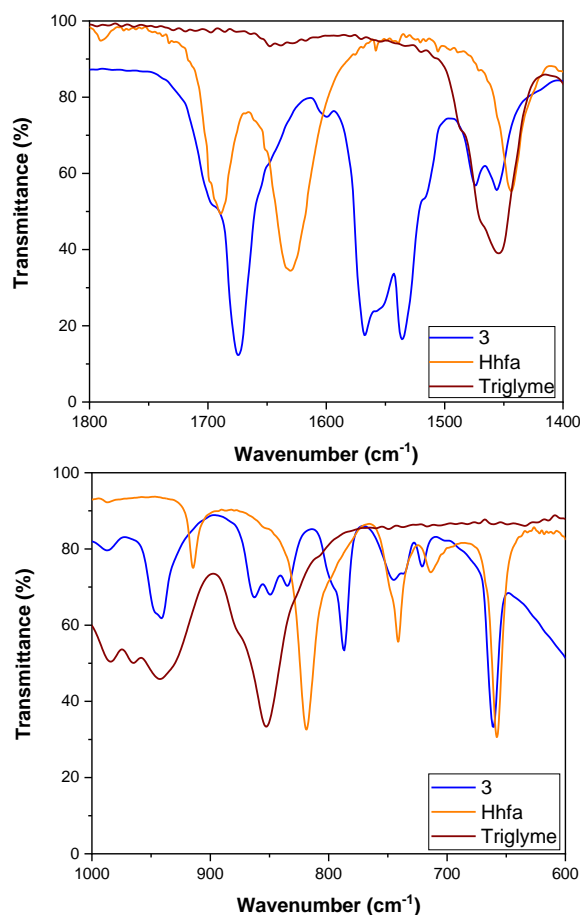


Fig. 3.14. FT-IR spectra of the compound **3**: **a)** C=O stretching region and **b)** triglyme stretching region.

NMR – Spectroscopy. The ^1H -NMR and ^{13}C -NMR spectra of the K(hfa)-glyme adducts have been carried out dissolving **5** & **6** in CD_3COCD_3 while **3** & **4** in CDCl_3 . All ^1H -NMR spectra (Fig. 3.15 – Fig. 3.18) show at $\delta \approx 3.3\text{--}3.4$ ppm a singlet consistent with the protons of the terminal methyl groups of the glyme ligand, while multiplets at $\delta = 3.4\text{--}3.7$ represent resonances of methylenic protons of the same ligand.

$^1\text{H-NMR}$ measurement was conducted by dissolving the adduct **5** in deuterated acetone as it is insoluble in chloroform. The obtained spectrum (Fig. 3.15a) shows a singlet at $\delta \approx 3.294$ ppm consistent with the protons of the terminal methyl groups of the glyme ligand. At around 3.472 ppm, the signals can be traced back to the CH_2 of monoglyme. At 5.514 ppm, the peak for the only proton of the hfa binder appears. Spectrum $^{13}\text{C-NMR}$ is recorded under decoupling conditions (Fig. 3.15b). At the chemical shift value of 83 ppm, the carbon signal falls into the two ketonic groups of the hfa. Finally, the two quartets at about 119 ppm and 173 ppm can be traced back to the C of the CF_3 and C-O groups of the binder. The quartets are due to coupling with the fluoride atoms of the CF_3 groups.

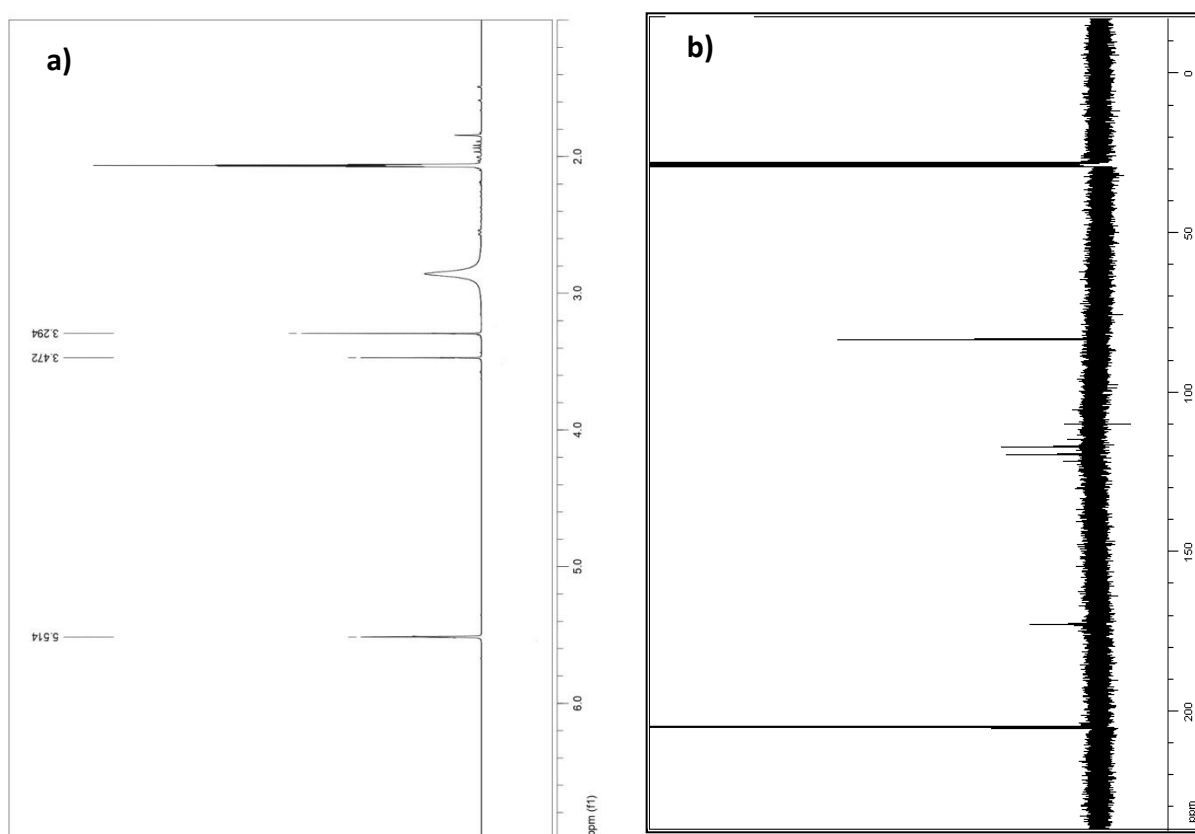


Fig. 3.15. a) $^1\text{H-NMR}$ spectrum of **5** (CD_3COCD_3 , 500 MHz, 27 °C) b) $^{13}\text{C-NMR}$ spectrum of **5** (CD_3COCD_3 , 125 MHz, 27 °C)

The $^1\text{H-NMR}$ spectrum of the adduct **6** was carried out in deuterated acetone (Fig. 3.16a). For adduct **6** in the ppm range of 3.3 ppm to 3.5 ppm, we find signals for the eight methylnic hydrogens of the polyether. At the chemical shift value of 5.514 ppm, the singlet signal of the hydrogen of the "diketonate" binder appears. Spectrum $^{13}\text{C-NMR}$ is recorded under decoupling conditions (Fig. 3.16b). At the chemical shift value of 86 ppm, the carbon signal falls into the two ketonic groups of the hfa. Finally, the two quartets at about 119 ppm and 174 ppm can be traced back to the C of the CF_3 and C-O groups of the binder. The quartets are due to coupling with the fluoride atoms of the CF_3 groups.

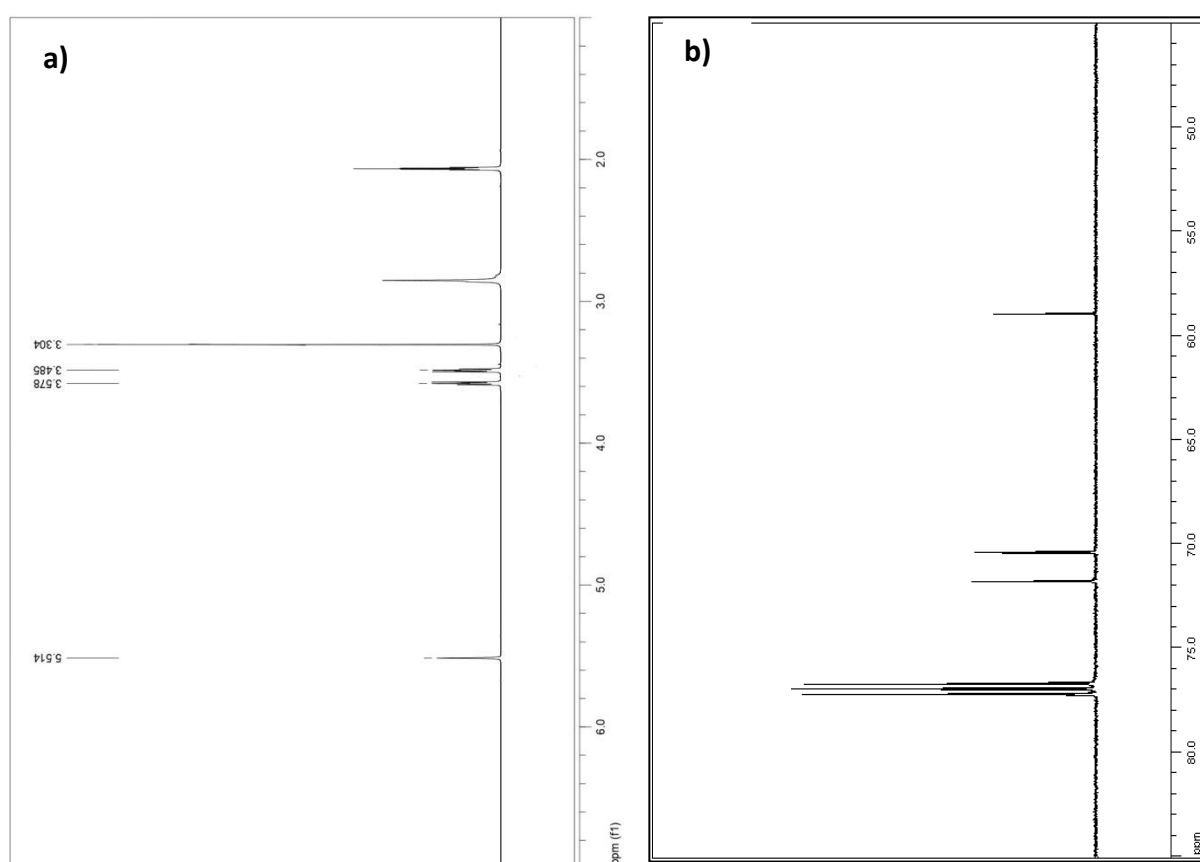


Fig. 3.16. a) $^1\text{H-NMR}$ spectrum of **6** (CD_3COCD_3 , 500 MHz, 27 °C) **b)** $^{13}\text{C-NMR}$ spectrum of **6** (CD_3COCD_3 , 125 MHz, 27 °C)

The $^1\text{H-NMR}$ spectrum of the adduct **7** was carried out in deuterated chloroform (Fig. 3.17a) and presented all the signals related to the resonant protons of the complex in question.

The integration of the intense 3.3 ppm singlet indicates the six equivalent protons of the two terminal methyl groups of the triglyme. In the chemical shift from 3.5 ppm to 3.7 ppm, two multiplets and one singlet can be seen from the polyether's twelve methylenic hydrogens. At 5.9 ppm, we find the singlet relative to the proton compared to the diketone's two carbonyl groups. Spectrum ^{13}C -NMR (Fig. 3.17b) is recorded in decoupling conditions. For a chemical shift value of 58 ppm, the signal for the two methyl carbons of the polyether is observed. Between 69 ppm and 71 ppm, the methylenic C of the triglyme resonates. At 77 ppm, the signal for the deuterated chloroform used as a solvent is observed. Finally, at the value of 85 ppm, the carbon resonates in the two ketonic groups. The two quartets at about 118 ppm and 173 ppm can be traced back to the C of the CF_3 and $\text{C}=\text{O}$ groups, respectively, of the β -diketone. The quartets are due to coupling with the fluoride atoms of the CF_3 groups.

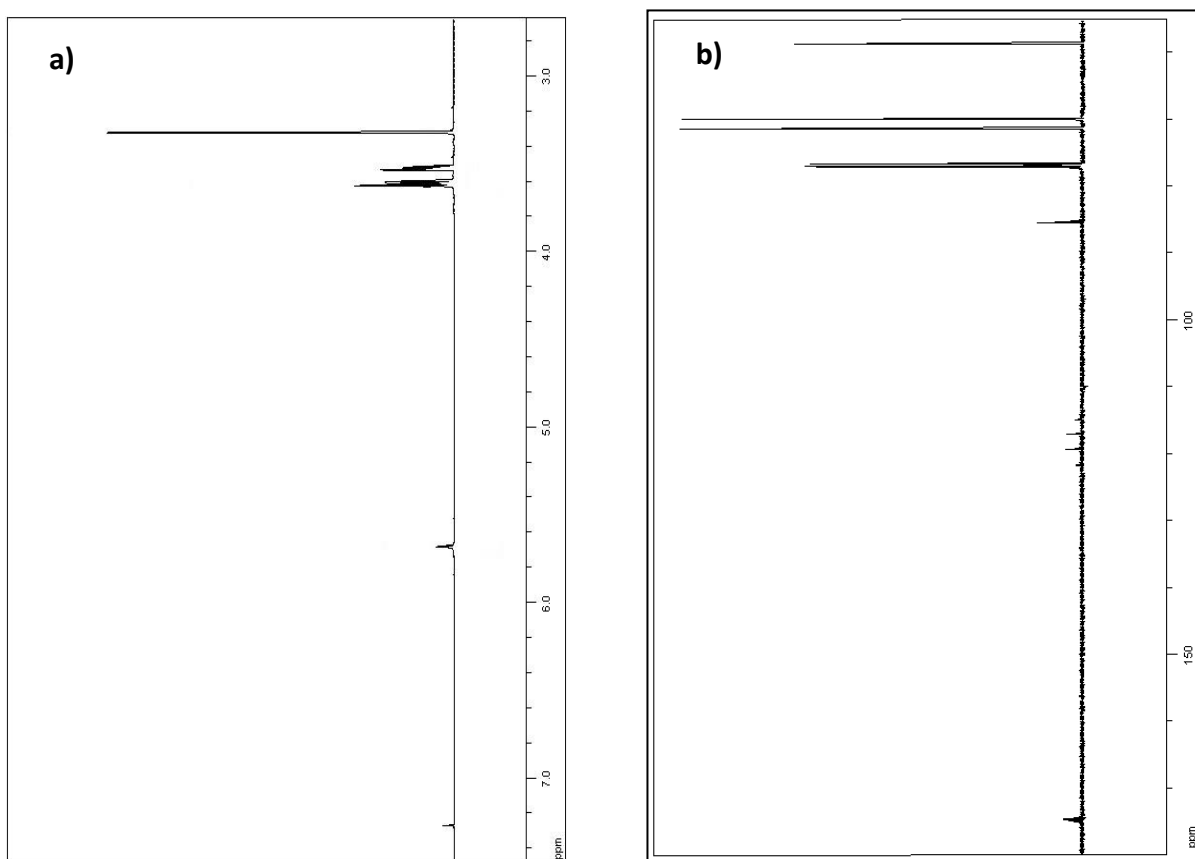


Fig. 3.17. a) ^1H -NMR spectrum of **7** (CDCl_3 , 500 MHz, 27 °C) b) ^{13}C -NMR spectrum of **7** (CDCl_3 , 125 MHz, 27 °C)

The ^1H -NMR spectrum of adduct **8** was carried out in deuterated chloroform (Fig. 3.18a) and showed an intense 3.3 ppm singlet, which relates to the resonance of the six equivalent protons of the two terminal methyl groups of the polyether. Signals ranging from 3.5 ppm to 3.7 ppm can be traced back to the sixteen methylenic protons of tetraglyme. The 5.691 ppm singlet is related to the proton linked to carbon dioxide in the two carbonyl groups of the hfa. Spectrum ^{13}C -NMR (Fig. 3.18b) shows an intense 59 ppm signal, typical of the two methyl C of the tetraglyme. Between 69 ppm and 71 ppm, signals are seen for the eight methylenic C of the polyether. At 77 ppm, the signal from the deuterated chloroform used as a solvent is observed. At the chemical shift value of 86 ppm, the carbon signal falls in the two ketonic groups of the hfa. Finally, the two quartets at about 118 ppm and 174 ppm can be traced back to the C of the CF_3 and $\text{C}=\text{O}$ groups of the binder. The quartets are due to coupling with the fluoride atoms of the CF_3 groups.

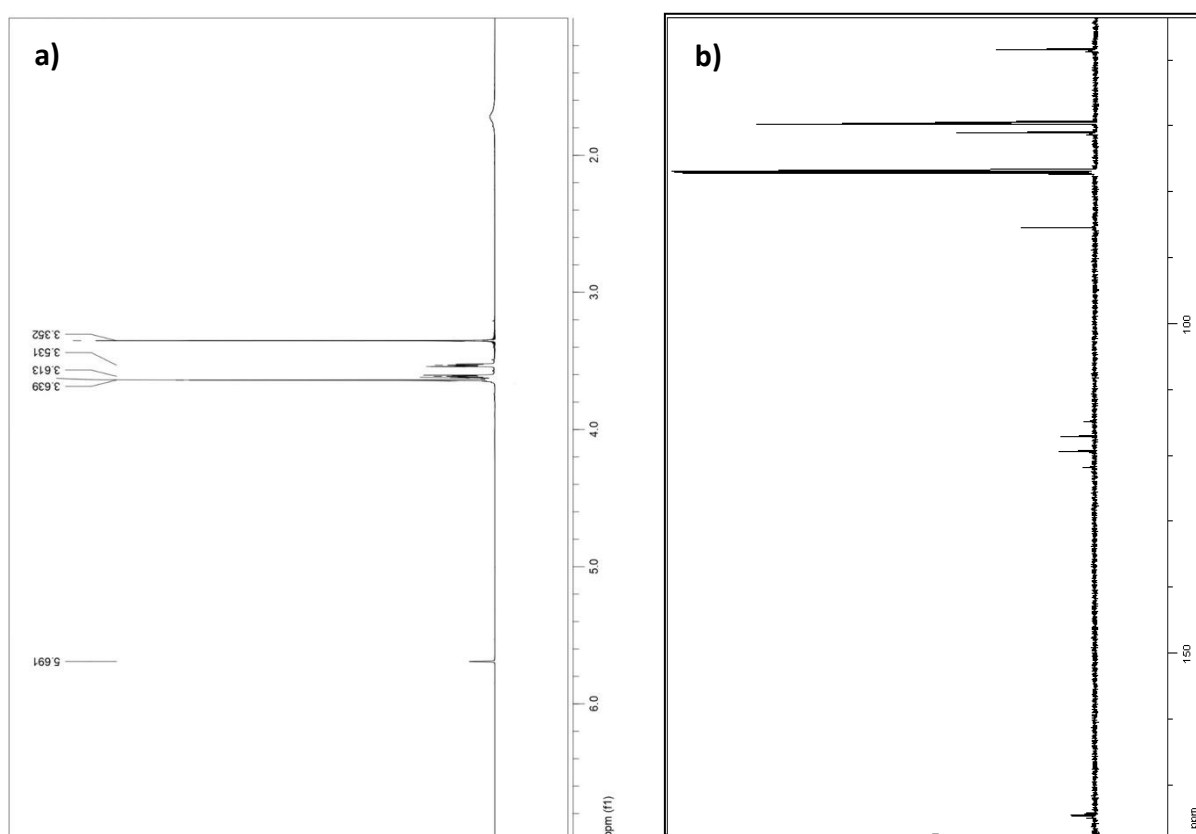


Fig. 3.18. a) ^1H -NMR spectrum of **8** (CDCl_3 , 500 MHz, 27 °C) b) ^{13}C -NMR spectrum of **8** (CDCl_3 , 125 MHz, 27 °C)

Thermal Analysis: The thermal behaviors of the as-synthesized precursors have been investigated by thermogravimetric (TG) measurements (Fig. 3.19a) and differential scanning calorimetry (DSC) (Fig. 3.19b). TG curves of the “K(hfa)•glyme” **6**, **7**, and **8** show a single-step mass loss associated with the clean decomposition of the adducts, while adducts **5** show two-step mass-loss. Adduct **5** shows a weight loss of about 10.2% in the range 25-95°C, which accounts for the loss of the monoglyme of the [K(hfa)]₃•monoglyme polymeric structure, the theoretical weight loss being equal to 10.8%. The primary mass loss due to the clean adduct decomposition occurs in the range 218-271 °C, with a residue of 36.1%, but this is not a drawback for its liquid-assisted MOCVD applications processes, given its solubility in common organic solvents.

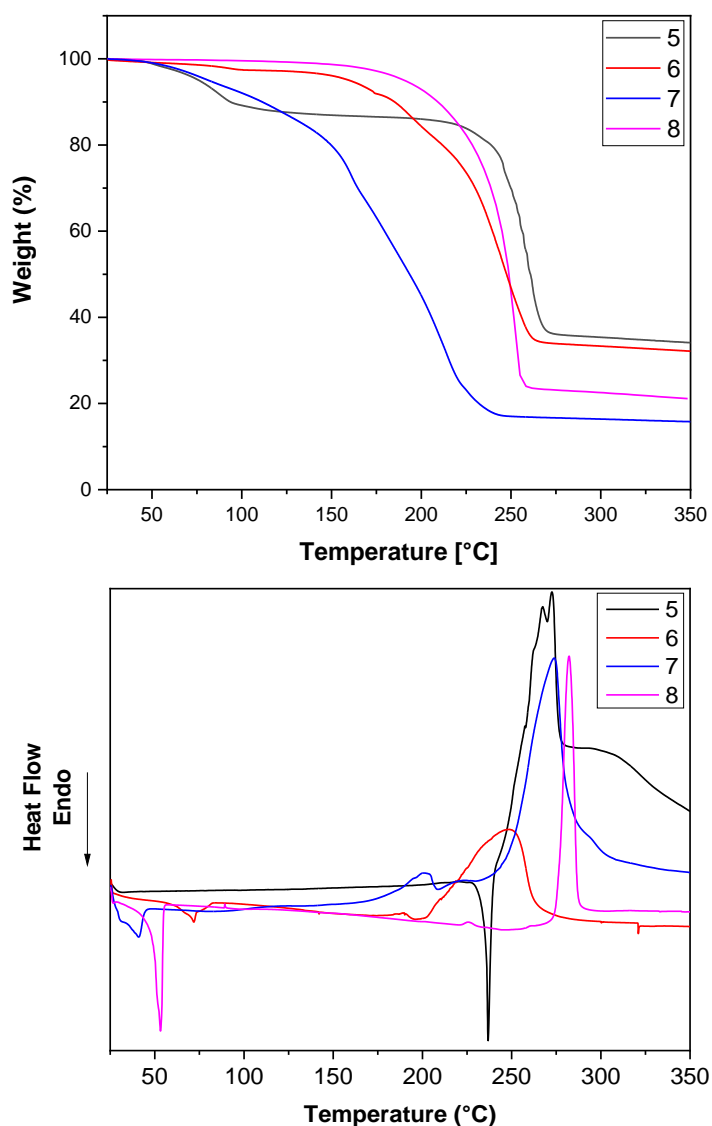


Fig. 3.19. (a) TGA of adducts 5, 6, 7, and 8 and (b) DSC of adducts 5, 6, 7 and 8

The TG curves of adducts **6**, **7**, and **8** show a single step weight loss with a residue of 34.1% at 264 °C, 17.33% at 246.70 °C and 23.5% at 260 °C, respectively.

The DSC curves of adduct **5** show a sharp endothermic peak at 236.9 °C, which may be related to the melting of the polymeric structure. The DSC curve of adduct **6** presents a small endothermic peak at 71.8 °C due to the adduct melting and a broad exothermic peak at 247.6 °C, which can be associated with its decomposition. In contrast, adduct **7** shows the exothermic peaks around 274.3 °C, which may be related to vaporization overlapped with a partial decomposition of the products. In adduct **8**, we observe a sharp endothermic peak at 53.3 °C, indicating the melting of the polymeric structure and a sharp exothermic peak at 282.5 °C, associated with the vaporization of the melt.

3.3 Conclusions

The reported research provides a detailed study on the syntheses of four novel adducts of potassium. In conclusion, a straightforward one-pot nature of the presently reported synthetic route envisages the possibility to efficiently synthesize and produce these precursors on a large scale for industrial applications and to store for longer time as the precursors are stable in air. Various glymes have been used to complete the K ion's coordination sphere, giving rise to volatile compounds by changing the coordination moieties. Functional validation of these precursors has been tested through their applications to sol-gel processes of $K_{0.5}Na_{0.5}NbO_3$ nanostructures.

REFERENCES

- [1] C. J. Pedersen, *J. Am. Chem. Soc.*, 1967, 89, 2495–2496.
- [2] C. J. Pedersen, *J. Am. Chem. Soc.*, 1967, 89, 7017–7036.
- [3] Z. Liu, S. K. M. Nalluri and J. Fraser Stoddart, *Chem. Soc. Rev.*, 2017, 46, 2459–2478.
- [4] L. Fabbrizzi, *ChemTexts*, 2020, 6, 10.

- [5] G. Tripathi, G. Ramanathan, *J. Molecular Structure*, 2018, 1156, 273-279.
- [6] Z. Dong, M. Schmidtman, and T. Meller, *Chem. Eur. J.*, 2019, 25, 10858 – 10865.
- [7] R. C. Mehrotra, *Pure Appl. Chem.*, 1988, 8, 60
- [8] P. A. Vigato, V. Peruzzo, S. Tamburini, *Coord. Chem. Rev.*, 2009, 253, 1099–1201.
- [9] S. Mishra and S. Daniele, *Chem. Soc. Rev.*, 2015, 115, 8379–8448.
- [10] Y. C. Tsai, *Coord. Chem. Rev.*, 2012, 256, 722– 758.
- [11] A. Hanft and C. Lichtenberg, *Organometallics*, 2018, 37, 1781–1787.
- [12] C. Gallegos, V. Taberner, M. E. G. Mosquera, T. Cuenca, and J. Cano, *Eur. J. Inorg. Chem.*, 2015, 5124-5132.
- [13] R.D. Shannon, *Acta Crystallogr.* 32, 751–767 (1976).
- [14] K. Kaiser, C. Ganesamoorthy, C. Wölper, and S. Schulz, *Z. Anorg. Allg. Chem.*, 2020, 681–691.
- [15] D. Tsybarenko, I. Korsakov, A. Mankevich, G. Girichev, E. Pelevina and A. Kaul, *ECS Trans.*, 2009, 25, 633-638.
- [16] E. Østreg, H. H. Sønsteby, S. Øien, O. Nilsena and H. Fjellvåga, *Dalton Trans.*, 2014, 43, 16666.
- [17] G. Dubois, C. Reye, R. J. P. Corriu and C. Chuit, *J. Mater. Chem.*, 2000, 10, 1091-1098.
- [18] Y. Sun, J. Xiong, Z. Dai, X. Pan, N. Tang, and J. Wu, *Inorg. Chem.*, 2016, 55, 136–143.
- [19] F. M. García-Valle, M. T. Muñoz, T. Cuenca, S. Milione, M. E.G. Mosquera, and J. Cano, *J. Organomet. Chem.*, 2019, 898, 120854.
- [20] S. Kim, I. H. Park, S. S. Lee, W. Sim, and J. Y. Lee, *CrystEngComm.*, 2020, 22, 5601.
- [21] P. Liebing, and K. Merzweiler, *Z. Anorg. Allg. Chem.*, 2015, 641, 1911–1917.
- [22] R. K. Kottalanka, A. Harinath, S. Rej and T. K. Panda, *Dalton Trans.*, 2015, 44, 19865–19879.

- [23] G. G. Condorelli, G. Malandrino and I. L. Fragalà, *Coord. Chem. Rev.*, 2007, 251, 1931-1950.
- [24] M. E. Fragalà, R. G. Toro, P. Rossi, P. Dapporto and G. Malandrino, *Chem. Mater.*, 2009, 21, 2062-2069.
- [25] G. Malandrino, I. L. Fragalà, D. A. Neumayer, C. L. Stern, B. J. Hinds and T. J. Marks, *J. Mater. Chem.*, 1994, 4, 1061-1066.
- [26] D. M. Tsymbarenko, A. M. Makarevich, A. E. Shchukin, I. P. Malkerova, A. S. Alikhanyan, N. P. Kuzmina, *Polyhedron*, 2017, 134, 246–256.
- [27] N. P. Kuzmina, D. M. Tsymbarenko, I. E. Korsakov, Z. A. Starikova, K. A. Lysenko, O. V. Boytsova, A. V. Mironov, I. P. Malkerova, A. S. Alikhanyan, *Polyhedron*, 2008, 27, 2811–2818.
- [28] H. Liu, S. Battiato, A. L. Pellegrino, P. Paoli, P. Rossi, C. Jiménez, G. Malandrino and D. Munoz-Rojas, *Dalton Trans.*, 2017, 46, 10986-10995.
- [29] A. Gulino, P. Dapporto, P. Rossi, and I. Fragalà, *Chem. Mater.*, 2003, 15, 3748-3752.
- [30] G. Malandrino and I. L. Fragalà, *Coord. Chem. Rev.*, 2006, 250, 1605-1620.
- [31] R. Lo Nigro, R. G. Toro, G. Malandrino, I. L. Fragalà, P. Rossi and P. Dapporto, *J. Electrochem. Soc.*, 2004, 151, F206.
- [32] N. Peddagopu, P. Rossi, C. Bonaccorso, A. Bartasyte, P. Paoli & G. Malandrino, *Dalton Trans.*, 2020, 49, 1002.
- [33] M. R. Catalano, A. L. Pellegrino, P. Rossi, P. Paoli, P. Cortelletti, M. Pedroni, A. Speghini, G. Malandrino, *New J. Chem.*, 2017, 41, 4771–4775.
- [34] A. L. Pellegrino, M. R. Catalano, P. Cortelletti, G. Lucchini, A. Speghini, G. Malandrino, *Photochem. Photobiol. Sci.*, 2018, 17, 1239.
- [35] S. Battiato, P. Rossi, P. Paoli, G. Malandrino, *Inorg. Chem.*, 2018, 57, 15035–15039.
- [36] S. Tanga and H. Zhao, *RSC Adv.*, 2014, 4, 11251.
- [37] Bruker (2012). Bruker APEX2. Bruker AXS Inc., Madison, Wisconsin, USA.

- [38] Bruker (2012). Bruker SAINT. Bruker AXS Inc., Madison, Wisconsin, USA.
- [39] Krause, L.; Herbst-Irmer, R.; Sheldrick G.M.; Stalke D. *J. Appl. Cryst.*, 2015, 48, 3-10.
- [40] CrysAlisPro, Version 1.171.34.44, Rigaku OD, 2010.
- [41] Burla, M. C.; Caliendo, R.; Camalli, M.; Carrozzini, B.; Cascarano, G. L.; Da Caro, L.; Giacovazzo, C.; Polidori, G.; Spagna, R., *J. Appl. Crystallogr.*, 2005, 38, 381-388.
- [42] Sheldrick, G. M. *Acta Crystallogr., Sect. C: Struct. Chem.*, 2015, 71, 3-8.
- [43] M. Nardelli *J. Appl. Crystallogr.* 1995, 28, 659.
- [44] C. F. Macrae, I. J. Bruno, J. A. Chisholm, P. R. Edgington, P. McCabe, E. Pidcock, E. Rodriguez-Monge, R. Taylor, J. van de Streek, P. A. Wood *J. Appl. Crystallogr.* 2008, 41, 466-470.
- [45] Dassault Systèmes BIOVIA, Discovery Visualizer, v19.1.0.18287 (2019), San Diego: Dassault Systèmes.
- [46] C. R. Groom, I. J. Bruno, M. P. Lightfoot, and S. C. Ward, *Acta Cryst.*, 2016, B72, 171-179.
- [47] Kudyakova, Y. S.; Slepukhin, P. A.; Valova, M. S.; Burgart, Y. V.; Saloutin, V. I.; Bazhin, D. N. *Eur. J. Inorg. Chem.*, 2020, 523-531.

CHAPTER 4

Sodium β -diketonate glyme adducts: Synthesis and Characterization

Metal β -diketonates $M(\text{RCOCHCOR})_n$ (R, alkyl; aryl, etc.) are the focal point in the study of coordination compounds. Their chemistry has been explored for most of the metals in the periodic table.^[1] Many publications have also been reported on the ligand's coordination tendencies (i.e., to form chelates with the metal and delocalize the negative charge over a 'metallocycle').^[2,3] The variations in the R group often influence the properties of this class of compound. Other than the bonding and structural features associated with these complexes, the ligands' ability to complete various metals' coordination spheres has provided inorganic chemists with examples of compounds of electropositive metal ions, which represent covalent characteristics, i.e., solubilities in organic solvents and high volatilities. These unique characteristics have been comprehensively exploited in the past for solvent extraction and gas-liquid chromatographic techniques.^[4,5]

Metal β -diketonate complexes also attract attention because of their application as contact shift reagents for the enhanced resolution of non-magnetic resonance (NMR) spectra laser technology and the polymer industry.^[1] The existence of trace quantities of β -diketonate complexes in fuels has also provoked interest.^[6-8] Few reviews have been published in this area^[9-13], and a remarkable book by Bradley, Mehrotra, and Gaur.^[1]

Sodium forms an integral part of higher research of functional materials with high technological potentials, such as thermoelectric (e.g., Na_xCoO_2)^[14, 15], superconductors (e.g., $\text{Na}_x\text{CoO}_2 \cdot y\text{H}_2\text{O}$)^[16] dielectrics (e.g., NaNbO_3)^[17], and piezoelectric ($\text{K}_{1-x}\text{Na}_x\text{NbO}_3$).^[18, 19] Lately, sodium has also established attention in less expensive sodium-ion batteries as an alternative to lithium-ion batteries.^[20, 21]

All the materials mentioned above, and their applications require the materials to be prepared in film form. Alkali metal-based compounds have been deposited as thin films by techniques such as pulsed laser deposition, metalorganic chemical vapor deposition

(MOCVD), chemical solution deposition, and more recently, Atomic Layer Deposition ALD.^[22–27] As such, the availability of precursors for sodium-containing materials is somewhat limited.

Concerning MOCVD, β -diketonates complexes are common precursors, while metal alkoxides or acetates are more frequently used as a solution-based method.^[23, 25–33] Metal-organic chemical vapor deposition (MOCVD) has steered workers to investigate β -diketonate complexes as potential molecular precursors for the fabrication of high-quality oxide thin films.^[34] Overall, such precursors must be volatile, have the necessary stability to transport to the deposition site, and decay cleanly to give the desired material. An added advantage of the metal β -diketonate complexes is that they often demonstrate excellent hydrolytic stability than their respective alkoxide counterparts. A variety of β -diketonate complexes of both main groups and transition metals have been used to deposit films of metals,^[35] metal oxides,^[35] metal sulfides,^[36] and metal fluorides.^[35]

β -diketonate ligands in metal complexes show a wide range of coordination modes, the degree of bridging being determined by the metal centre, the steric bulk of the ligand, and the presence of any Lewis bases. Thus, for example, $[\text{Mn}(\text{acac})_3]$ ^[37] is a monomer in the solid-state with purely chelating β -diketonate ligands, whereas $[\text{Pr}(\text{tmhd})_3]_2$ (although the larger β -diketonate tetramethyl-3,5-heptanedionate, tmhd ligand, is present) is a dimeric solid with chelating and bridging tmhd ligands.^[38]

The degree of oligomerization of some of the large ionic radius metals, e.g., groups 1, 2, and the lanthanides, can be broken by coordination of one of the many different Lewis base types of ligands.^[39] For a molecular precursor, further tailoring of such chelates system has been quite successful, following this strategy. Furthermore, entropy and enthalpy play a large role in this process.

We have previously examined the promising properties of a large family of single-source precursors to fabricate high-quality alkaline-earth films,^[40] rare-earth fluorides,^[41–47] and oxides. These precursors' molecular structure consisted of a fluorinated β -diketonate metal array, whose coordinative deficiency was saturated by various Lewis base ligands, such as glyme, yielding monomeric, water-free, stable, volatile, and low melting point metal precursors.^[48–50] All these properties are of relevance. In particular, low melting point

precursors represent the most desirable sources due to the more significant and stable vapor pressure since their liquid nature under process conditions avoids any effects of crystallite size on the evaporation, hence, on the film growth rate.

Here, we report on the synthesis of novel sodium complexes of the type “Na(hfa)•glyme”, [Hhfa = 1,1,1,5,5,5-hexafluoro-2,4-pentanedione, glyme = monoglyme (1,2-Dimethoxyethane), diglyme (bis(2-methoxyethyl)ether), triglyme (2,5,8,11-tetraoxadodecane) and tetraglyme (2,5,8,11,14-pentaoxapentadecane)], with glymes performing like crown ethers in terms of coordinating/solvating ions, i.e. in terms of chelating properties.^[39] Single crystal X-ray diffraction experiments provide evidence of interesting coordination moieties. They have also been characterized by FT-IR spectroscopy, ¹H, and ¹³C NMR.

4.1 Experimental Section

Materials. The sodium hydroxide [NaOH, >98%] and 1,1,1,5,5,5-hexafluoro-2,4-pentanedione (H-hfa, >98%), were purchased from Strem Chemicals and used as received. Monoglyme (1,2-Dimethoxyethane, 99.5%), diglyme (bis(2-methoxyethyl)ether, 99.5%), triglyme (2,5,8,11-tetraoxadodecane, >98%), tetraglyme (2,5,8,11,14-pentaoxapentadecane, >99%), dichloromethane (CH₂Cl₂, >99.5%) and n-pentane were purchased from Sigma Aldrich.

General procedures. Fourier Transform Infrared (FT-IR) spectra were recorded using a Jasco FT/IR-430 spectrometer with nujol mull between NaCl plates. Melting points were taken on tiny single crystals using a Kofler hot-stage microscope. Thermogravimetric analyses were made using a Mettler Toledo TGA2 and the STAR^e software. Dynamic thermal studies were carried out under purified nitrogen flow (50 sccm) at atmospheric pressure with a 5°C min⁻¹ heating rate. The weights of the samples were between 7–10 mg. Differential scanning calorimetry analyses were carried out using a Mettler Toledo Star System DSC 3 under purified nitrogen flow (30 sccm) at atmospheric pressure with a 5°C/min heating rate. The weights of the samples were between 5-8 mg. NMR tests were carried out at 27°C using a 500 MHz spectrometer (¹H at 500 MHz, ¹³C NMR at 125.7 MHz) equipped with a pulse-field

gradient module (Z-axis) and a tunable 5mm Varian inverse detection probe (ID-PFG); chemical shifts (δ) are stated in ppm and are referenced to residual deuterated solvent. NMR data were analyzed using the MestReC software.

Synthesis of Na(hfa) (9). The Na(OH) (0.367 g, 9.18 mmol) 30% excess was suspended in dichloromethane (40 mL), Hhfa (1.47 g, 7.06 mmol) was added after 10 min, and the mixture was refluxed under stirring for one hour. The excess of NaOH was filtered off. White crystals were collected after the evaporation of the solvent. The reaction yield was 88%. The crude product melts around 125 °C using the Kofler hot-stage microscope (760 Torr).

Synthesis of "Na(hfa)•monoglyme" (9a). The Na(OH) (0.367 g, 9.18 mmol) 30% excess was first suspended in dichloromethane (40 mL) followed by monoglyme (0.636 g, 7.06 mmol), and finally, Hhfa (1.47 g, 7.06 mmol) was added after 10 min, and the mixture was refluxed under stirring for one hour. The excess of NaOH was filtered off. The colorless crystals precipitated after partial evaporation of the solvent. The crystals were collected, washed with pentane, and filtered. The compound was sticky even after several cleaning steps. The reaction yield was 85%.

Synthesis of [Na₄(hfa)₆]•[Na(diglyme)₂]₂ (10). The Na(OH) (0.367 g, 9.18 mmol) 30% excess was first suspended in dichloromethane (40 mL) followed by diglyme (0.636 g, 7.06 mmol), and finally, Hhfa (1.47 g, 7.06 mmol) was added after 10 min, and the mixture was refluxed under stirring for one h. The excess of NaOH was filtered off. The colorless crystals precipitated after partial evaporation of the solvent. The crystals were collected, washed with pentane, filtered, and dried under vacuum. The reaction yield was 80%. The melting point of the crude product was 107°C (760 Torr).

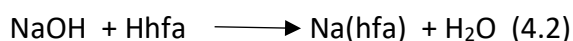
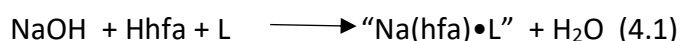
Synthesis of Na(hfa)•triglyme•H₂O (11). The Na(OH) (0.367 g, 9.18 mmol) 30% excess was first suspended in dichloromethane (40 mL) followed by triglyme (1.25 g, 7.06 mmol), and finally, Hhfa (1.47 g, 7.06 mmol) was added after 10 min, and the mixture was refluxed under stirring for one h. The excess of NaOH was filtered off. The obtained product did not crystallize and is an oil.

Synthesis of Na(hfa)•tetraglyme (12). The Na(OH) (0.367 g, 9.18 mmol) 30% excess was first suspended in dichloromethane (40 mL) followed by tetraglyme (1.57 g, 7.06 mmol), and finally, Hhfa (1.47 g, 7.06 mmol) was added after 10 min, and the mixture was refluxed under stirring for one h. The excess of NaOH was filtered off. The crystals were collected, washed with pentane, filtered, and dried under vacuum. The reaction yield was 87%. The crude product melts around 62°C using the Kofler hot-stage microscope (760 Torr).

Single crystal X-ray structure. Intensity data from a single crystal of adduct **9** and adduct **10** were collected at 100K using a Bruker APEX-II CCD using the Cu-K α radiation ($\lambda = 1.54184 \text{ \AA}$). Data collections were performed with the program CrysAlis CCD.^[51] Data reductions were carried out with the program CrysAlis RED.^[51-52] Finally, absorption corrections were performed with the program ABSPACK in CrysAlis RED. Structures were solved using the SIR-2004 package^[52] and subsequently refined on the F^2 values by the full-matrix least-squares program SHELXL-2013.^[53] Geometrical calculations were performed by PARST97^[54], and molecular plots were produced by the program Mercury (v3.7).^[55] All the non-hydrogen atoms of the two structures were refined using anisotropic thermal parameters. In contrast, the hydrogen ones were set in a calculated position and refined in agreement with the carbon atom to which they are bound.

4.2 Results & Discussions

Novel sodium complexes have been synthesized, in a single-step reaction, from the sodium hydroxide, hexafluoroacetylacetone, and glyme ligands dichloromethane. The mixture was refluxed under stirring for 1 hour (Eq. (4.1)) initially and then later corrected to (Eq. (4.2))



- 9.** Na(hfa)
- 9a.** Na(hfa)•monoglyme
- 10.** [Na₄(hfa)₆]•[Na•(diglyme)₂]₂
- 11.** Na(hfa)•triglyme•H₂O
- 12.** Na(hfa)•tetraglyme

After the solvent evaporation, the precursors **10** and **12** are obtained as white crystals and melt respectively at 107°C and 62°C. Compound **9** has a white sticky crystal-like consistency, while precursor **11** is a colorless oil at room temperature. The adducts are mostly soluble in common organic solvents such as ethanol, dichloromethane, and acetone. Complexes **9**, **10**, and **12** are non-hygroscopic and can be handled in the air. Thus, our synthetic strategy produces anhydrous adducts, except for the adduct **11**, with high yields (80-90%) in a single and low-cost route from commercially available chemicals.

In-depth analysis of adduct **9a** proved that the monoglyme is not coordinated (see ¹H NMR section in the following). Therefore, a different synthetic procedure was applied [eq. (2)] from the sodium hydroxide and hexafluoroacetylacetone to produce the pure Na(hfa) (**9**). Further characterization (FT-IR, single-crystal structures, TGA, DSC) has been carried for compound **9**.

NMR spectra. The ¹H -NMR and ¹³C-NMR studies of the "Na(hfa)-glyme" adducts have been carried out dissolving adducts **2**, **3**, and **4** in CDCl₃ while the **1a** in CD₃COCD₃. ¹H -NMR spectra of adducts **2**, **3**, and **4** show at δ≈3.3-3.4 ppm a singlet consistent with the protons of the terminal methyl groups of the glyme ligand, while multiplets at δ=3.6-3.7 represent resonances of methylenic protons of the same ligand. Also, at δ=5.6-5.8, there is a singlet for the one proton of the hfa ring ligand for the **1**, **2**, **3**, and **4** adducts.

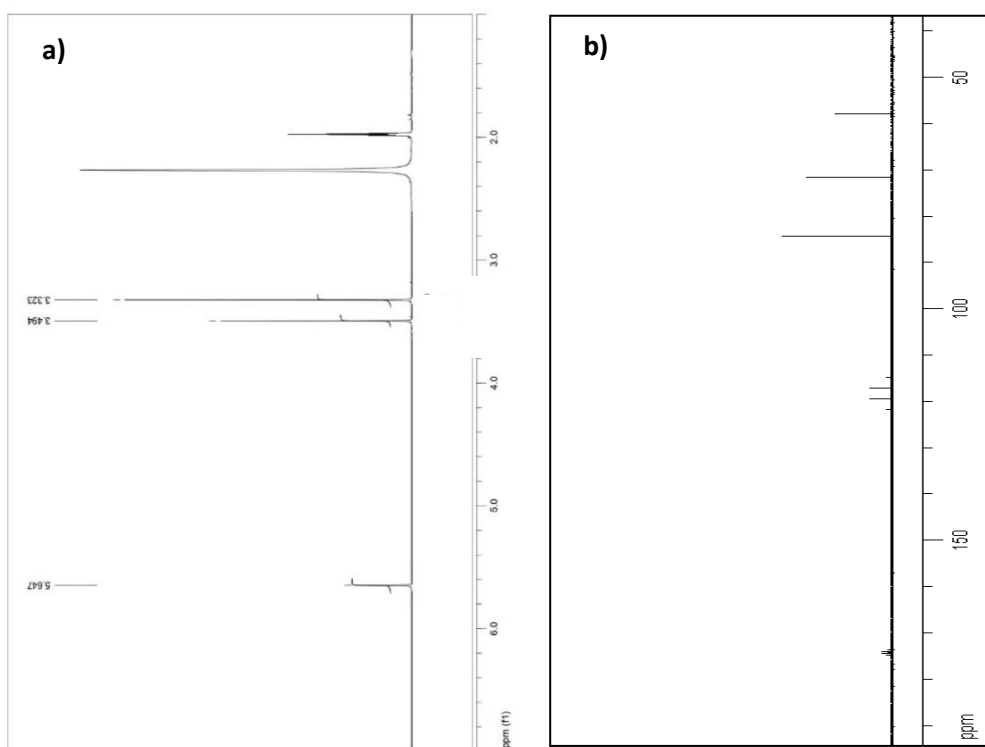


Fig. 4.1 a) ¹H-NMR spectrum of **9a** (CD₃COCD₃, 500 MHz, 27 °C) **b)** ¹³C-NMR spectrum of **9a** (CD₃COCD₃, 125 MHz, 27 °C)

¹H-NMR measurement was conducted by dissolving the adduct **9a** in deuterated acetone as it is insoluble in chloroform. The obtained spectrum (Fig. 4.1a) shows signals consistent with the terminal methyl groups' protons or the CH₂ of monoglyme, which can be traced back to glyme coordination. Nevertheless, given the sticky nature of the compound **9a**, its NMR spectra were compared with the ¹H-NMR spectrum of the free monoglyme ligand to ascertain from the position of the peak if monoglyme is coordinated or is present as contamination. Methyl groups of the monoglyme are found at 3.323 ppm (Fig. 4.2), which is at the same position as the compound **9a** and confirms monoglyme contamination. The unique proton of the hfa ligand appears at 5.647 ppm. Spectrum ¹³C-NMR is recorded under decoupling conditions (Fig. 4.1b). At the chemical shift value of 84 ppm, the carbon signal falls into the two ketonic groups of the hfa. Finally, the two quartets at about 118 ppm and 174 ppm can be traced back to the C of the CF₃ and C-O groups of the ligand. The quartets are due to coupling with the fluoride atoms of the CF₃ groups.

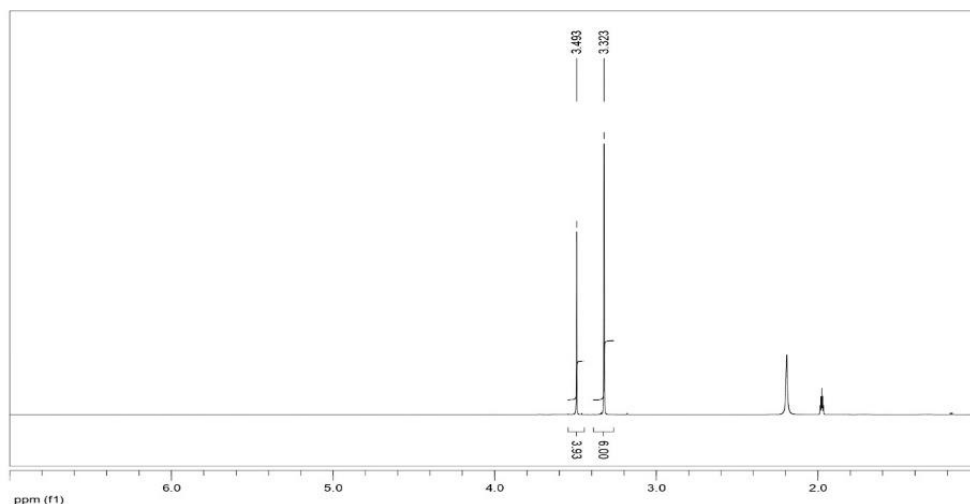


Fig. 4.2. ^1H -NMR spectrum of monoglyme ligand (CD_3COCD_3 , 500 MHz, 27 °C)

The ^1H -NMR spectrum of the adduct **10** was carried out in deuterated chloroform (Fig. 4.3a). For adduct **10**, signals for the eight methylenic hydrogens of the polyether were found in the 3.5 ppm to 3.6 ppm range. At the chemical shift value of 5.8 ppm, the singlet signal of the only hydrogen of the "diketonate" ligand appears. Spectrum ^{13}C -NMR is recorded under decoupling conditions (Fig. 4.3b). Between 70 ppm and 71 ppm, the signals for the eight polyether methyl carbons are observed. At 77 ppm, the signal attributable to deuterated chloroform used as a solvent is observed. At the chemical shift value of 87 ppm, the carbon signal falls into the two ketonic groups of the hfa. Finally, the two quartets at about 118 ppm and 176 ppm can be traced back to the C of the binder's CF_3 and C-O groups. The quartets are due to coupling with the fluoride atoms of the CF_3 groups.

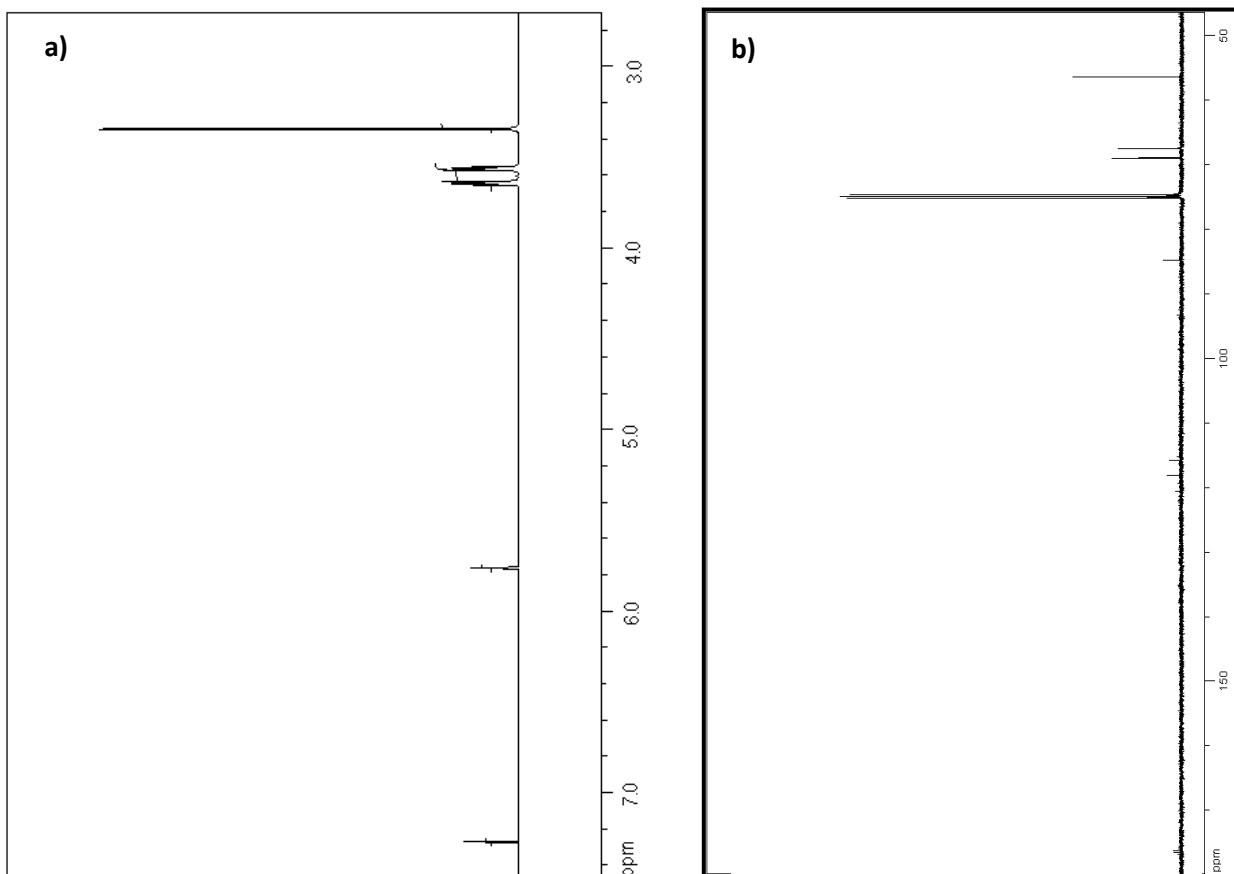


Fig. 4.3 a) ^1H -NMR spectrum of **10** (CDCl_3 , 500 MHz, 27 °C) b) ^{13}C -NMR spectrum of **10** (CDCl_3 , 125 MHz, 27 °C)

The ^1H -NMR spectrum of the adduct **11** was carried out in deuterated chloroform (Fig. 4.4a) and presented all the signals related to the complex's resonant protons. The integration of the intense 3.3 ppm singlet indicates the six equivalent protons of the two terminal methyl groups of the triglyme. In the chemical shift from 3.5 ppm to 3.7 ppm, two multiplets and one singlet can be seen from the polyether's twelve methylenic hydrogens. At 5.8 ppm, we find the singlet relative to the proton of the diketone. Spectrum ^{13}C -NMR (Fig. 4.4b) is recorded in decoupling conditions. For a chemical shift value of 59 ppm, the signal for the two methyl carbons of the polyether is observed. Between 69 ppm and 71 ppm, the methylenic C of the triglyme resonates. At 77 ppm, the signal for the deuterated chloroform used as a solvent is observed. Finally, at the value of 86 ppm, the carbon resonates in the two ketonic groups. The two quartets at about 118 ppm and 176 ppm can be traced back to

the C of the CF₃ and C=O groups, respectively, of the β-diketone. The quartets are due to coupling with the fluoride atoms of the CF₃ groups.

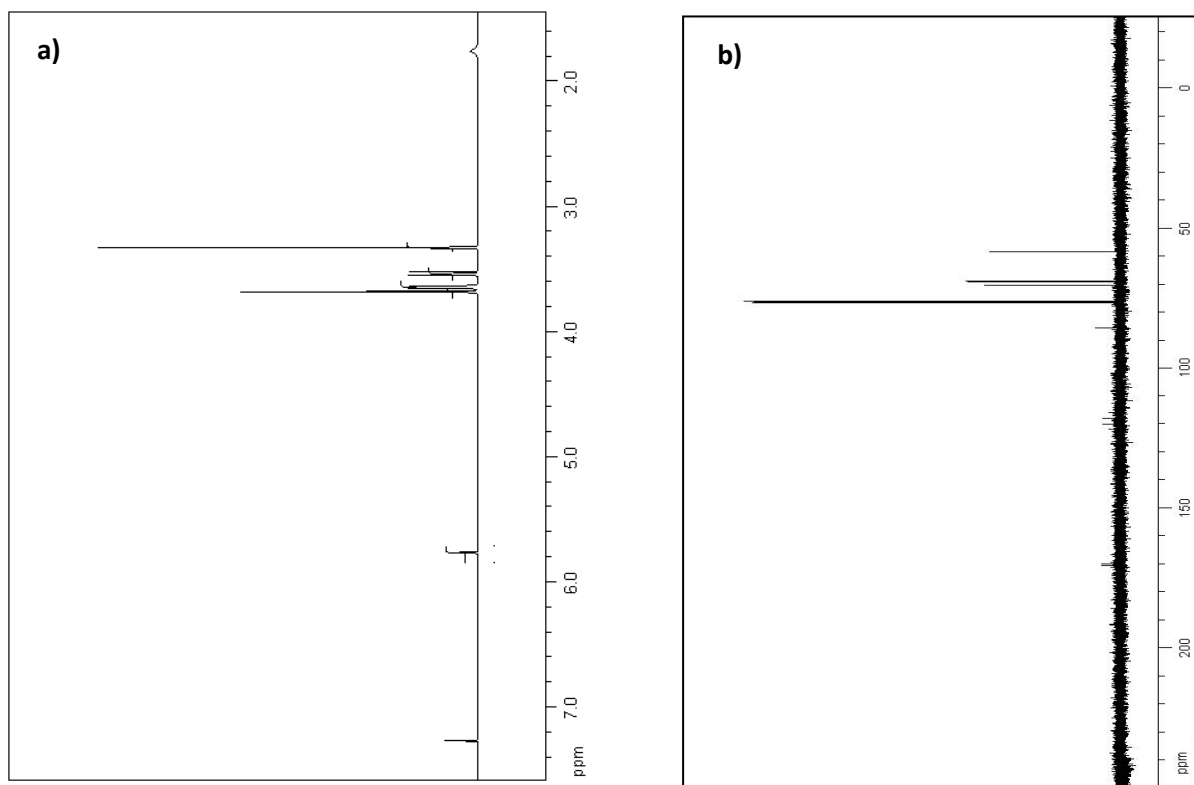


Fig. 4.4. a) ¹H-NMR spectrum of **11** (CDCl₃, 500 MHz, 27 °C) b) ¹³C-NMR spectrum of **11** (CDCl₃, 125 MHz, 27 °C).

The ¹H-NMR spectrum of adduct **12** was carried out in deuterated chloroform (Fig. 4.5a) and showed an intense 3.4 ppm singlet, which relates to the resonance of the six equivalent protons of the two terminal methyl groups of the polyether. Signals ranging from 3.5 ppm to 3.7 ppm can be traced back to the sixteen methylenic protons of tetraglyme. The 5.8 ppm singlet is related to the proton linked to the hfa. Spectrum ¹³C-NMR (Fig. 4.5b) shows an intense 59 ppm signal, typical of the two methyl C of the tetraglyme. Between 69 ppm and 71 ppm, signals are seen for the eight methylenic C of the polyether. At 77 ppm, the signal from the deuterated chloroform used as a solvent is observed. At the chemical shift value of 86 ppm, the carbon signal falls in the two ketonic groups of the hfa. Finally, the two quartets at about 118 ppm and 176 ppm can be traced back to the C of the CF₃ and C=O groups of the binder. The quartets are due to coupling with the fluoride atoms of the CF₃ groups.

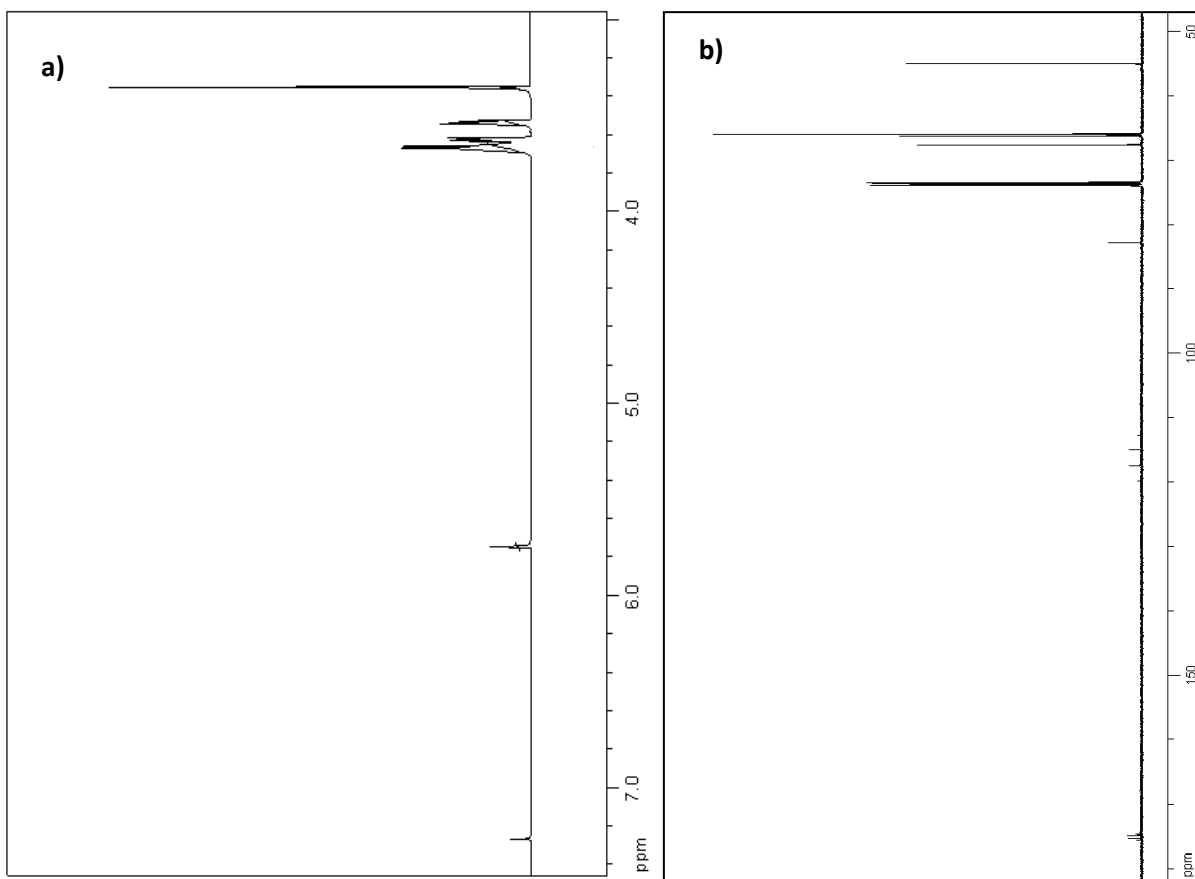


Fig. 4.5 a) $^1\text{H-NMR}$ spectrum of **12** (CDCl_3 , 500 MHz, 27 °C) b) $^{13}\text{C-NMR}$ spectrum of **12** (CDCl_3 , 125 MHz, 27 °C)

FT-IR – characterization. The sodium precursors have been characterized by Fourier transform (FT)-IR in the range $4000\text{-}500\text{ cm}^{-1}$. All the FT-IR transmittance spectra (fig. 4.6) of the "Na(hfa)•glyme" (**10**, **11** and **12**) and of Na(hfa) (**9**) show the peaks at 1674 cm^{-1} and 1560 cm^{-1} associated with C=O stretching and C=C stretching, respectively (fig. 4.6, Inset: enlarged image), due to the β -diketonate ligand. The broadband observed in the $1000\text{-}1300\text{ cm}^{-1}$ range may be related to vibrations due to coordination of the polyether C-O bending and/or stretching overlapped with the C-F stretching. Also, bands at 1015 , 861 , and 837 cm^{-1} can be associated with glyme modes **10**, **11**, and **12**. The C-H glyme stretching modes, lying in the $2800\text{-}3000\text{ cm}^{-1}$ range, overlap with nujol features, except compound **11**, whose spectrum has been recorded in the neat sample. The nujol shows peaks at 2923 cm^{-1} , at 1461 cm^{-1} , and 1377 cm^{-1} . In the adduct **11** (liquid) spectrum, we may observe a broad band at the 3600 cm^{-1} range due to the OH stretching modes of pooled water. In contrast, spectra of adducts **9**, **10**, and **12** show no band at 3600 cm^{-1} , indicating that no water molecules are

coordinated to the metal ion, thus pointing to the metal centre's saturation due to the Lewis base glyme.

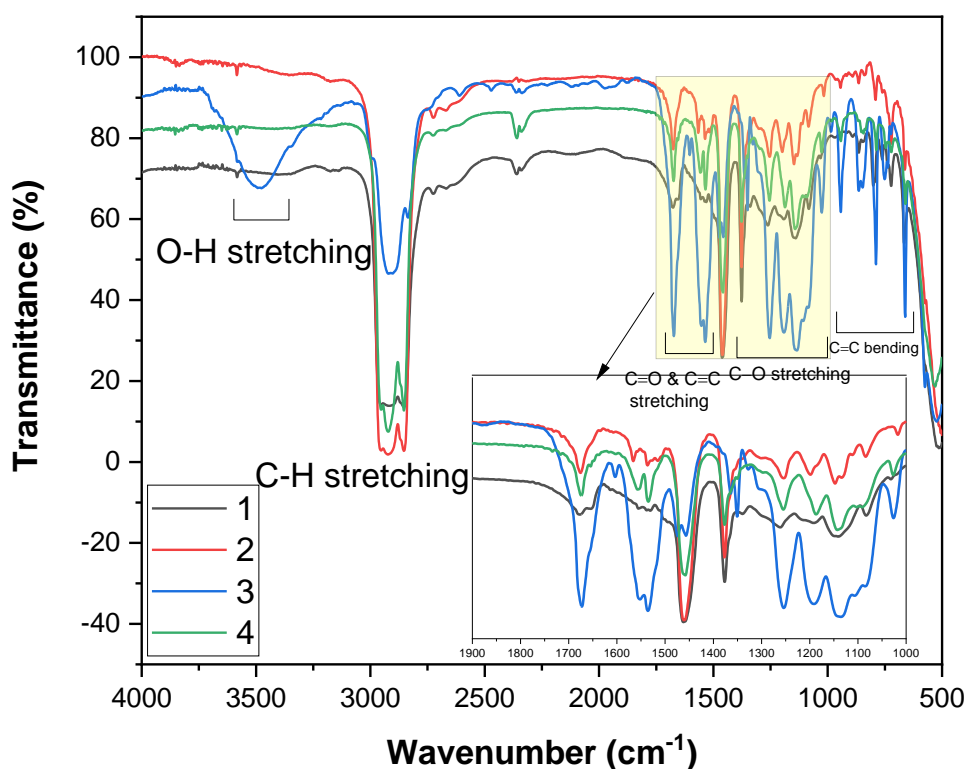


Fig. 4.6. Infrared spectra and (Inset: enlargement of the “Na(hfa)glyme” and Na(hfa) FT-IR adducts in the 1900-1000 cm⁻¹ range.)

Comparing different FT-IR spectra, in the carbonyl range, of the compounds **9**, **10**, **11**, and **12**, and H-hfa ligand (Fig. 4.7), it is possible to observe two carbonyl peaks at 1689 and 1629 cm⁻¹ for the H-hfa free ligand. We observe one of the distinct H-hfa peaks, the C=O stretching, slightly shifted to 1675 cm⁻¹ for adducts **10**, **11**, and **12**, while for adduct **9**, a splitting of this peak is observed producing signals at 1678 and 1651 cm⁻¹. The peaks for all the adducts are shifted to those of the free ligand, suggesting that the H-hfa ligand is coordinated to the sodium ion for all the samples.

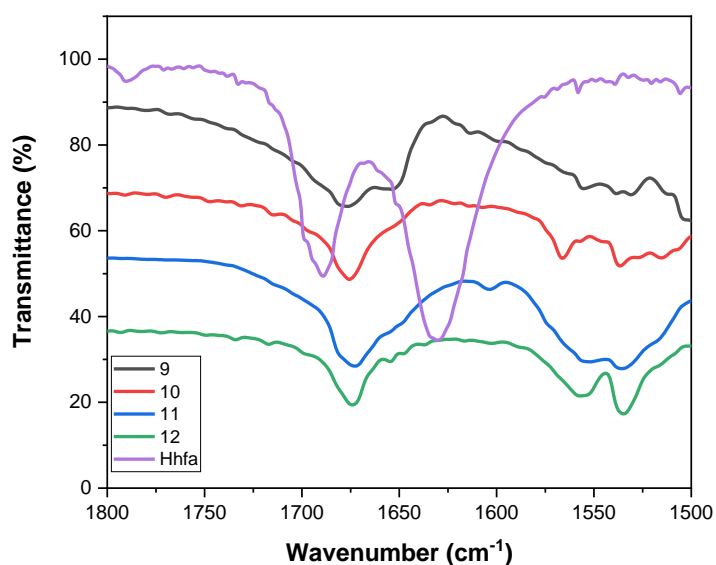


Fig. 4.7. FT-IR spectra of the adducts **9**, **10**, **11**, and **12**, and H-hfa ligand in the carbonyl range.

To confirm the glyme coordination, the typical ether signals at 1030 and 860 cm^{-1} were found for adducts **10**, **11**, and **12**. In the case of compound **9**, no signals are present in the 1100-800 cm^{-1} region, as expected, considering that no monoglyme is present in this compound. (fig. 4.8a). In adduct **10** (fig. 4.8b), we observe the glyme signals shifted to 1017 cm^{-1} and 790 cm^{-1} . Similarly, adduct **11** in fig. 4.9a and adduct **12** in fig. 4.9b shows the glyme coordinated peak slightly shifted to 1020 and 850 cm^{-1} .

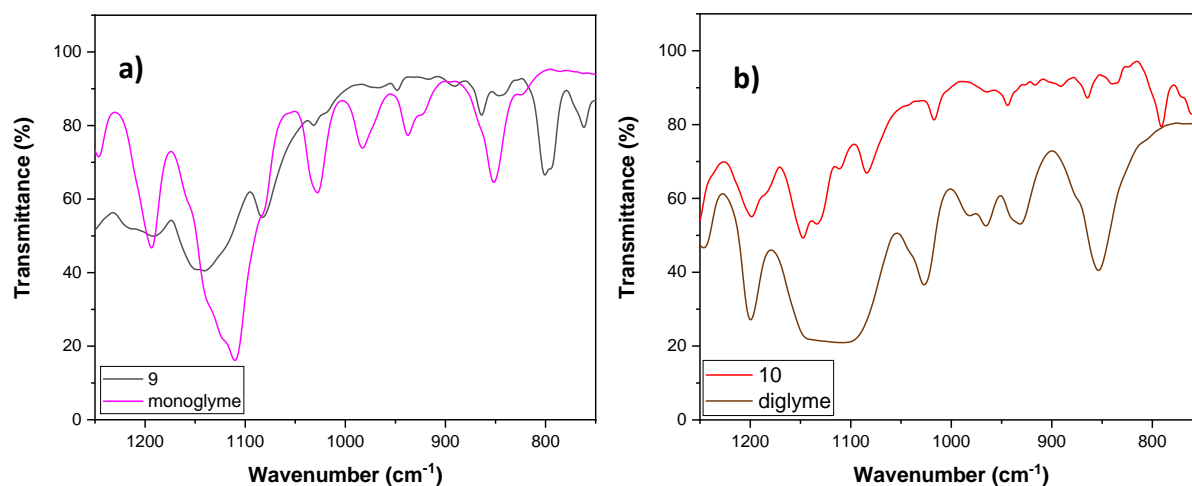


Fig. 4.8 a) Comparison of FT-IR spectra of free monoglyme and adduct **9** in the monoglyme range vibration **b)** Comparison of FT-IR spectra of free diglyme and adduct **10** in the diglyme range vibration.

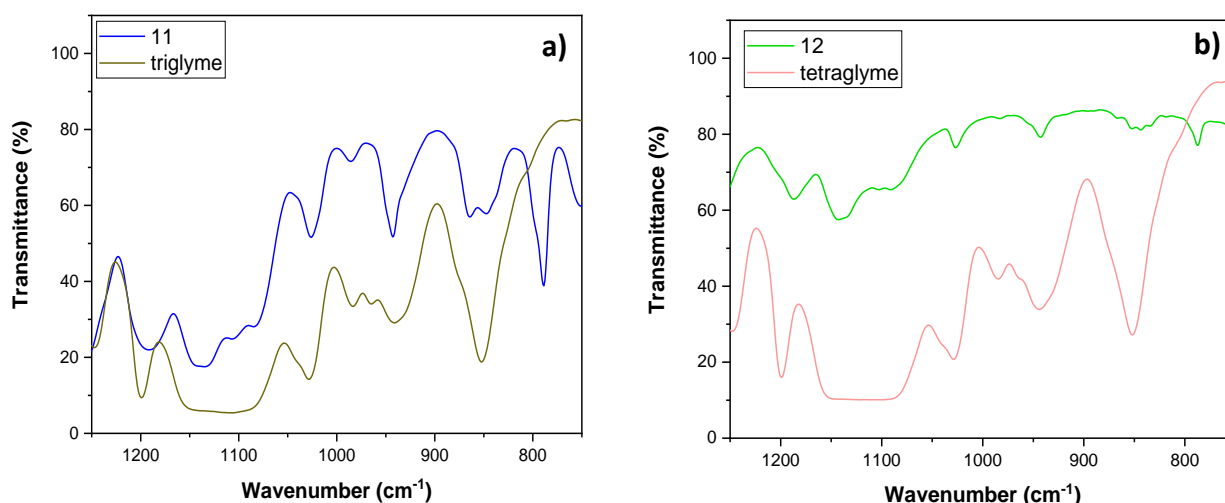


Fig. 4.9. a) Comparison of FT-IR spectra of free triglyme and adduct **11** in the triglyme range vibration; b) Comparison of FT-IR spectra of free tetraglyme and adduct **12**.

Single crystal structures. The structures of **9** and **10** have been defined through single-crystal X-ray diffraction data. In Fig. 4.10 and Fig. 4.11, ball and stick views of the asymmetric units of the two compounds, **9** and **10**, are reported. Crystallographic data and refinement parameters are reported in Table 4.1. Ball and stick view of compound **12**, published by Catalano et al., is shown in figure 4.12 and used only for comparison purposes.

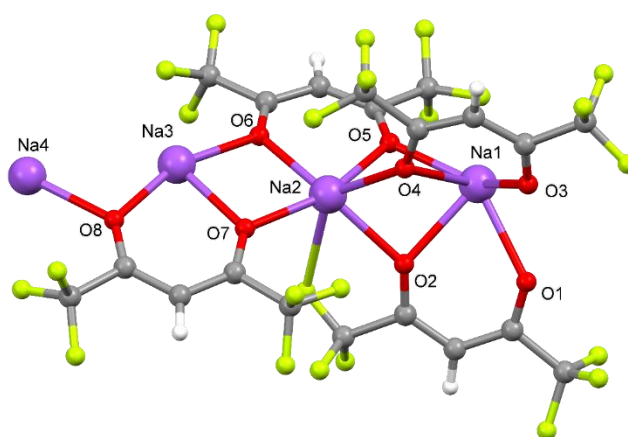


Figure 4.10. Ball and stick view of the asymmetric unit **9**.

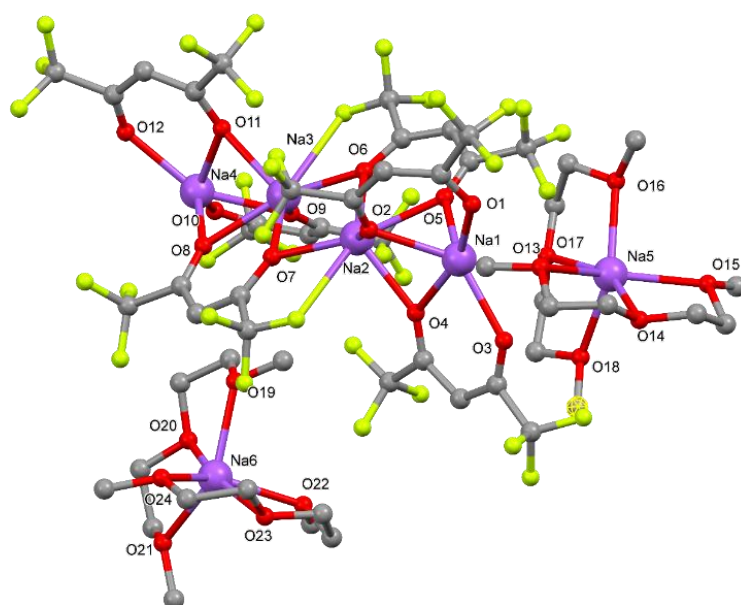


Figure 4.11. Ball and stick view of the asymmetric unit **10**. For the sake of clarity, hydrogen atoms have been omitted.

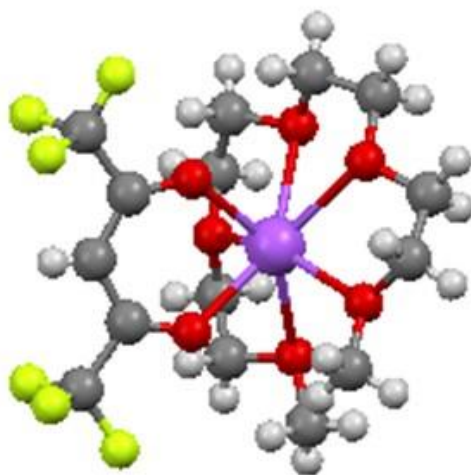


Fig. 4.12 Ball and stick view of the Na(hfa)•tetraglyme complex ^[56]

Table 4.1. Crystallographic data and refinement parameters for **9** and **10**

	9	10
Empirical formula	Na(hfa)	[Na ₄ (hfa) ₆]•[Na•(diglyme) ₂] ₂
Formula weight	230.05	1916.97
Temperature (K)	100	100
Wavelength (Å)	1.54184	1.54184
Crystal system, space group	tetrahedral, I-4	Triclinic, P-1
Unit cell dimensions (Å, °)	a = 24.4916(7) b = 24.4916(7) c = 9.8714(3)	a = 11.460(1) α = 83.860(4) b = 17.019(1) β = 87.651(5) c = 21.816(2) γ = 71.840(4)
Volume (Å ³)	5921(2)	4019.6(6)
Z, D _c (mg/cm ³)	8, 2.064	2, 1.584
μ (mm ⁻¹)	2.803	1.839
F(000)	3584	1936
θ range (°)	2.551-68.403	2.037-68.696
Reflections collected / unique	18361 / 5247	100935 / 14654
Data / parameters	5247 / 505	14654 / 1082
Goodness-of-fit on F ²	0.993	1.927
Final R indices [I > 2σ(I)]	R1 = 0.0821, wR2 = 0.2238	R1 = 0.01584, wR2 = 0.4446
R indices (all data)	R1 = 0.1087, wR2 = 0.2541	R1 = 0.1751, wR2 = 0.4627

In the asymmetric unit of **9**, four sodium cations and four hfa anions are present. Five oxygen atoms coordinate all the sodium cations, and their coordination sphere is completed by several fluorine atoms ranging from 2 to 4, giving rise to a coordination number in the 7-9 range (Na2 and Na3 are hepta-coordinated, Na4 is octa-coordinated, while Na1 is nona-coordinated). The oxygen atoms of two hfa anions (O1, O2, and O3, O4) act as μ_3 -bridging atoms towards three sodium cations, while the oxygen atoms of the other two hfa anions (O5, O6, and O7, O8) bridge two metal cations (see Fig. 4.13). Due to these bridging atoms' presence, a 3D polymer is formed (see Fig. 4.14).

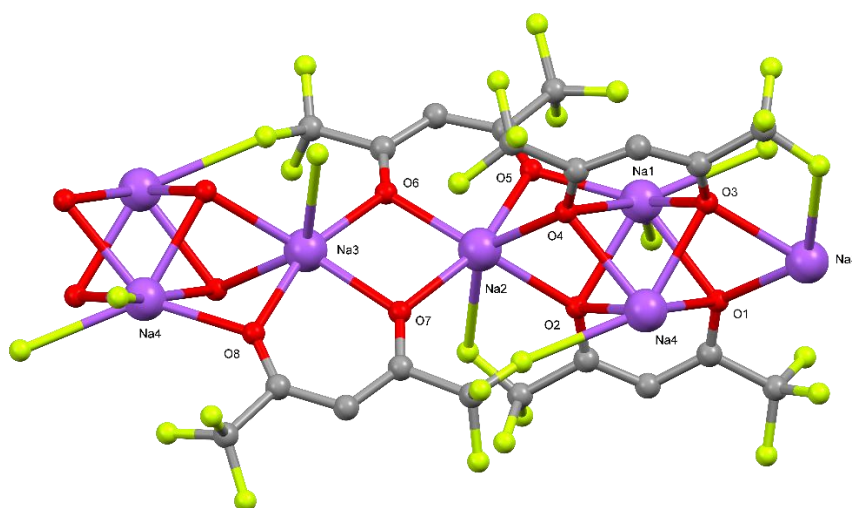


Fig. 4.13. Bridging scheme of the hfa ligand in **9**.

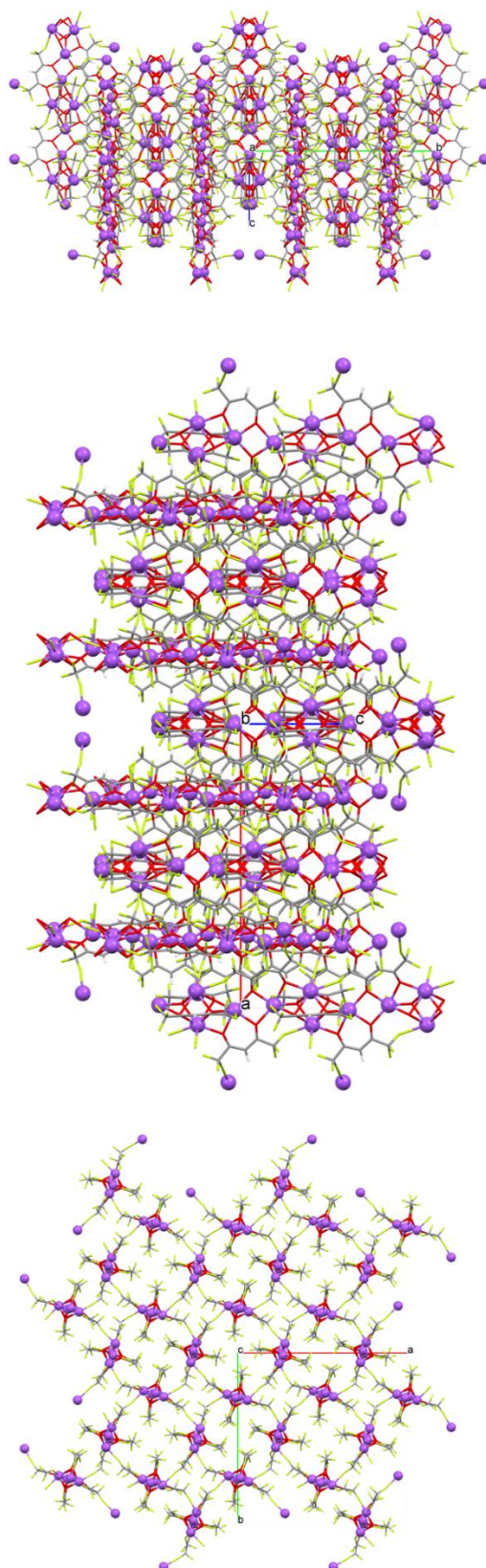


Fig. 4.14. Crystal packing of **9**, views along the a, b, and c axes (top, middle, and bottom, respectively).

Inside the 3D polymer, it is possible to localize a group of four sodium cations that occupy a rhombus's vertices (see Fig. 4.15 and Table A.6.). These rhombuses form a chain that propagates along the c axis (see Figure 4.15).

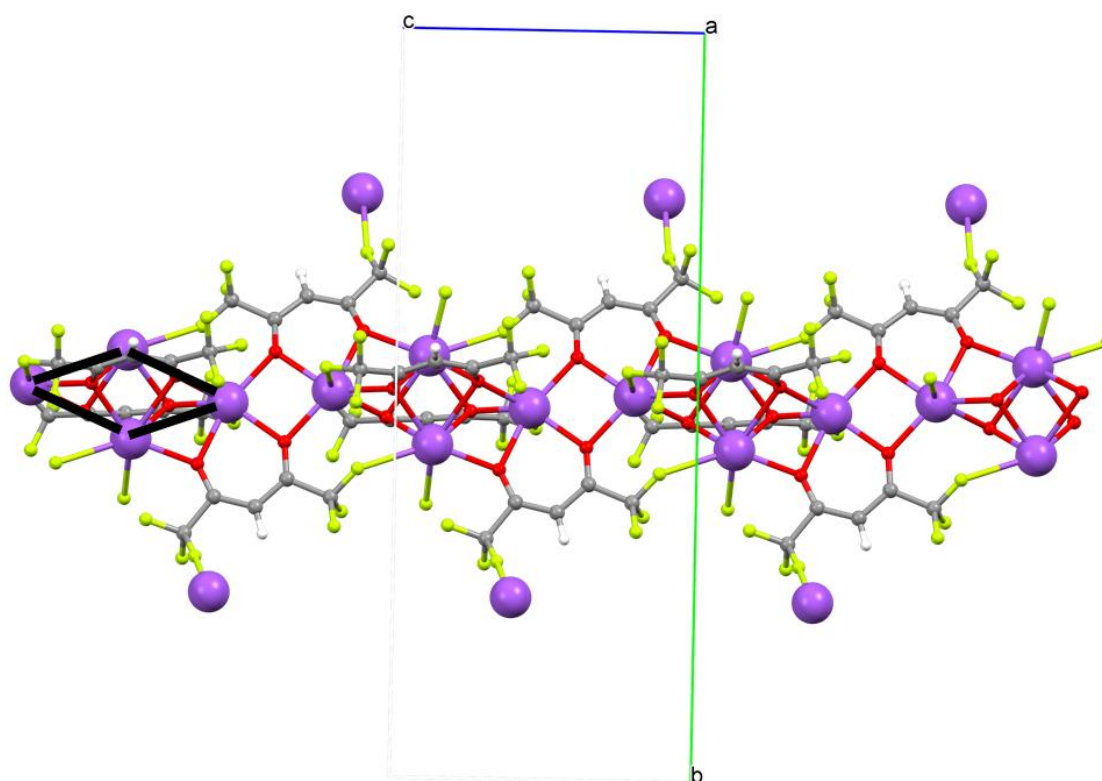


Fig. 4.15. In black, the rhombus defined by four proximal sodium atoms is evidenced.

In the asymmetric unit of compound **10**, two $\text{Na}(\text{diglyme})_2^+$ cations and one $\text{Na}_4(\text{hfa})_6^{2-}$ anion are present. In the $\text{Na}(\text{diglyme})_2^+$ cation, the sodium atom is hexa-coordinated by all the three oxygen atoms of the two diglyme molecules. Concerning the $\text{Na}_4(\text{hfa})_6^{2-}$ anion, all the sodium atoms are coordinated by five oxygen atoms; in addition to these, the central metal cations Na2 and Na3 are bonded to a fluorine atom as well (see table A.6.). All the oxygen atoms of the four hfa anions of $\text{Na}_4(\text{hfa})_6^{2-}$ act as μ_2 -bridging atoms with the exceptions of O1, O3, O10, and O12, which belong to hfa anions situated at both ends of the $\text{Na}_4(\text{hfa})_6^{2-}$ unit (see figure 4.16).

In the $\text{Na}_4(\text{hfa})_6^{2-}$ anion, the four sodium atoms are aligned; concerning their relative distances, the couples Na1/Na2 and Na3/Na4, that are bridged by three oxygen atoms, are significantly nearer than the central one Na2/Na3 (see Table A.6).

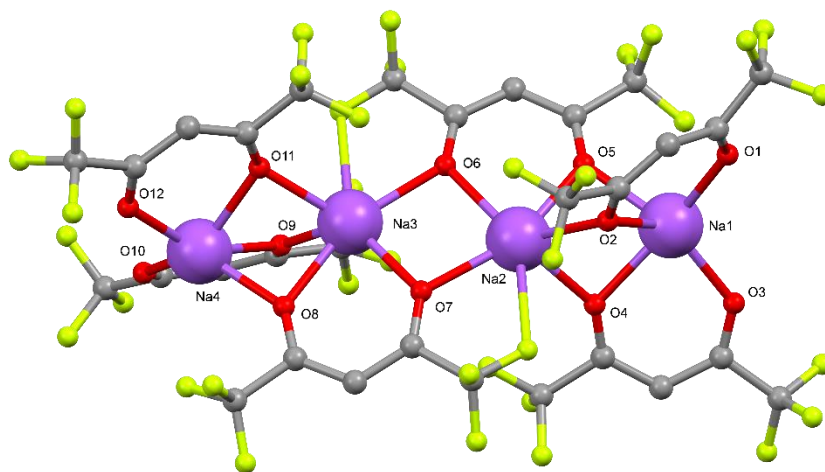


Fig. 4.16. Ball and stick view of the $\text{Na}_4(\text{hfa})_6^{2-}$ anion.

In the reported work of the $\text{Na}(\text{hfa}) \bullet \text{tetraglyme}$ complex,^[56] the sodium cation is seven-coordinated by the five oxygen atoms of the ether and by the two oxygen atoms of the hfa anion. The present synthesis of adducts **9**, **10**, **11**, and adduct **12** gives us a good understanding of the polyether chain's effect on the central metal β -diketonate structure's coordination chemistry. With the introduction of monoglyme and diglyme essentially providing ionic complexes, the mass transport property is eventually affected, as we will observe in the coming sections on the thermal analysis. Meanwhile, adduct **12** forms a covalent structure and provides critical essential features of higher volatility due to the large polyether chain and higher solubility in organic complexes.

Thermal analysis. The thermal behaviors of the as-synthesized precursors have been investigated by thermogravimetric (TG) measurements (fig. 4.17) and differential scanning calorimetry (DSC) (fig. 4.18). TG curves of adducts **11** and **12** show a single-step mass loss associated with the adducts' vaporization, while adducts **9** shows two-step mass-loss and adduct **10** shows a multiple-step mass loss. Adduct **9** shows a weight loss of about 13.8% in the range 25-107°C, which is not that straightforward and needs further analysis. The primary mass loss due to the adduct vaporization occurs in the range 215-295°C, with a residue of 16%, that most likely corresponds to 4[NaF] formation, which gives a theoretical value of 18.2%, but this is not a drawback for its applications in liquid assisted MOCVD processes, given its solubility in common organic solvents.

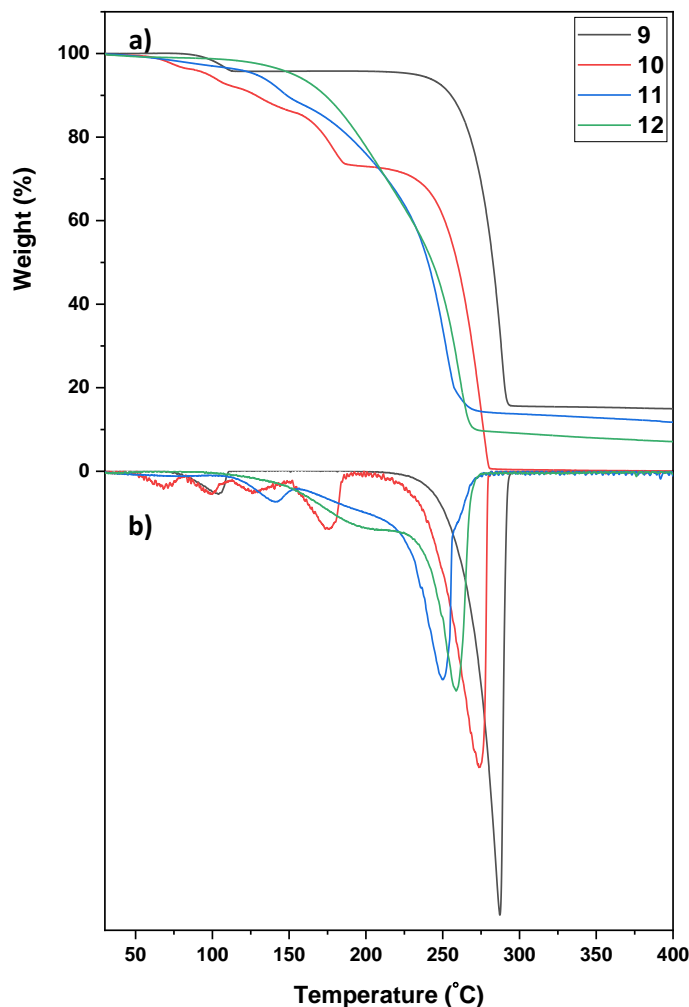


Fig. 4.17. **a)** TG, and **b)** DTG profiles of "Na(hfa)glyme" and Na(hfa) under N₂ flow at atmospheric pressure in the temperature range 30-400°C.

The TG curves of adducts **11** and **12** (fig. 4.17a) show a nearly single step weight loss with a residue of 14.2% at 274.3°C and 9.8% at 270°C, respectively. The adduct **10** curve shows a multi-step weight loss, with a residue of about 1 % at 280°C. Interpretation of the individual steps is not straightforward, but NaF would be the most likely final residue; further analysis needs to be carried out to support the hypothesis.

The DSC curves (fig. 4.18) of adduct **9** show a small peak at 125°C, signifying the complex melting. The DSC curve of adduct **10** presents a small endothermic peak at 107 °C due to the adduct melting and a broad exothermic peak at 256.9°C, which can be associated with its partial vaporization decomposition. In contrast, adduct **11** shows the exothermic peaks around 244.3°C, which may be related to vaporization overlapped with a partial

decomposition of the products. In adduct **12**, we observe a sharp endothermic peak at 62°C, indicating the melting of the polymeric structure and a sharp exothermic peak at 245.64°C, associated with the vaporization of the melt.

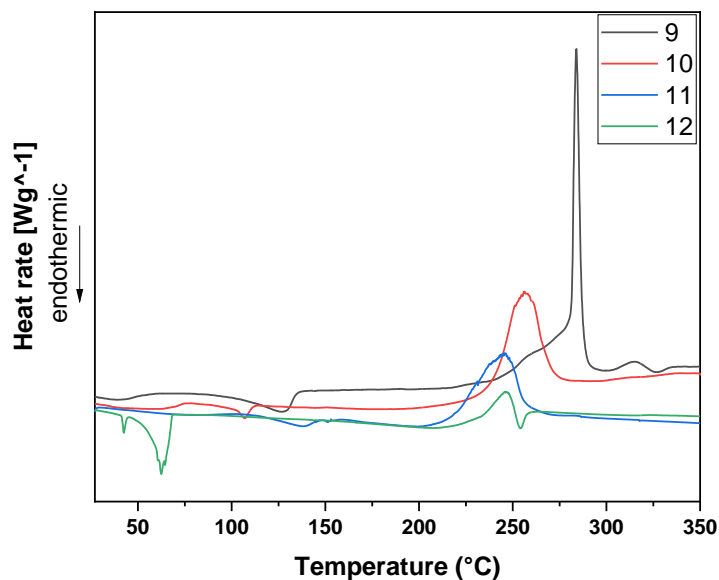


Fig. 4.18. DSC profiles of "Na(hfa)glyme" and Na(hfa) under N₂ flow at atmospheric pressure in the temperature range 30-350°C.

4.3 Conclusions

In summary, a one-pot synthesis method has been applied with high yield for the synthesis of the precursors using β -diketonate to counter-balance the charge of the cation, and different glymes have been used to complete the coordination sphere. Depending on the glyme nature, the precursors demonstrate an interesting structural motif. Precursors **9**, **10**, and **12** are solid, whereas **11** is liquid. Single crystal X-ray diffraction studies of precursor **9** show interesting coordination moieties as adduct **9** and adduct **10** are present as ionic species held together in a β -diketonate cage counteract the charge of the central metal cation. FT-IR spectrum confirms the glyme ligand's coordination in the region 1030 cm⁻¹ and 850 cm⁻¹ for all the adducts except for adduct **9**. The thermal analysis reveals a single step mass loss for adducts **11** and **12** with a residue of 14.2% and 9.8%. Adduct **9** shows a two-step mass loss with a residue of 16% and adduct **10** shows a five-step mass loss with a very low residue. Functional validation of these precursors is taken up in chapter 6 by applying to sol-gel and liquid-assisted MOCVD processes of (K, Na)NbO₃ films.

REFERENCES

- [1] R.C. Mehrotra, R. Bohra, DP Gaur, Metal b-Diketonates and Allied Derivatives, Academic Press, London, 1978.
- [2] L.G. Hubert-Pfalzgraf, Appl. Organomet. Chem. 6 (1992) 627.
- [3] A.R. Barron, W.S. Rees Jr, Adv. Mater. Opt. Electron. 2 (1993) 271.
- [4] J.E. Schwarberg, R.E. Sievers, R.W. Moshier, Anal. Chem. 42 (1970) 1828.
- [5] R.W. Moshier, R.E. Sievers, Gas Chromatography of Metal Chelates, Pergamon Press, Oxford, 1975.
- [6] J.M. Suighara, L.T. McRee, J. Org. Chem. 22 (1957) 795.
- [7] J.R. Vallentyne, Can. J. Bot. 33 (1955) 304.
- [8] G.E. Mapstone, J. Proc. R. Soc. N. S. W. 82 (1948) 79.
- [9] NS. Poonia, A.V. Bajaj, Chem. Rev. 79 (1979) 389.
- [10] L.G. Hubert-Pfalzgraf, Polyhedron 13 (1994) 1181.
- [11] R.E. Sievers, S.B. Turnipseed, L. Huang, A.F. Lagalante, Coord. Chem. Rev. 128 (1993) 285.
- [12] R.C. Mehrotra, J. Ind. Chem. Soc. 55 (1978) 1.
- [13] W.A. Wojtczak, P. Fleig, M.J. Hampden-Smith, Advances in Organometallic Chemistry, vol. 31, Academic Press, New York, 1996.
- [14] P. Brinks, H. Heijmerikx, T. A. Hendriks, G. Rijnders and M. Huijben, RSC Adv., 2012, 2, 6023–6027 RSC.
- [15] J. Y. Son, Y. H. Shin and C. S. Park, J. Appl. Phys., 2008, 104
- [16] Sugiura K, Ohta H, Nomura K, Yanagi H, Hirano M, Hosono H, Koumoto K., Inorg Chem. 2006 Mar 6;45(5):1894-6
- [17] A. Duk, M. Schmidbauer and J. Schwarzkopf, Appl. Phys. Lett., 2013, 102

- [18] J. Schwarzkopf, M. Schmidbauer, T. Remmele, A. Duk, A. Kwasniewski, S. Bin Anooz, A. Devi and R. Fornari, *J. Appl. Crystallogr.*, 2012, 45, 1015–1023
- [19] M. Blomqvist, J.-H. Koh, S. Khartsev, A. Grishin and J. Andreasson, *Appl. Phys. Lett.*, 2002, 81, 337–339
- [20] D. Kim, E. Lee, M. Slater, W. Lu, S. Rood and C. S. Johnson, *Electrochem. Commun.*, 2012, 18, 66–69
- [21] M. D. Slater, D. Kim, E. Lee and C. S. Johnson, *Adv. Funct. Mater.*, 2013, 23, 947–958
- [22] N. Janne and T. Marina, *J. Phys.: Condens. Matter*, 2012, 24, 325901
- [23] C.-R. Cho and B.-M. Moon, *Integrated Ferroelectrics*, 2002, 45, 39–48
- [24] J. Schwarzkopf, M. Schmidbauer, A. Duk, A. Kwasniewski, S. B. Anooz, G. Wagner, A. Devi and R. Fornari, *Thin Solid Films*, 2011, 520, 239–244
- [25] R. Kužel and J. Buršík, *Thin Solid Films*, 2013, 530, 2–8
- [26] Š. Kunej, A. Veber and D. Suvorov, *J. Am. Ceram. Soc.*, 2013, 96, 442–446
- [27] K.-i. Katsumata, C. E. J. Cordonier, T. Shichi and A. Fujishima, *J. Am. Chem. Soc.*, 2009, 131, 3856–3857
- [28] J. Schwarzkopf, M. Schmidbauer, T. Remmele, A. Duk, A. Kwasniewski, S. Bin Anooz, A. Devi and R. Fornari, *J. Appl. Crystallogr.*, 2012, 45, 1015–1023
- [29] D. Tsymbarenko, I. Korsakov, A. Mankevich, G. Girichev, E. Pelevina and A. Kaul, *ECS Trans.*, 2009, 25, 633–638
- [30] B. M. Nichols, B. H. Hoerman, J.-H. Hwang, T. O. Mason and B. W. Wessels, *J. Mater. Res.*, 2003, 18, 106–110
- [31] M. V. Romanov, I. E. Korsakov, A. R. Kaul, S. Y. Stefanovich, I. A. Bolshakov and G. Wahl, *Chem. Vap. Deposition*, 2004, 10, 318–324
- [32] A. Onoe, Y. Tasaki, and K. Chikuma, *J. Cryst. Growth*, 2005, 277, 546–554
- [33] P. Chin Goh, K. Yao and Z. Chen, *Appl. Phys. Lett.*, 2011, 99

- [34] W.S. Rees Jr, Introduction, in: W.S. Rees Jr (Ed.), CVD of Non-Metals, VCH Publishers, 1996.
- [35] D.C. Bradley, *Polyhedron* 13 (1994) 1121.
- [36] J. Aarik, A. Aidla, A. Jaek, M. Leskela, L. Niinisto, *J. Mater. Chem.* 4 (1994) 1299.
- [37] J.P. Fachler, A. Avdeef, *Inorg. Chem.* 13 (1974) 1864.
- [38] C.R. Erasmus, J.C.A. Boyens, *Acta Crystallogr. B* 26 (1970) 1843.
- [39] S.R. Drake, M.B. Hursthouse, K.M.A. Malik, D.J. Otway, *J. Chem. Soc. Dalton Trans.* (1993) 2579.
- [40] Malandrino, G.; Castelli, F.; Fragalà, I. L. *Inorg. Chim. Acta*, 1994, 224, 203
- [41] Zaira Lipani, Maria R. Catalano, Patrizia Rossi, Paola Paoli, and Graziella Malandrino *Chem. Vap. Deposition* 2013, 19, 22–28
- [42] Malandrino, G.; Perdicaro, L. M. S.; Fragalà, I. L. *Chem. Vap. Deposition*, 2006, 12, 736
- [43] Lo Nigro, R.; Toro, R.; Malandrino, G.; Fragalà, I. L.; Rossi, P.; Dapporto P. J. *Electrochem. Soc.* 2004 151, F206.
- [44] Lo Nigro, R.; Malandrino, G.; Fragalà, I. L.; Bettinelli, M.; Speghini, A. *J. Mater. Chem.*, 2002, 12, 2816
- [45] Malandrino, G.; Benelli, C.; F. Castelli, F.; Fragalà I. L. *Chem. Mater.* 1998, 10, 3434
- [46] Malandrino, G.; Fragalà, I. L.; Aime, S.; Dastrù, W.; Gobetto, R.; Benelli, C. *J. Chem. Soc. Dalton Trans.* 1998, 1509.
- [47] Malandrino, G.; Incontro, O.; Castelli, F.; Fragalà, I. L.; Benelli, C. *Chem. Mater.* 1996, 8, 1292.
- [48] Drake, S. R.; Lyons, A.; Otway, D. J.; Slawin, A. M. Z.; Williams, D. J. *J. Chem. Soc. Dalton Trans.* 1993, 2379.
- [49] Drake, S. R.; Hursthouse, M. B.; Malik, K. M. A.; Miller, S. A. S.; Otway, D. J. *Inorg. Chem.* 1993, 32, 4464.

- [50] Bradley, D. C.; Chudzynska, H.; Hursthouse, M. B.; Motevalli, M. *Polyhedron* 1994, 13, 7.
- [51] CrysAlisPro, Agilent Technologies (2011).
- [52] Burla, M.C.; Caliandro, R.; Camalli, M.; Carrozzini, B.; Cascarano, G. L.; Da Caro, L.; Giacovazzo, C.; Polidori, G.; Spagna, R. *J. Appl. Cryst.*, 2005, 38, 381-388.
- [53] Gruene, T.; Hahn, H. W.M; Luebben, A. V.; Meilleur, F.; Sheldrick, G. M. *J. Appl. Cryst.*, 2014, 47, 462-466.
- [54] Nardelli, M. *J. Appl. Cryst.*, 1995, 28, 659.
- [55] Macrae, C. F.; Bruno, I. J.; Chisholm, J. A.; Edgington, P. R.; McCabe, P.; Pidcock, E.; Rodriguez-Monge, E.; Taylor, R.; van de Streek; J. Wood, P. A. *J. Appl. Crystallogr.* 2008, 41, 466-470.
- [56] M. R. Catalano, A. L. Pellegrino, P. Rossi, P. Paoli, P. Cortelletti, M. Pedroni, A. Speghini, and G. Malandrino, *New J. Chem.*, 2017, 41(12), 4771-4775.

CHAPTER 5

Validation of “Li(hfa)•glyme” through applications in PI-MOCVD processes of Lithium Niobate films

Coordination chemistry of alkali (M^+) and alkaline earth cations (M^{2+}) started developing rapidly in the 1970s. The reasons for such a delayed interest in the field could be attributed to the following: (i) the chemistry of these elements had been considered modest and noticeable only with the help of the ionic model;^[1] (ii) compared to the commonly studied transition metal ions, the complexing ability of alkali and alkaline metals is weaker; and above all (iii) there had been no apparent necessity for an interest in such studies. Consequently, any observation which evidenced a coordinative interaction of these alkali and alkaline-earth was given little importance.

With the advancement in the scientific understanding of alkali metal coordination chemistry, there has been a growing interest in lithium, which is mainly due to the actual and potential applications of Li^+ in science, medicine, and technology.^[2] Out of these, Lithium niobate ($LiNbO_3$, LN) is a crucial technological material with numerous piezoelectric, pyroelectric, acousto-optic, electro-optic, and non-linear optical devices. $LiNbO_3$ thin films are appealing due to their potential to enhance optical devices' quality through energy-saving and single crystal, miniaturization, and hybridization with silicon technologies. Countless deposition techniques have been tested for the growth of $LiNbO_3$ films: pulsed laser deposition,^[3,4] sol-gel,^[5,6] rf-sputtering,^[7,8] metal-organic chemical vapor deposition (MOCVD)^[9-17]. MOCVD has stronger benefits over other techniques, such as elevated oxygen partial pressure, better compositional control of crystalline phase, and even epitaxial growth for lattice-matched substrates, scalability, and enhanced step coverage. For LN deposition, numerous MOCVD processes have been tested: low pressure-single reliable source MOCVD, using a mixture of solid Li and Nb metal-organic precursors, introduced into a hot evaporation zone for simultaneous evaporation,^[10,12,13] conventional low-pressure thermal MOCVD, evaporating Li and Nb precursors separately,^[11, 13-17] or atmospheric pressure aerosol assisted MOCVD, in which precursor solution was carried into

the evaporator in the form of ultrasonically generated aerosol^[9]. Several combinations of Li and Nb precursors have been studied: Li(tmhd) and Nb(tmhd)₄^[10,12,13] (only in single solid source MOCVD), both alkoxide precursors Li(OBut) and Nb(OEt)₅^[11,15] or mixture of Li(tmhd) and Nb(OEt)₅^[14,16,17] (Htmhd=2,2,6,6-tetramethyl-3,5-heptanedionate). In aerosol-assisted MOCVD,^[8] a complex bimetallic precursor has been used, which is developed as a reaction product between Li(tmhd) and Nb(OEt)₅ in organic solution. LiNbO₃ films on different substrates have been deposited by MOCVD as polycrystalline or epitaxial twinned or not twinned. Despite these promising advantages, industrial applications of an MOCVD process are still limited, likely because starting molecular compounds' commercial availability is insufficient.

Lithium precursors for vapor phase processes, either MOCVD or atomic layer deposition, are very scarce.^[18,19] Thus, there has been a growing need to engineer these kinds of precursors. In this regard, the status of β -diketonates as anionic ligands for M^{Z+} is respectable and is one of the earliest to be recognized.^[20] The presence of highly electronegative fluorine atoms favored the conditions for the formation of stable complexes.

In this regard, our previous studies have revealed the importance of glyme in stabilizing complexes with the desired thermal properties for MOCVD applications.^[21,22] They promote thermally stable, and volatile adducts by behaving like crown ethers in terms of coordinating/solvating ions of the alkaline-earth,^[23,24] the transition^[25,26] and the rare-earth metals^[22,27] through oxygen-ion complexation, i.e., chelating properties. Also, glymes have many other beneficial properties, including being liquid at various temperatures (typically >200°C), low viscosity, high chemical, thermal stability, relatively low vapor pressure, and low toxicity.^[28] Due to these excellent solvent properties, glymes have been significantly used as solvents in liquid-assisted MOCVD processes, either liquid injection or aerosol assisted.^[29,30] Glymes have high boiling points and exist as a liquid over a wide range of temperatures (>200°C, or even >300°C) except monoglyme. Most glymes show low vapor pressures (<0.5 mmHg at 20 °C) except mono- and diglyme compared to some volatile organic solvents. Furthermore, many simple glymes exhibit low viscosities in the range 1–4 mPa s at 20°C. They are entirely miscible with both water and organic solvents (such as ethanol, acetone, benzene, and octane).^[28]

Cumulatively, from all considerations mentioned above, we report on a simple direct liquid injection metal-organic chemical vapor deposition approach which is applied to the fabrication of LiNbO_3 nanostructured thin films using the fluorinated β -diketonate complexes, i.e., novel lithium, “Li(hfa)•L” (Hhfa= hexafluoroacetylacetone, L = dimethoxyethane (monoglyme) **1**, bis(2-methoxyethyl)ether (diglyme) **2**, 2,5,8,11-tetraoxadodecane (triglyme) **3** and 2,5,8,11,14-pentaoxapentadecane (tetraglyme) **4** adducts as they represent single-source precursors of lithium along with commercially purchased $\text{Nb}(\text{tmhd})_4$. Structural, morphological, and compositional characterization of the films shows the formation of polycrystalline thin films with a very uniform surface. The depositions are compared in respect to the deposition from the commercially available $\text{Li}(\text{tmhd})$ for the functional validity of the precursors synthesized.

5.1 Experimental Section

Materials and methods. The “Li(hfa)•glyme” precursors were synthesized as previously reported in refs.^[31] The films were deposited on C-sapphire (0001), R-sapphire (1102), A-sapphire (1120), and Si (100) under low-pressure in a pulsed liquid injector MOCVD reactor at temperature > 700 °C. Li's appropriate ratio: Nb complexes were dissolved in organic solvent 1,2-dimethoxyethane (monoglyme) and evaporated at 200-240°C, a suitable temperature for efficient vaporization without thermal degradation. The subsequent mixture of precursors and solvent vapor is transported by a carrier gas ($\text{Ar}+\text{O}_2$) into a deposition chamber to the hot substrate where precursor decomposition occurs, causing the growth of the oxide film. The phase structure of films was studied by X-ray diffraction (XRD) using a Panalytical Benchtop diffractometer equipped with $\text{Cu K}\alpha$ operating at 40 kV and 30 mA using a scan step 0.02° . Film morphology was analyzed by FE-SEM using a Thermo Scientific APERO field emission microscope. The EDX spectra were recorded using a Thermo Scientific UltraDry silicon drift windowless X-ray detector, measuring 5.89 keV as the full width half maximum (FWHM) $\text{Mn-K}\alpha$. Raman spectra were collected at room temperature using a Jobin-Yvon/Horiba LabRam and Renishaw Raman RM-1000 spectrometers in backscattering geometry. The 514.5 nm line of a He^+ ion laser-focused on a spot size of about $1 \mu\text{m}$ and 100x magnification. The study was conducted in a cross-

polarization mode where Incident laser and scattering light have been polarized perpendicular to each other (HV).

5.2 Results and Discussions

The novel Li precursors synthesized as reported in chapter 2^[31] have been the starting point for the MOCVD growth of LiNbO₃. It is worth noting that the complexes have been synthesized with a high yield in a single step, low-cost route from commercially available chemicals. The adducts **1** and **2** are solid, while **3** and **4** are liquid and are soluble in common organic solvents such as ethanol, dichloromethane, acetone.

The structure of adduct $[\text{Li}_{12}(\text{hfa})]_{12} \cdot \text{monoglyme} \cdot 4\text{H}_2\text{O}$ (**1**) and $[\text{Li}_2(\text{hfa})_2 \cdot \text{diglyme} \cdot \text{H}_2\text{O}]$ (**2**), is depicted in fig. 5.1a) and 5.1b). The adduct **1** has a polymeric structure in which, in addition to the β -diketonate hfa, an H₂O molecule is also coordinated to the Li-ion. Adduct **2** shows a dimeric structure.

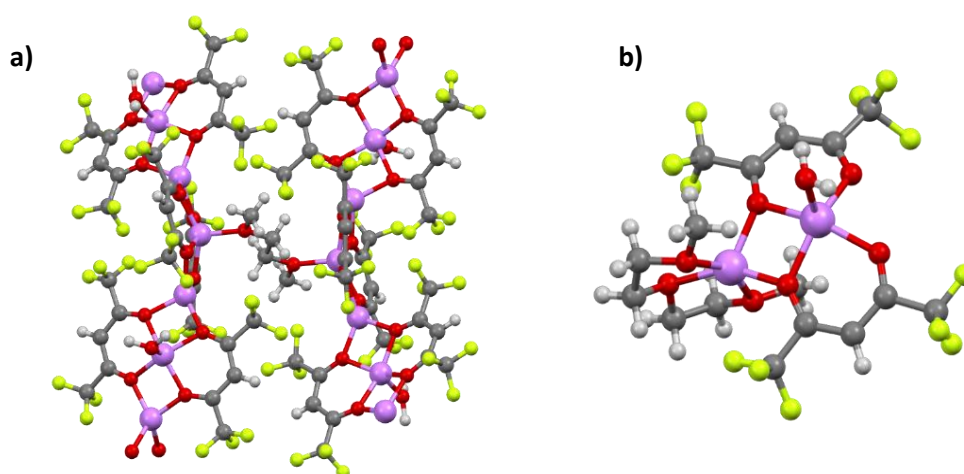


Fig. 5.1 a) Ball and stick view of the adduct **1** and **b)** adduct **2**

Regarding applications in MOCVD processes, these precursors' thermal properties and solubility make them attractive to prepare solid oxide phases through a liquid-assisted MOCVD approach. Also, the presence of H₂O is not a drawback as an excellent thermal behavior for MOCVD applications has been previously observed for the $\text{Mg}(\text{hfa})_2 \cdot 2\text{H}_2\text{O} \cdot 2\text{diglyme}$ ^[32] and $\text{Co}(\text{hfa})_2 \cdot 2\text{H}_2\text{O} \cdot \text{tetraglyme}$ ^[33] adducts, despite the presence of H₂O molecules in the coordination sphere.

The films deposited were characterized by XRD and FE-SEM analysis. These investigations allowed us to evaluate and validate the precursors' functional property to deposition alkali metal oxide phases.

XRD analysis

In fig. 5.2, 5.3, 5.4, the XRD patterns of the LiNbO_3 films, obtained through PI-MOCVD, are reported in the different adducts' functions and the substrates used.

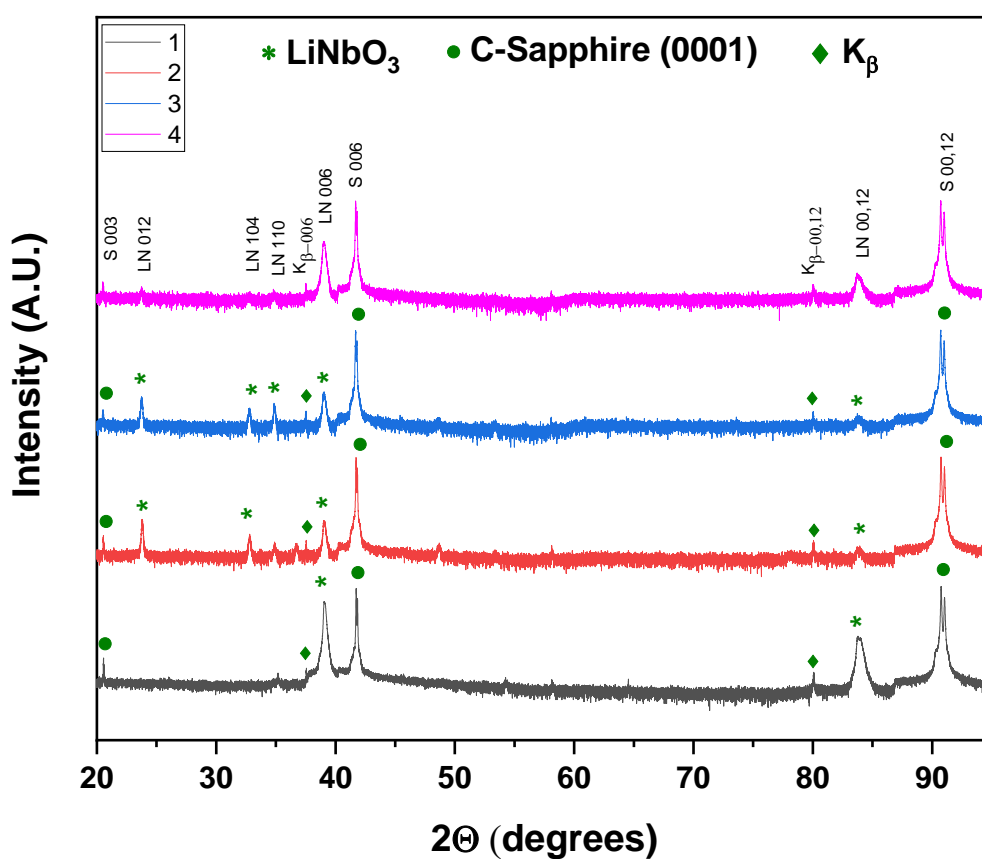


Fig. 5.2. X-ray diffraction patterns of the LN films deposited on C-sapphire (0001).

The XRD measurements of LiNbO_3 deposited on C-Sapphire (0001) (fig. 5.2) are polycrystalline in nature and exhibit patterns associated with a rhombohedral phase according to the space group $R3c$, JCPDS no. 020-0631. The corresponding peaks at 2θ values of 23.83° , 32.79° , 34.94° , 39.08° , and 83.83° are attributed to 012, 104, 110, 006 and 00,12 reflection planes.

The XRD measurements of LiNbO_3 deposited on A-Sapphire (1120) (fig. 5.3) exhibit patterns associated with a rhombohedral phase according to the space group $R3c$, JCPDS no. 020-0631.^[34] The corresponding 2θ values of 23.73° , 34.84° , 39.08° , 73.61° , and 83.83° are attributed to 012, 110, 006, 220, and 00,12 reflection planes.

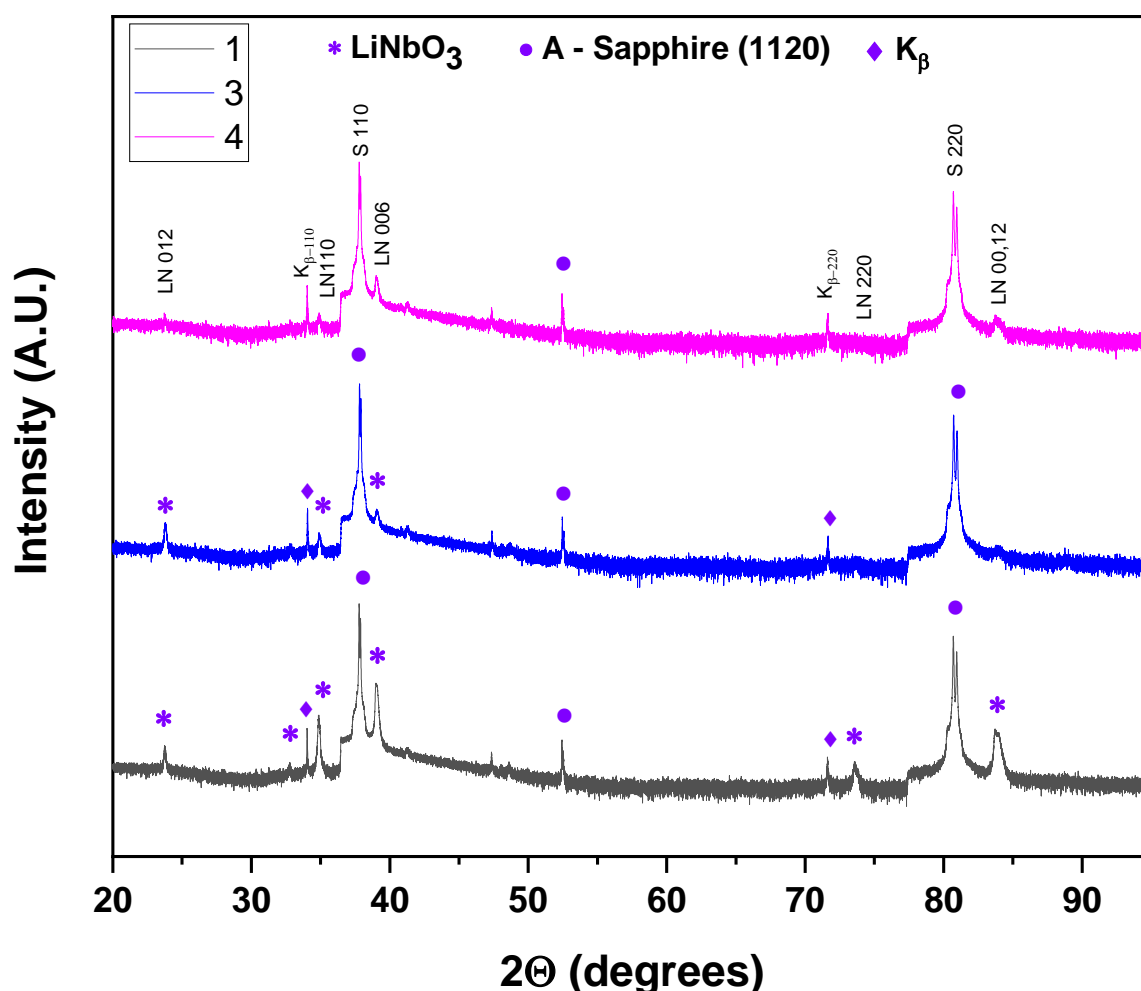


Fig. 5.3 X-ray diffraction patterns of the LN films deposited on A-sapphire (1120).

The XRD measurements of LiNbO_3 deposited on R-Sapphire (1102) (fig. 5.4) exhibit patterns associated with a rhombohedral phase according to the space group $R3c$, JCPDS no. 020-0631. The corresponding 2θ values of 23.85° , 34.95° , 48.65° , and 62.50° are attributed to 012, 110, 024, and 300 reflection planes.

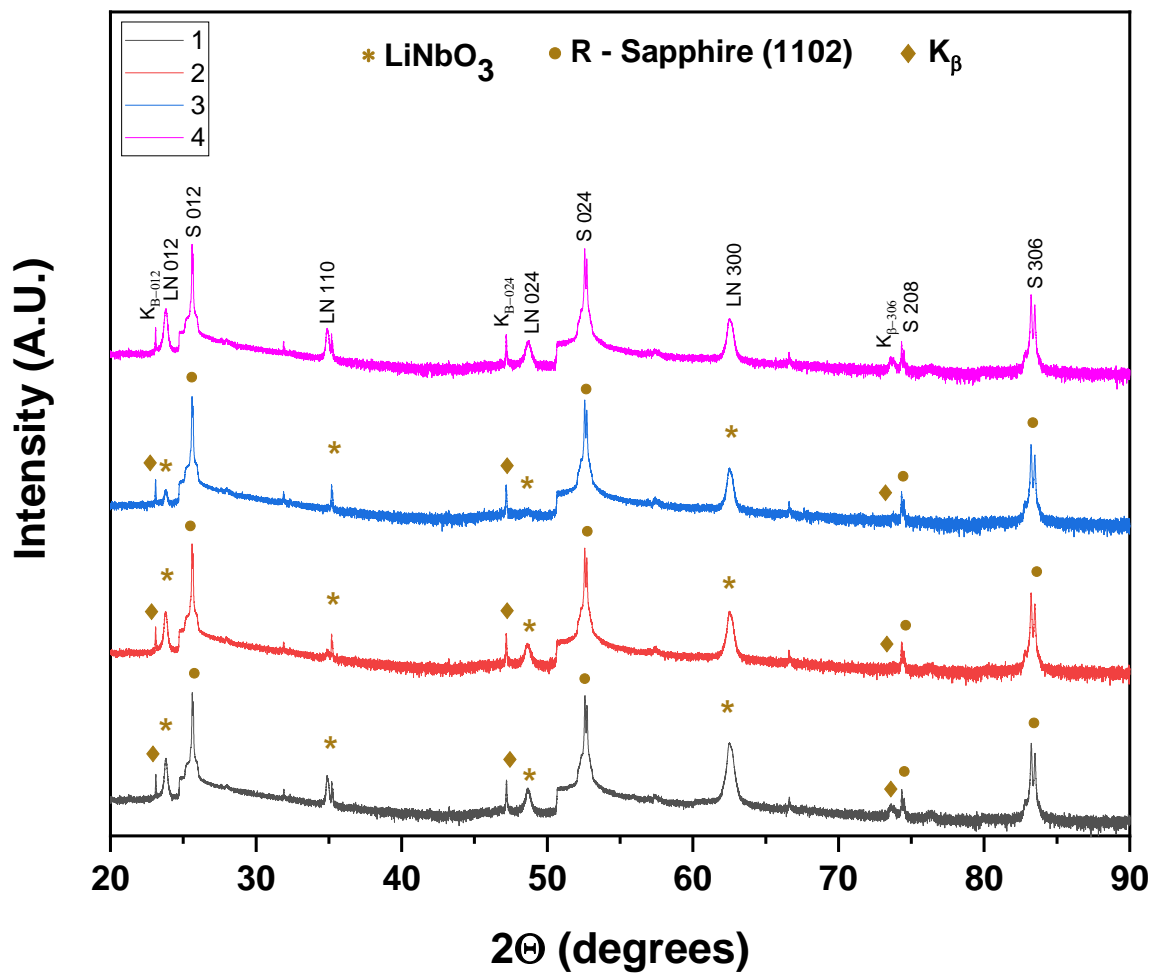


Fig. 5.4. X-ray diffraction patterns of the LN films deposited on R-sapphire (1102).

The XRD measurements of LiNbO₃ deposited on Si (100) (fig. 5.5) exhibit patterns associated with a rhombohedral phase according to the space group *R3c*, JCPDS no. 020-0631. The corresponding 2θ values of 23.77°, 34.95°, and 39.19° are attributed to 012, 110, and 006 reflection planes.

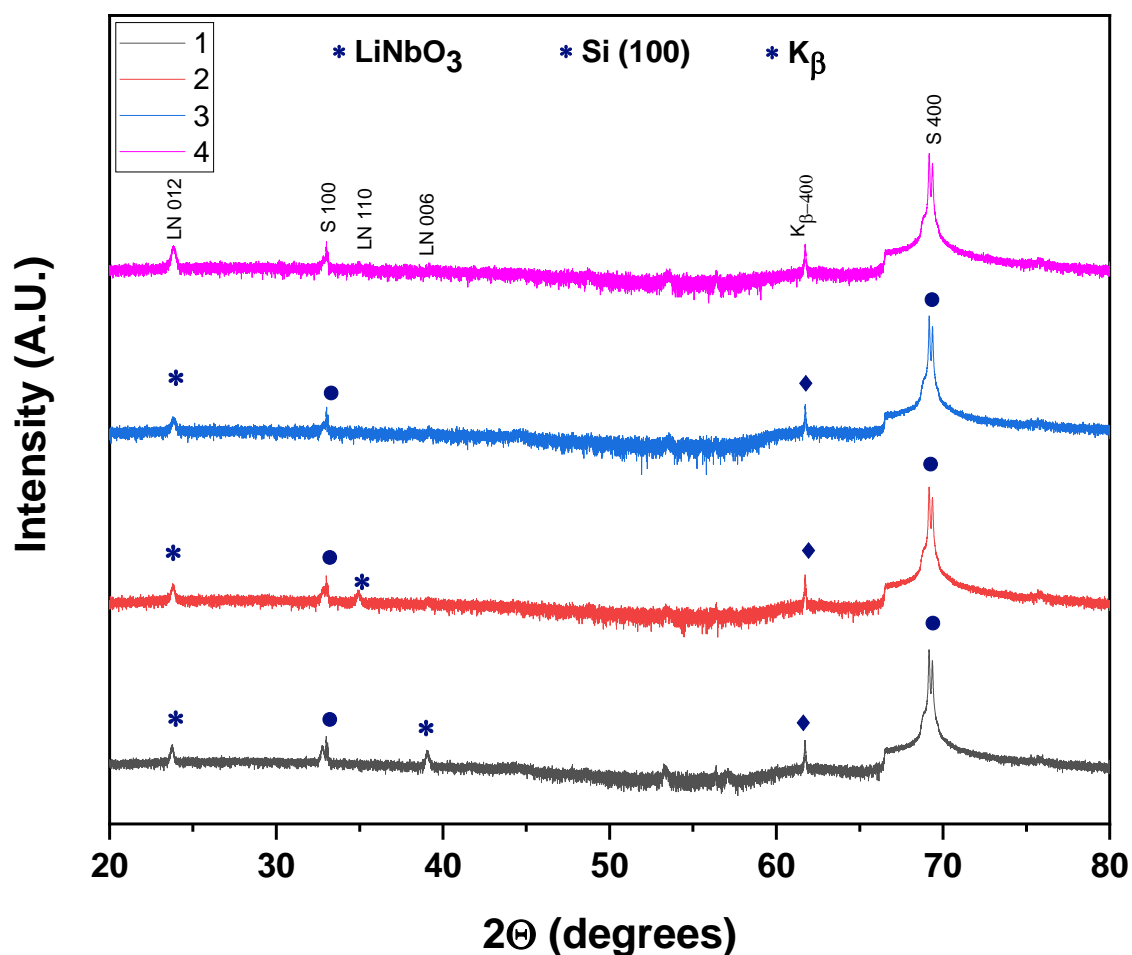


Fig. 5.5. X-ray diffraction patterns of the LN films deposited on Si (100).

EDX analysis

Energy dispersive X-ray (EDX) analysis (fig. 5.6a –5. 6d) was performed to support further the hypothesis that no fluorine phases are present after the deposition. The quantitative analysis was not performed owing to the ultra-light Li K X-rays at 55 eV. Thus, the analysis is

only limited to support Nb's presence and the absence of fluorine contamination in the synthesized phase. The adduct's EDX spectrum shows the typical L line of the Nb and the $K\alpha$ of the Al and O. We also observe Si $K\alpha$ for the depositions on the Si substrate and we also observe a small Carbon peak at 0.277 KeV in case of deposition with adduct **4** on C-sapphire.

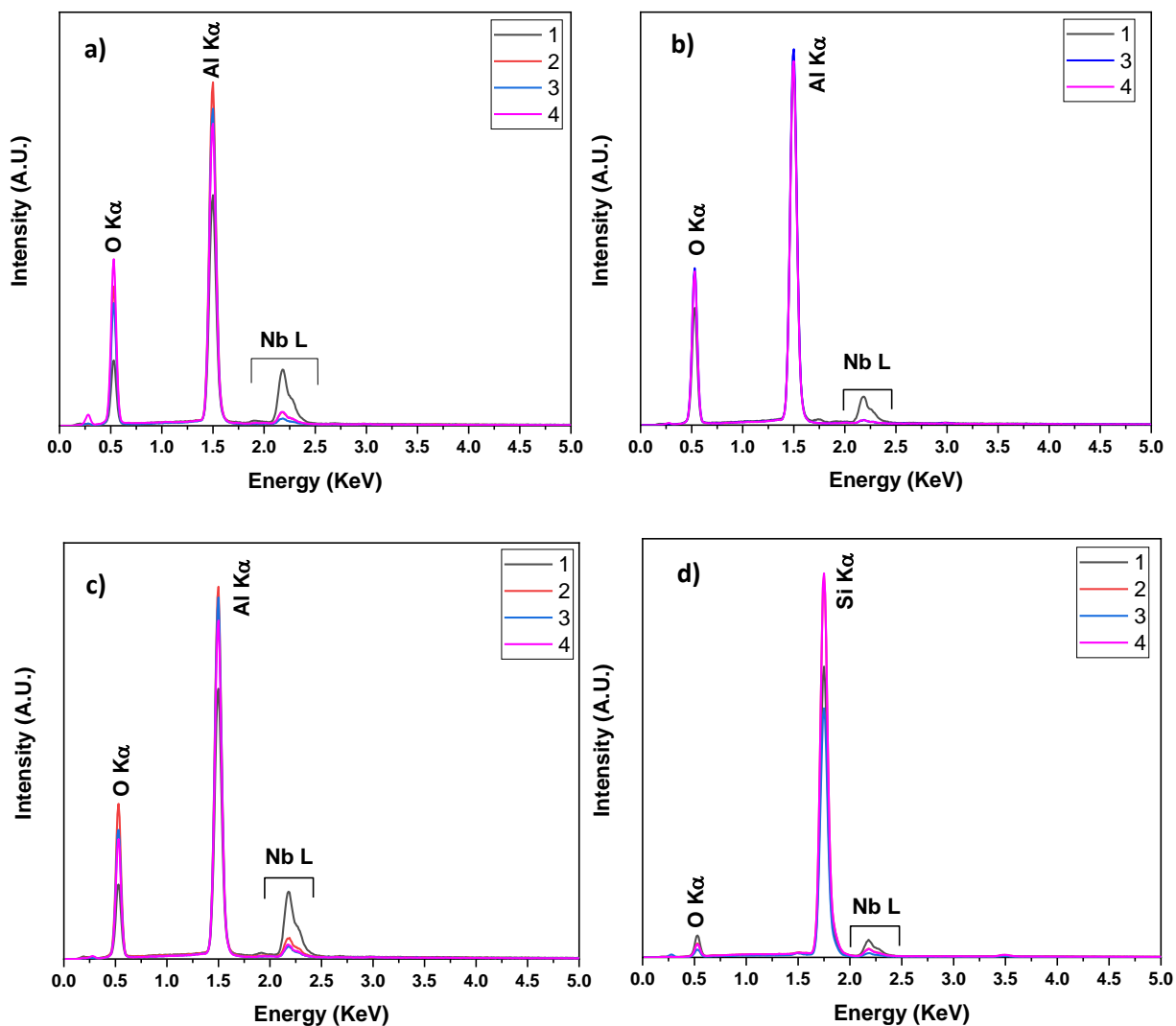


Fig. 5.6 EDX spectra of the LiNbO_3 films deposited on **a)** C-sapphire (0001) **b)** A-sapphire (1120), **c)** R-sapphire (1102), and **d)** Si (001).

FE-SEM characterization

The microstructure and morphology of LiNbO_3 films in fig. 5.7 – fig. 5.10 have been studied by field emission scanning electron microscopy (FE-SEM). The FE-SEM images of the films

deposited do not show homogeneous surfaces. The size, shape, and forms of the grains are strictly influenced by the precursor's nature and the substrate used. The films show two distinct morphology, i.e., the presence of trigonal and needle-shaped structures., which are about 1.3 μm to 5 μm large. The film grown from adduct **1** (Fig. 5.7a) shows a close packing of the crystalline grains coalesced together with an average size of about 500 nm, while LN deposition with adduct **2**, **3**, and **4** shows a non-homogenous film morphology with a grain size of about 1-2 μm , predominantly triangular.

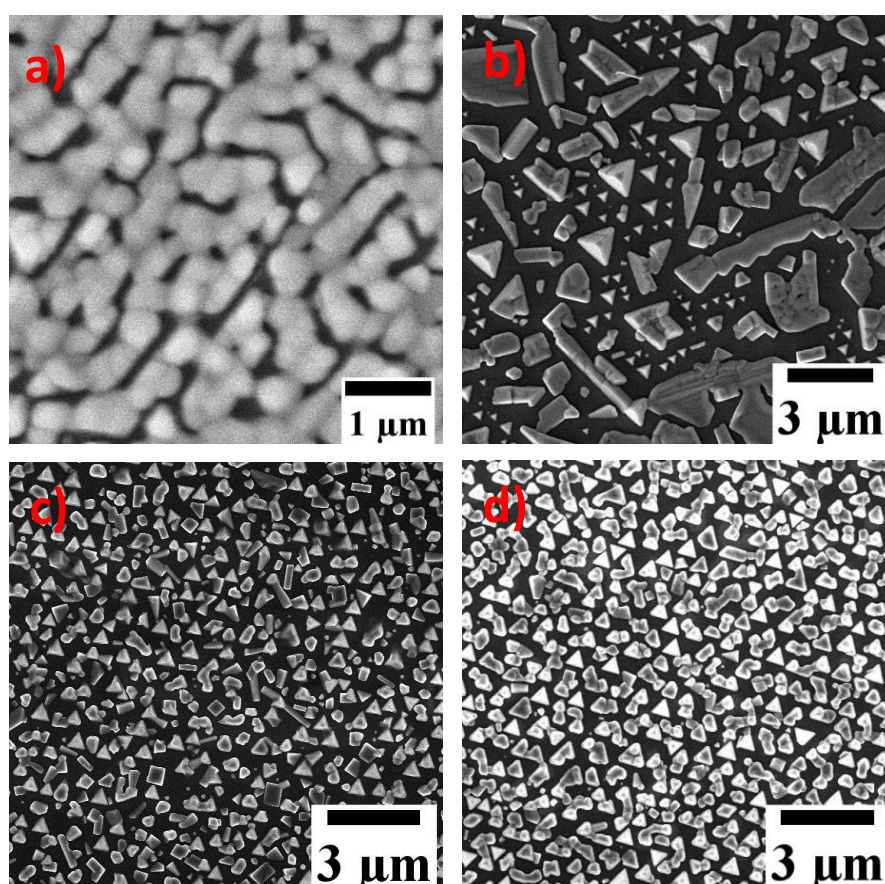


Fig. 5.7. FE-SEM images of the deposited Lithium Niobate at 775°C on C-sapphire (0001) using **a)** adduct **1**, **b)** adduct **2**, **c)** adduct **3**, **d)** adduct **4**

The LN films' FE-SEM images deposited on A-sapphire (1120) (fig. 5.8) using adduct 1 show a homogenous surface with coalesced grains. The average size of the grains is about 700 nm.

On the contrary, LN films using adduct **3** show non-homogenous films with grains of different sizes, dimensions, and shapes, predominantly triangular in nature and grain size of about 1-3 μm in size. Similarly, the LN film using adduct **4** shows a similar nature to the film obtained from adduct **3** with different granular structures and sizes.

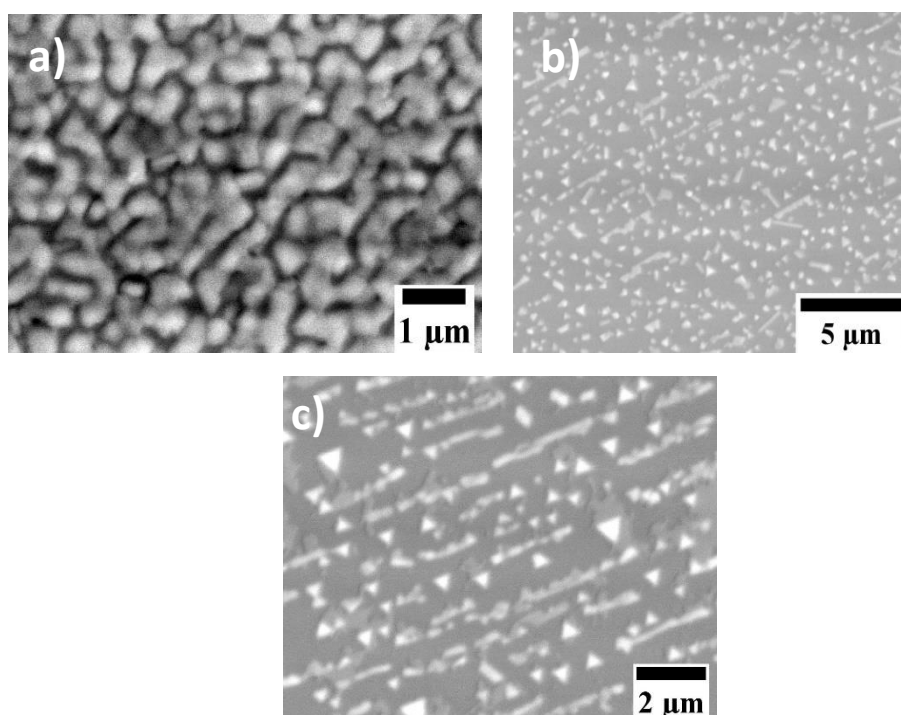


Fig. 5.8. FE-SEM images of the deposited Lithium Niobate at 775°C on A-sapphire (1120) using **a)** adduct **1**, **b)** adduct **3**, **c)** adduct **4**

The LN films' FE-SEM images deposited on R-sapphire (1102) (fig. 5.9) using adduct 1 show a homogenous surface with coalesced grains. The average size of the grain is about 500 nm. The LN films using adducts **2** and **3** show homogenous films with much smaller grains, of about 100-500 nm in size, of different shapes. Similarly, the LN films using adduct **4** show similar nature to those grown from adducts **2** and **3**, but with much smaller granular structures and about 100 nm.

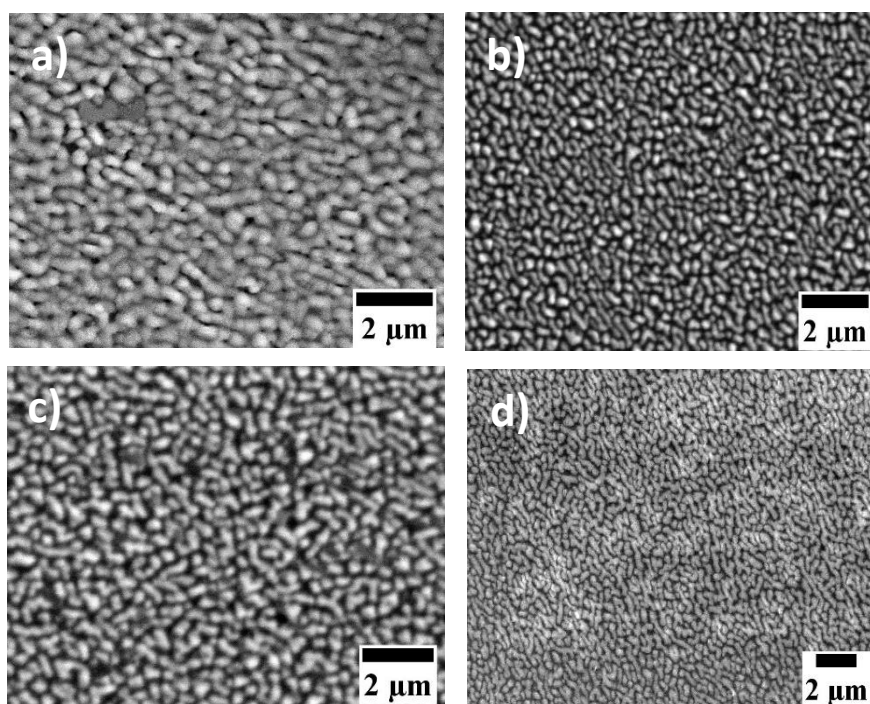


Fig. 5.9. FE-SEM images of the deposited Lithium Niobate at 775°C on R-sapphire (1102) using **a)** adduct **1**, **b)** adduct **2**, **c)** adduct **3**, and **d)** adduct **4**

The LN films' FE-SEM images deposited on Si (100) (fig. 5.10) using adduct 1 show a homogenous surface with a large plate-like grain. The average size of the grain is about 5-7 μm . LN films using adduct 2 and 3 show homogenous films with much smaller grains of different shapes coalesced together and an average grain size of about 100 nm. Similarly, the LN films using adduct 4 show a similar nature but with much smaller granular structures.

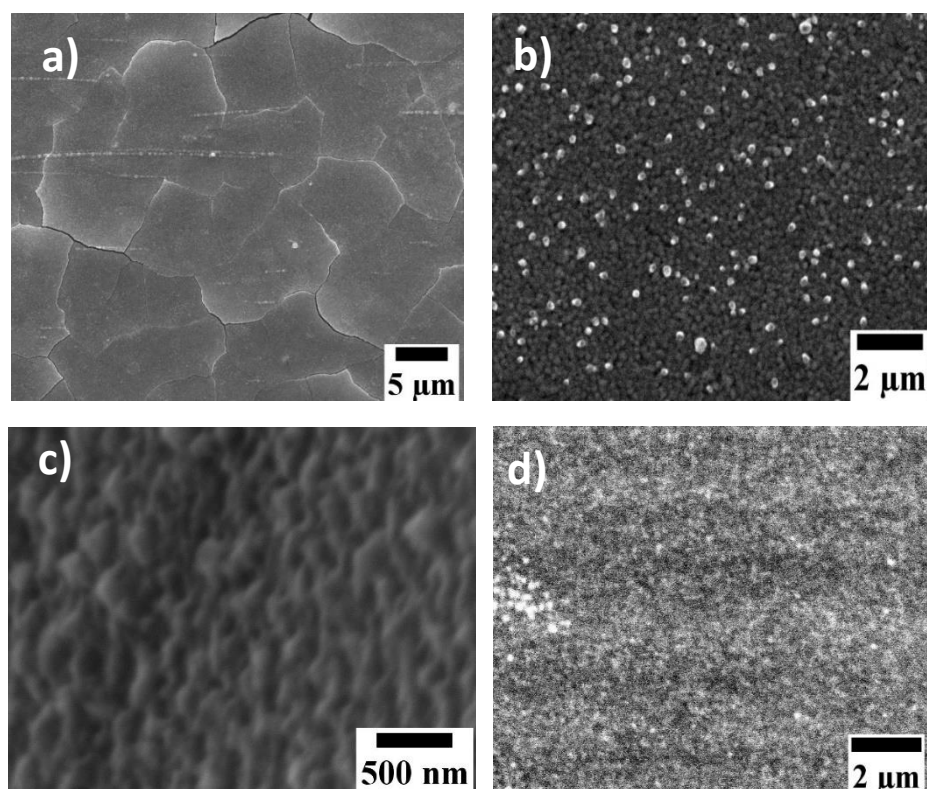


Fig. 5.10. FE-SEM images of the deposited Lithium Niobate at 775°C on Si (100) using **a)** adduct **1**, **b)** adduct **2**, **c)** adduct **3**, and **d)** adduct **4**.

Raman Spectroscopy

LN film phase characterization through Raman spectroscopy has been done in great length by Margueron et al.^[35] and Bartaszyte et al.^[36] Accordingly, the present study incorporates the method and analysis^[36-38] to work published by them in this regard. LiNbO_3 has $4A_1 + 9E$ Raman active modes as calculated by the lattice data.^[35] So, generally, one should observe 13 modes of LiNbO_3 but in the contrary, a much lesser number of modes are observed than expected, which can be explained by the close frequencies of several modes and the spectrum's overlapping mode profiles. Additionally, one may observe the peaks' wavenumbers significantly shifted from the standard values due to strain effects.^[36] Furthermore, the oblique modes may well be observed with intermediate frequencies between those of normal modes^[39] due to the oblique orientation of the *c*-axis^[40] with respect to the laser beam. Also, another critical thing to note is that according to Raman selection rules,^[35] only *E*(TO) modes have been observed in crossed polarization

configuration for films deposited by MOCVD and E(5TO) overlaps with E(6TO), and thus we only observe them as a single peak in the spectra.

Cumulatively, gathering information from the previous work, the Raman spectra were measured in crossed polarization configurations,^[35] i.e., LN films deposited on C-sapphire A-sapphire, R-sapphire, and Si substrates by PI-MOCVD. The wavenumbers of Raman modes of LiNbO₃ have been tabulated in Table 5.2.

Table 5.2: (Bartasyte et al.^[37])

Phase	Space group	Raman active modes (cm ⁻¹)
LiNbO ₃	R3c	155, 199, 240, 241, 253, 265, 276, 277, 298, 334, 334, 343, 364, 370, 421, 425, 433, 457, 580, 632, 659, 667, 870, 879

In the fig. 5.11, we observe the LiNbO₃ phase according to the modes previously reported corresponding to the wavenumbers as suggested, and thus it confirms the presence of only LiNbO₃ phase on C-sapphire deposition using adducts **1**, **2**, **3**, and **4**. We observe some oblique modes that arise due to microstrain or the film orientation, as explained previously.^[38] This aspect is not so straightforward and needs to be analyzed further. It might be further noted that adduct **1** shows only the dominant Raman modes, indicating a pure phase Lithium niobate film, highly oriented on C-sapphire. While adducts **2**, **3**, and **4** show the required LN modes, as supported by XRD analysis, it reveals a polycrystalline nature.

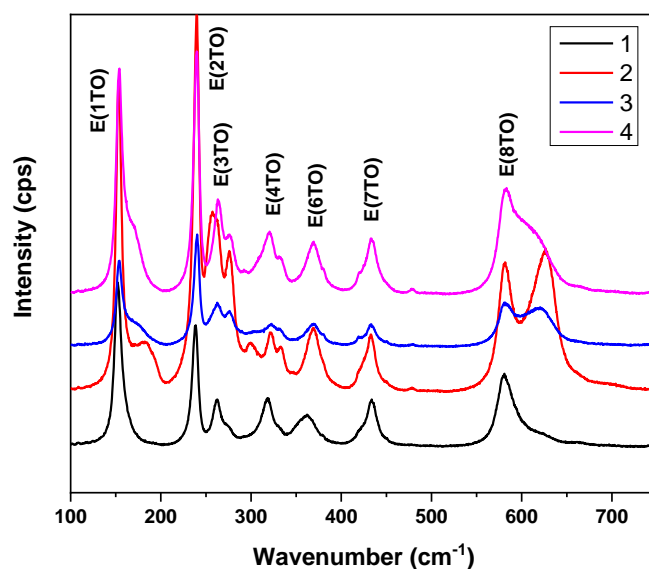


Fig. 5.11. Raman spectra of the deposited LiNbO_3 on C-sapphire (0001) at cross-polarization mode HV.

In the fig. 5.12, we observe the LiNbO_3 phase according to the wavenumbers as suggested, and thus it confirms the presence of only the LiNbO_3 phase on A-sapphire deposition using adducts **1**, **2**, **3**, and **4**. We observe the presence of some oblique modes much lesser than the depositions on c-sapphire, which might suggest lesser strain on the film orientation, as explained previously. This aspect is not so straightforward and needs to be further analyzed. We also observe some sharp peaks which arise due to the sapphire substrate.

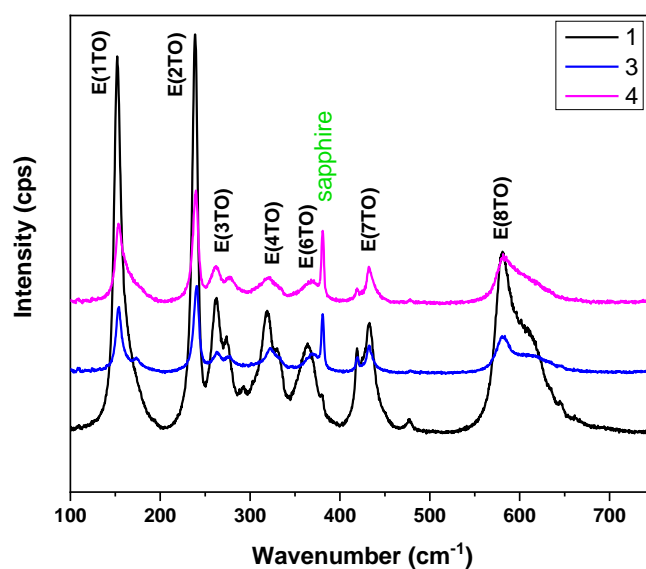


Fig. 5.12 Raman spectra of the deposited LiNbO_3 on A-sapphire (1120) at cross-polarization mode HV.

In the fig. 5.13, we observe the LiNbO_3 phase according to the wavenumbers as suggested, and thus it confirms the presence of only the LiNbO_3 phase on R-sapphire deposition using adducts **1**, **2**, **3**, and **4**. We do observe the presence of some oblique modes as well.

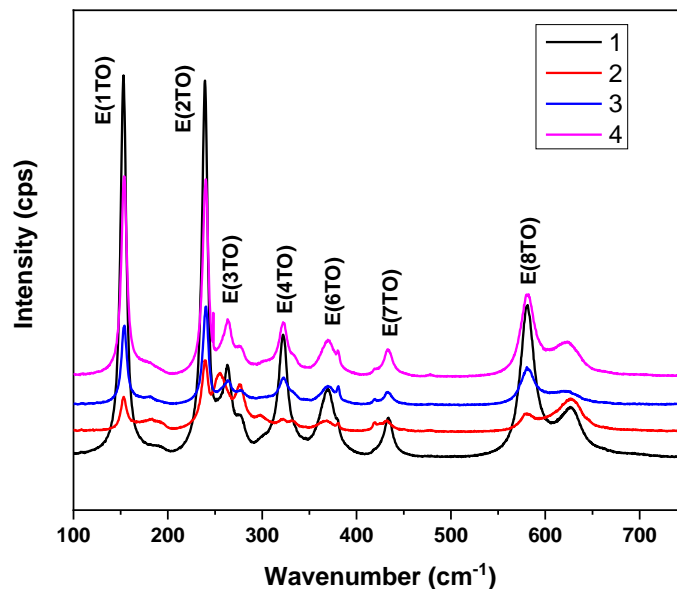


Fig. 5.13. Raman spectra of the deposited LiNbO_3 on R-sapphire (1102) at cross-polarization mode HV.

It is challenging to analyze the deposition on the Si substrate (fig. 5.14) due to the substrate's large peak. Still, the Raman spectra from the depositions show no secondary phases.

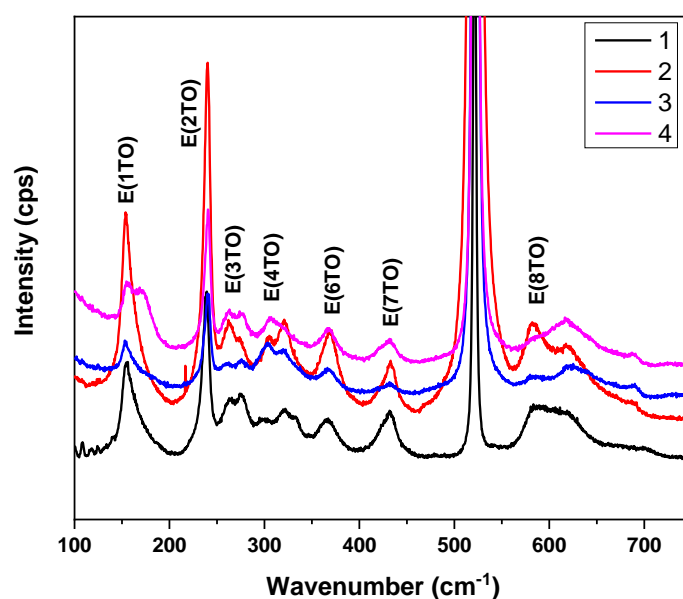


Fig. 5.14. Raman spectra of the deposited LiNbO_3 on Si (100) at cross-polarization mode HV.

In comparing the above characterization data and the XRD analysis, one can indeed observe a highly oriented growth of pure phase LN films on C-sapphire (0001) using adduct **1**. The claim is further supported by EDX measurement, which shows no presence on fluorine and Raman spectra, which shows all the active Raman modes in cross-polarization configuration with no oblique modes, suggesting potential epitaxial film characteristics.

5.3 Conclusions

In summary, a simple direct liquid injection PI-MOCVD process has been applied to the fabrication of LiNbO₃ based films, using the “Li(hfa)•glyme” complexes, which act as single-source precursors for oxide phases. The deposited films exhibit LiNbO₃ phases depending on the substrate nature, and precursors used. Nevertheless, the present results of films without any fluorine contamination indicate the synthesized Li adducts as promising sources for the deposition of LiNbO₃ films.

The preliminary results confirm that the MOCVD approach yields reproducibly and selectively the synthesis of the pure LiNbO₃ phase on C-sapphire (0001) substrate and primarily with the adduct **1**, i.e. [Li(hfa)]₁₂•monoglyme•4H₂O complex. These final goals have been achieved through an accurate optimization of the operative parameters, such as the deposition temperature and the precursors' vaporization temperature.

Finally, the current PI-MOCVD approach provides a strong alternative for using alkali metal precursors in the liquid state. This strategy paves the way for the synthesis of other precursors to be utilized to fabricate thin films and oxide phases, irrespective of any substantial consideration to high residues.

REFERENCES

- [1] C. S. G. Phillips and R. J. P. Williams, Vol. 2, Oxford University Press, Oxford, 1966, Chapter 20.

- [2] Lithium-Current Applications in Science, Medicine, and Technology; Bach, R. 8, Ed.; Wiley-Interscience: New York, NY, 1985.
- [3] Shih, W.-C. and Sun, X.-Y., *Physica B* 405, 1619–1623 (2010).
- [4] Akazawa, H. and Shimada, M. J., *Vacuum Sci. Technol.* 26, 281-287 (2008).
- [5] Takahashi, M., Otowa, R., Mori, H., and Sato, S., *J. Appl. Phys.* 96, 6569 (2004).
- [6] Takahashi, M., Iyoda, K., Maeda, Y., Miyauchi, T., Ohkido S. and Sato, S., *J. Appl. Phys.* 103, 034101 (2008).
- [7] Shandilya, S., Tomar, M. and Gupta, V., *J. Appl. Phys.* 111, 102803 (2012).
- [8] Iyevlev, V., Kostyuchenko, A., Sumets, M. and Vakhtel, V., *J Mater Sci: Mater Electron* 22, 1258–1263 (2011).
- [9] Wernberg, A.A., Gysling, H.J., Filo, A.J. and Blanton, T. N., *Appl. Phys. Lett.* 62 (9), 946-948 (1993).
- [10] Lu, Z., Hiskes, R., Dicarolis, S.A., Route, R.K., Feigelson, R.S., Leplingard, F. and Fouquet, J.E., *J. Mat. Res.* 9 (9), 2258-2263, (1994).
- [11] Tanaka, A., Miyashita, K., Tashiro, T., Kimura, M. and Sukegawa, T., *J. Cryst. Growth* 148 (3), 324-326 (1995).
- [12] Feigelson, R.S., *J. Cryst. Growth* 166, 1-16 (1996).
- [13] Lee, S.Y. and Feigelson, R.S., *J. Cryst. Growth* 186, 594-606 (1998).
- [14] Shiratsuyu, K., Sakurai, A., Tanaka, K. and Sakabe, Y., *Jap. J. Appl. Phys.* p1 38 (9B) 5437-5441 (1999).
- [15] Saulys, D., Joshkin, V., Khoudiakov, M., Kuech, T.F., Ellis A.B., Oktyabrsky, S.R. and McCaughan, L., *J. Cryst. Growth* 217, 287-301 (2000).
- [16] Shin, Y. S., Yoshida, M., Akiyama, Y., Imaishi, N. and Jung, S. C. *Jpn. J. Appl. Phys.* 42, 5227-5232 (2003).
- [17] Morohashi, R., Wakiya, N., Kiguchi, T., Yoshioka, T., Tanaka, J. and Shinozaki, K. *Key Eng. Mat.* 388, 179-182 (2009).

- [18] J. A. Ocón, J. G. Murillo, M. Miki-Yoshida, M. N. Cardoza, and O. E. Contreras-López, *J. Cryst. Growth*, 2014, 408, 64–70.
- [19] M. Nisula, Y. Shindo, H. Koga and M. Karppinen, *Chem. Mater.*, 2015, 27, 6987–6993.
- [20] G. A. Guter and G. S. Hammond, *J. Am. Chem. Soc.*, 78, 5166 (1956).
- [21] G. G. Condorelli, G. Malandrino and I. L. Fragalà, *Coord. Chem. Rev.*, 2007, 251, 1931-1950.
- [22] G. Malandrino and I. L. Fragalà, *Coord. Chem. Rev.* 2006, 250, 1605-1620.
- [23] G. Malandrino, I. L. Fragalà, D. A. Neumayer, C. L. Stern, B. J. Hinds and T. J. Marks, *J. Mater. Chem.*, 1994, 4, 1061-1066.
- [24] M. E. Fragalà, R. G. Toro, P. Rossi, P. Dapporto and G. Malandrino, *Chem. Mater.*, 2009, 21, 2062-2069.
- [25] H. Liu, S. Battiato, A. L. Pellegrino, P. Paoli, P. Rossi, C. Jiménez, G. Malandrino and D. Munoz-Rojas, *Dalton Trans.*, 2017, 46, 10986-10995.
- [26] A. Gulino, P. Dapporto, P. Rossi, and I. Fragalà, *Chem. Mater.*, 2003, 15, 3748-3752.
- [27] G. Malandrino, R. Lo Nigro, C. Benelli, F. Castelli and I. L. Fragalà, *Chem. Vap. Deposition*, 2000, 6, 233-238.
- [28] S. Tanga and H. Zhao, *RSC Adv.*, 2014, 4, 11251-11287.
- [29] S. Battiato, J.L. Deschanvres, H. Roussel, L. Rapenne, B. Doisneau, G. G. Condorelli, D. Munoz-Rojas, C. Jiménez and G. Malandrino, *Dalton Trans.*, 2016, 45, 17833-17842
- [30] S.-T. Zhang, M. Modreanu, H. Roussel, C. Jiménez and J.-L. Deschanvres, *Dalton Trans.*, 2018, 47, 2655-2661.
- [31] N. Peddagopu, P. Rossi, C. Bonaccorso, A. Bartasyte, P. Paoli & . Malandrino, *Dalton Trans.*, 2020, 49, 1002.
- [32] M. E. Fragalà, R. G. Toro, P. Rossi, P. Dapporto and G. Malandrino, *Chem. Mater.*, 2009, 21, 2062-2069.

- [33] A. Gulino, P. Dapporto, P. Rossi, G. Anastasi and I. Fragalà, *J. Mater. Chem.*, 2004, 14, 2549-2553.
- [34] Lunberg M 1971 *Acta Chem. Scand.* 25 3337.
- [35] Margueron S, Bartasyte A, Glazer A M, Simon E, Hlinka J and Gregora I 2012 *J. Appl. Phys.* 111 104105
- [36] Bartasyte A, Plausinaitiene V, Abrutis A, Murauskas T, Boulet P, Margueron S, Gleize J, Robert S, Kubilius V and Saltyte Z 2012 *Appl. Phys. Lett.* 101 122902
- [37] Bartasyte A., Plausinaitiene V., Abrutis A., Stanionyte S., Margueron S., Boulet P., T Kobata ,Y. Uesu and J. Gleize., *J. Phys.: Condens. Matter.*, 2013, 25(20):205901.
- [38] A. Bartasyte , V. Plausinaitiene , A. Abrutis, S. Stanionyte, S. Margueron, V. Kubilius c, P. Boulet, S. Huband, P.A. Thomas, *Materials Chemistry and Physics* 149-150 (2015) 622e631
- [39] Veithen M and Ghosez P 2002 *Phys. Rev. B* 65 214302
- [40] He Z B, Setter N, Ono T and Shinozaki K 2009 *Appl. Phys. Lett.* 95 062905

CHAPTER 6

Functional validation of the Na and K β -diketonate glyme adducts: fabrication of Potassium Sodium Niobate nanostructures

Ferroelectric materials exhibit a wide range of functional properties. Some of these materials' sought-after features include piezoelectricity, pyroelectricity, non-linear dielectric behavior, high non-linear optical activity, and switchable polarization.^[1-3] The interest in alternative lead-free piezoelectric ceramics has been the driving factor to develop potassium sodium niobate (KNN) as a prospective source of lead-free piezoelectric materials. KNN is non-toxic, has a high piezoelectric constant, and a high Curie temperature.^[4] These features make it one of the most potentially useful contenders to replace lead-based ferroelectrics.

The synthesis and study of nanoscale perovskite crystals are appealing because of their novel and exciting properties. The general understanding of these nanostructures is that the quantum restraint of electrons by the potential wells of nanometer-sized structures may provide one of the most versatile and potent means to control the electrical, magnetic, optical, and thermoelectric properties of solid-state functional materials.^[5] In this regard, perovskite materials comprising of ferroelectric and piezoelectric nanostructures have been extensively investigated due to the size effect, which can change the magnitude and direction of spontaneous electric polarization, the crystal structure, and the Curie temperature comparing with their ferroelectric bulk counterparts.^[3,6-7] Thus, ferroelectric materials in fiber form that can be incorporated into smart ceramic-polymer composites could answer all structural issues in KNN. The main advantage of using fibers instead of monolithic ferroelectric ceramics is the improvement attained by the composites' design flexibility. A higher aspect ratio is necessary to increase the active nano elements performance, which can be achieved as 1D nanofiber structures with high length to diameter ratios. Furthermore, the fiber structures increase the electromechanical coupling in nano-composites and enable more adsorption of molecules on the larger surface of nano-material-based sensors.^[8]

Extensive studies on (K,Na)NbO₃ based systems have already been carried out.^[9-12] These investigations focus primarily on obtaining perovskite phases through fabrication techniques involving one or two milling stages and prolonged calcination at high temperatures.^[13-16] Wet chemical techniques, such as hydrothermal, alkoxide (sol-gel), and polymerized complex methods, have distinct advantages in stoichiometric control and homogeneous mixing molecular level. Studies have revealed that fine oxide ceramic powders can be synthesized using commercially available inorganic powders (oxides, carbonates, and hydroxides) as starting chemicals^[17-18] compared to conventional mixing processes. These techniques can be further applied to KNN, resulting in lower processing temperatures, and reducing alkali metal oxides' loss. Consequently, smaller particle sizes are produced with improved chemical uniformity and enhanced densification kinetics.^[19]

Sol-gel is a very flexible technique that can be utilized with a substrate having any geometry. This is not possible with other techniques. Moreover, using sol-gel, the composition of matter can be controlled to a higher degree than other methods.^[20] Additionally, it can be developed further as the starting material for the generation of nanofibers. The essential criteria for nanostructure synthesis as thin-films or nanofibers rely heavily on the precursors. A better understanding of sol-gel processed materials' crystallization behavior is needed to fabricate ferroelectrics that meet desired requirements.^[21] Conceivably, the crystallization behavior and the sol-gel processed ferroelectrics' final properties are closely related to the xerogels' structure. Conventionally different complex systems such as alkoxides, alcohols, carboxylates, nitrates, and citrates can be utilized as precursors owing to their distinct advantages.^[22]

In sol-gel processing, the gels are formed by cross-linking the organometallic precursors such as metal alkoxides M(OR)_n where the metal atom, M, is bonded through oxygen to one or more alkyl groups, R, and n is the valence of the cation. The cross-linking comes in two steps, i.e., hydrolysis and condensation. The hydrolysis of metal alkoxides involves replacing one or more alkoxy groups with hydroxyl groups.^[23] An obvious way of changing the degree of hydrolysis and condensation to vary the gel structure is to change the added water's pH value, which has been shown^[24] to produce no significant effect on the properties of the ferroelectric thin films. A more drastic way of changing the gel structure is to modify the precursor molecular structure. In other words, if the molecular structure of precursors is

modified as $M(OR)_m(OR')_{n-m}$ such that the hydroxyl groups only replace certain alkyl groups R but not R' groups during hydrolysis, the number of bonds per molecule that can cross-link during condensation is therefore reduced. The resultant polymeric structure is expected to be more linear, i.e., with a smaller fractal dimension. The gel network's structural units are also likely to be smaller as the degree of hydrolysis and condensation decreases. The reduction in the structural units' size should result in changes in the final products' microstructure. It is well known^[25] that β -diketonate likes to chelate with a metal ion that replaces the ligand's enolic hydrogen. At room temperature and without acid catalysis, the hydrolysis of β -diketonate ligands is very difficult. Therefore, the substitution of alkoxy groups in the precursor molecules by the less hydrolyzable groups such as β -diketonate can slow down hydrolysis and condensation.^[26]

Cumulatively from the acquired understanding, the present investigation reports on an innovative sol-gel process and spin coating method to produce KNN thin films, whereas the electrospinning technique is used to synthesize KNN nano-fibres. A mixture of β -diketonate sodium adducts, the $Na(hfa) \bullet tetraglyme$,^[27] with novel $[K(hfa)]_4 \bullet tetraglyme$, and $Nb(tmhd)_4$ (Hhfa = 1, 1, 1, 5, 5, 5 - hexafluoro - 2, 4 - pentanedione; tetraglyme = 2, 5, 8, 11, 14 - Pentaioxapentadecane; tmhd = 2,2,6,6-Tetramethyl-3,5-heptanedione) acts as single sources of metals. Structural, morphological, and compositional characterizations of the films and nanofibers are carried out through X-ray diffraction, field emission scanning electron microscopy, and energy dispersive X-ray analysis.

6.1 Experimental Section

Materials. $Nb(tmhd)_4$ (Tetrakis(2,2,6,6-tetramethyl-3,5-heptanedionato)niobium(IV)), Sodium hydroxide (NaOH, >98%), Potassium hydroxide (KOH, >98%) and 1,1,1,5,5,5-hexafluoro-2,4-pentanedione (H-hfa, >98%) was purchased from Strem Chemicals and used as received. Tetraglyme (2,5,8,11,14-pentaioxapentadecane, >99%), dichloromethane (CH_2Cl_2 , >99.5%) and n-pentane were purchased from Sigma Aldrich. Niobium ethoxide ($Nb(OCH_2CH_3)_5$, >99%) was purchased from abcr gmbh. Isopropanol (propan-2ol) was synthesized in-house and Polyvinylpyrrolidone (1-ethenylpyrrolidin-2-one) was purchased from Alfa Aesa.

Synthetic Method. The sol-gel reaction occurred in Isopropanol solution of Na(hfa)•tetraglyme, [K(hfa)]₄•tetraglyme and Nb(tmhd)₄ (for Nb⁴⁺) while Nb(OCH₂CH₃)₅ (for Nb⁵⁺). The Na(hfa)•tetraglyme adduct has been prepared according to the procedure reported in ref. [27] and described in chapter 4. The [K(hfa)]₄•tetraglyme complex was synthesized as previously reported in chapter 3. For the sol hydrolysis, acetic acid (CH₃COOH) was used as a catalyst.

The K, Na, and Nb precursors were mixed with isopropanol and acetic acid in the ratio of 1:1:2:130:4. The sol was aged at 60°C for 12 hrs and then was in part treated in temperature and calcined at 600°C in air for 1 hr with a ramp rate of 10°C/min for powder XRD analysis and then remaining sol-gel was used to spin-coat on Si(100) substrates. The spin-coating process was carried out using a Spin-Coater SCV-10, at 2000 revolutions per minute (RPM) for 60s. The deposition is alternated to fast annealing steps at 650°C in air for 10 min. After four steps, films were annealed at 10°C/min till 650°C in air for 30 min.

Materials characterization. Film structure was analyzed by X-ray diffraction (XRD) in grazing incidence mode (0.5°) using a Smartlab Rigaku diffractometer, equipped with a rotating anode of Cu K α radiation operating at 45 kV and 200 mA. The powder and nanofibers were analyzed through an STOE-STADI MP diffractometer operating in reflection mode and using Mo K α radiation ($\lambda = 0.7093 \text{ \AA}$). Film surface morphology was investigated using the field emission scanning electron microscope, ZEISS Supra 55 VP. The atomic composition of the sample was performed by energy dispersive X-Ray (EDX) analysis.

The sol-gel solution for electrospinning was made by mixing KNN precursor solution with PVP solution (0.7g PVP/5 ml isopropanol) in the ratio of 2:1. The sol was aged at 60°C for 12 hrs, and then electrospun using a needle tip of 21-gauge and 0.514 mm (inner diameter) at a voltage of 15 kV with a volumetric flow rate of 10 μ l/min and collected on an aluminum foil at 15 cm from the tip of the syringe according to the fig. 6.1. The collected fibers are then calcined by first heating at 5°C/min until 300°C for 1 hr and then heating at 1°C/min till 700°C for 1 hr.

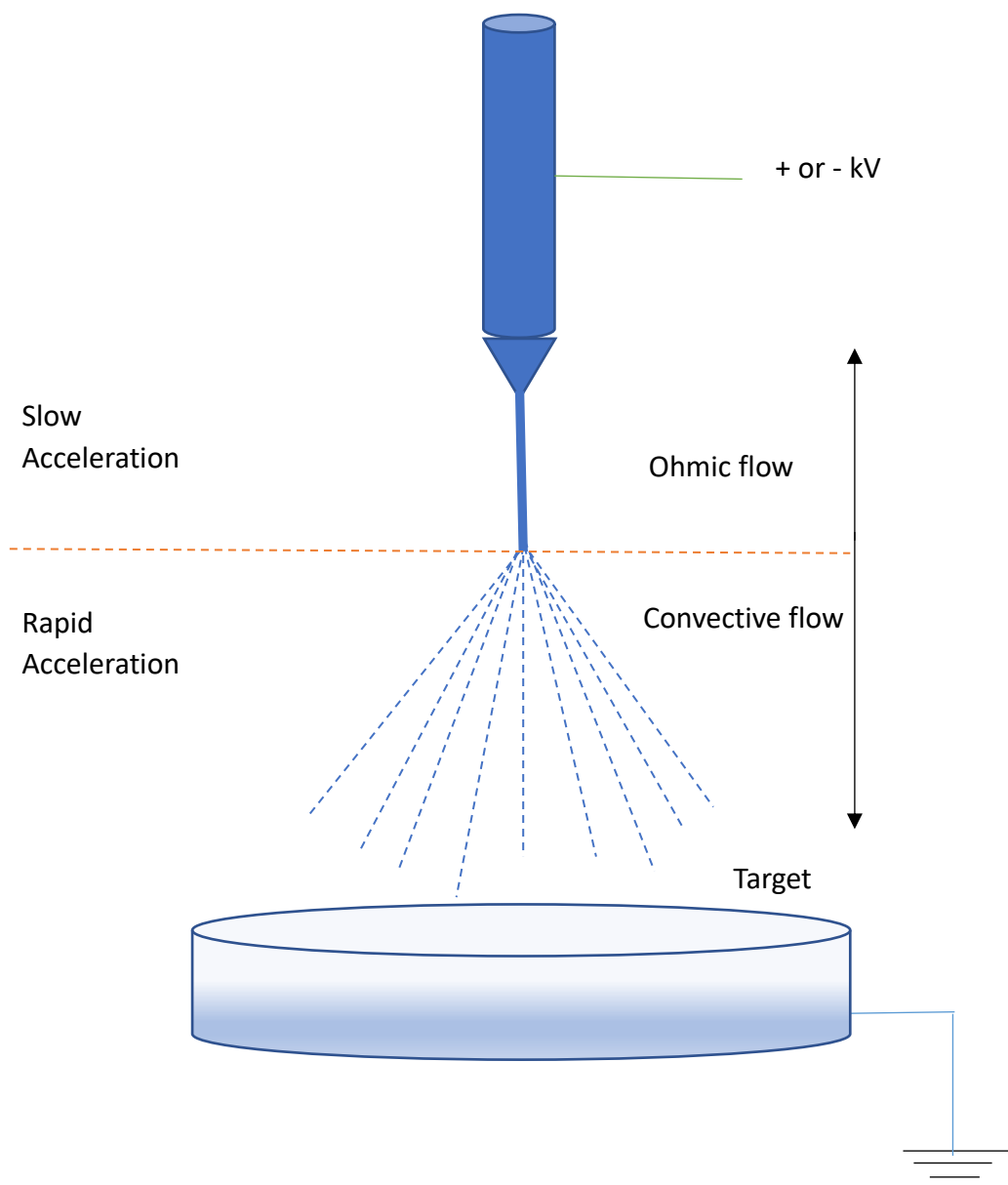


Fig. 6.1. Schematic representation of the electrospinning set-up (the image gives an enlarged perspective different from the real dimensions).

6.2. Results and Discussions

Structural determination

Three different approaches have been applied to synthesize KNN nanostructures using two different Nb-precursors, with a 4+ or 5+ oxidation test. For the sake of simplicity, KNN with Nb⁴⁺, which utilizes Nb(tmhd)₄, will be called KNN-Nb⁴⁺; similarly, KNN-Nb⁵⁺ utilizes Nb(ethoxide)₅ as the niobium source, and finally, KNN-Nb⁴⁺Nb⁵⁺ utilizes Nb(ethoxide)₅ and Nb(tmhd)₄ in a 1:1 ratio according to the required amount.

It might well be noted that KNN exists at Morphotropic Phase Boundary (MPB) and shows for the composition of K_{0.5}Na_{0.5}NbO₃. These superior ferroelectric and piezoelectric properties undergo three phase transitions: rhombohedral to orthorhombic (T_{R-O}) around -110 °C, orthorhombic to tetragonal (T_{O-T}) around 180 °C, and tetragonal to cubic (T_{T-C}) around 400°C.^[28-30] One way to understand the phases of KNN synthesized, researchers have most often referred to the reflection plane 200 at 2θ value of 45°.^[31] Thus, a much more rigorous analysis is required to assess the phases of the KNN synthesized in this research work.

The fig. 6.2. shows a comparative analysis of the XRD pattern obtained from using Nb(tmhd)₄ and Nb(ethoxide)₅ as the source of Nb metal into the lattice. Here, we study where the KNN has been deposited with Nb⁴⁺ and Nb⁵⁺ into the crystal structure. We can observe perovskites like structure with 2θ values around 22.67°, 32.16°, 39.67°, 46.33°, 52.00° and 57.57° which attributes to 100, 110, 111, 200, 201, and 211 reflection planes that are consistent according to K_{0.5}Na_{0.5}NbO₃.^[32] It is evident from the analysis that KNN-Nb⁴⁺ and KNN-Nb⁴⁺Nb⁵⁺ show tetragonal phase (JCPDS-ICDD 2001, file No.71-0945) of the perovskite structure in comparison to the KNN-Nb⁵⁺, which shows higher crystallinity and larger crystallite size owing to narrow peaks observed. The shift of the KNN-Nb⁴⁺ and KNN-Nb⁴⁺Nb⁵⁺ compared to the KNN-Nb⁵⁺ might suggest a different crystal structure attributed to the presence of the secondary phase. It also suggests a smaller unit cell for Nb⁴⁺ and Nb⁴⁺Nb⁵⁺ ions into the lattice. However, it may be noted that the thin film also shows some secondary phases that have been marked. The dominant peak at 27.62° suggests a secondary phase corresponding to K₄Nb₆O₁₇ (JCPDS 76-0977).

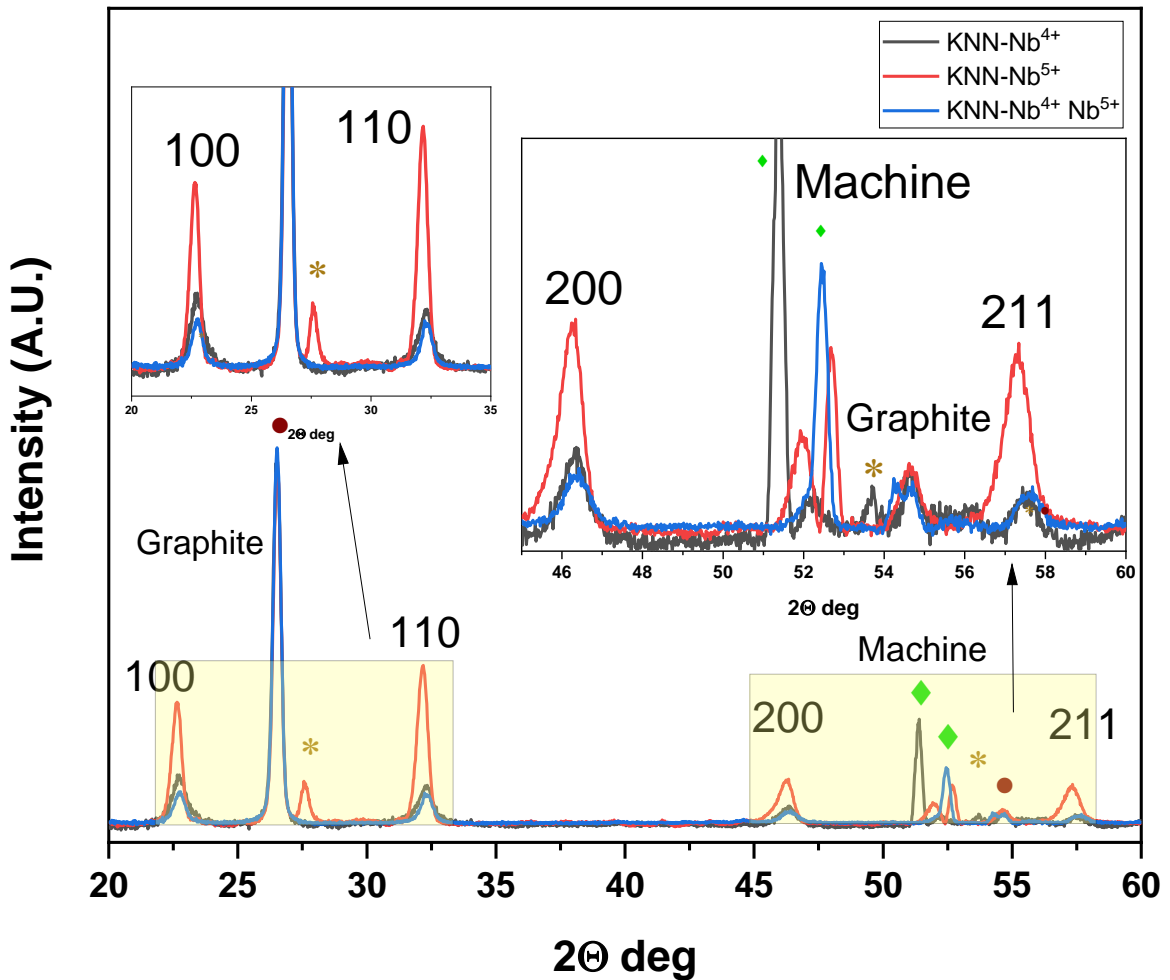


Fig. 6.2. XRD patterns (Cu K α) comparing the thin-film depositions of the KNN-Nb⁴⁺, KNN-Nb⁵⁺, and KNN-Nb⁴⁺Nb⁵⁺ on Si(100) substrate using sol-gel (Inset: enlarged view of the distinct peaks)

Please see the XRD measurements of the KNN-powders and KNN-fibres were carried out in collaboration with the University of Cologne, where an STOE-Stadi MP X-ray diffractometer with Mo source and K α = 0.70926 Å was used, and thus we see the XRD measurements of samples as mentioned above between 10°-60°.

Fig. 6.3 shows the comparison of KNN-fibres based on different niobium precursors used for the synthesis process. We can observe perovskites like structure with 2θ values of 22.40°, 31.7°, 39.30°, 45.20°, 51.21°, and 56.82°, which attributes to 100, 110, 111, 200, 201, and

211 reflection planes that are consistent according to $K_{0.5}Na_{0.5}NbO_3$. On closer inspection, we can speculate on the existence of orthorhombic phase for $KNN-Nb^{5+}$ fibers based on 002 and 200 peaks merging and tetragonal phase for $KNN-Nb^{4+}$ and $KNN-Nb^{4+}Nb^{5+}$, which may suggest the coexistence of orthorhombic – tetragonal phase.^[33] The shifting of the $KNN-Nb^{4+}$ and $KNN-Nb^{4+}Nb^{5+}$ signifies lattice contraction, but this needs to be studied further with more analysis.

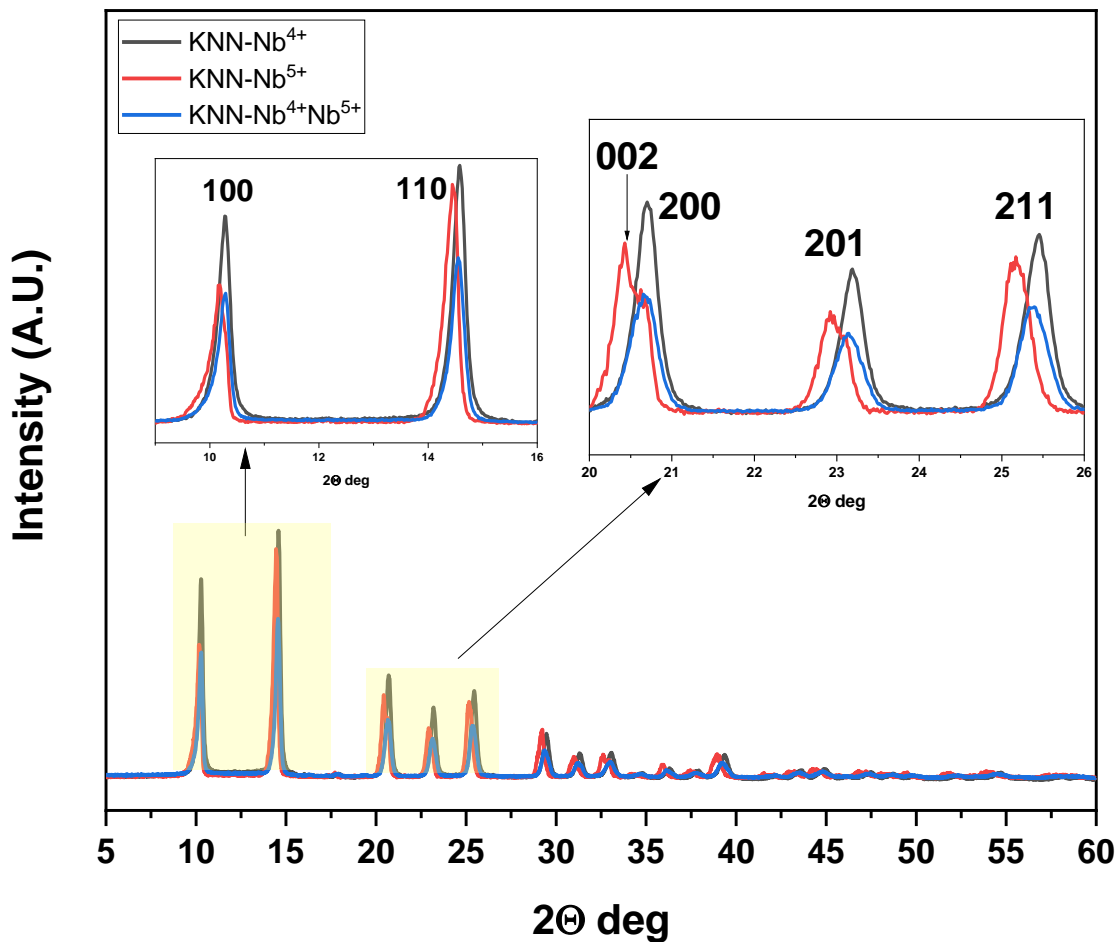


Fig. 6.3. XRD patterns (Mo $K\alpha$) comparing the KNN-fibres of the $KNN-Nb^{4+}$, $KNN-Nb^{5+}$, and $KNN-Nb^{4+}Nb^{5+}$ (Inset: Enlarged image of 100 and 110 peaks and enlarged image of 200 (002 peaks included), 201 and 211 peaks).

Fig. 6.4 shows the comparison of KNN-powders based on different niobium precursors used for the synthesis process. We can observe perovskites like structure with 2θ values of 22.40° , 31.7° , 39.30° , 45.20° , 51.21° , and 56.82° , which attributes to 100, 110, 111, 200, 201, and 211 reflection planes. We also observe the orthorhombic phase of KNN (JCPDS-ICDD 2001, file No. 71-2171) in the case of powder. A shift towards a higher angle may be observed between KNN-Nb⁵⁺ and KNN-Nb⁴⁺, KNN-Nb⁴⁺Nb⁵⁺ samples, but no substantial difference concerning the shift can be observed between KNN-Nb⁴⁺ and KNN-Nb⁴⁺Nb⁵⁺.

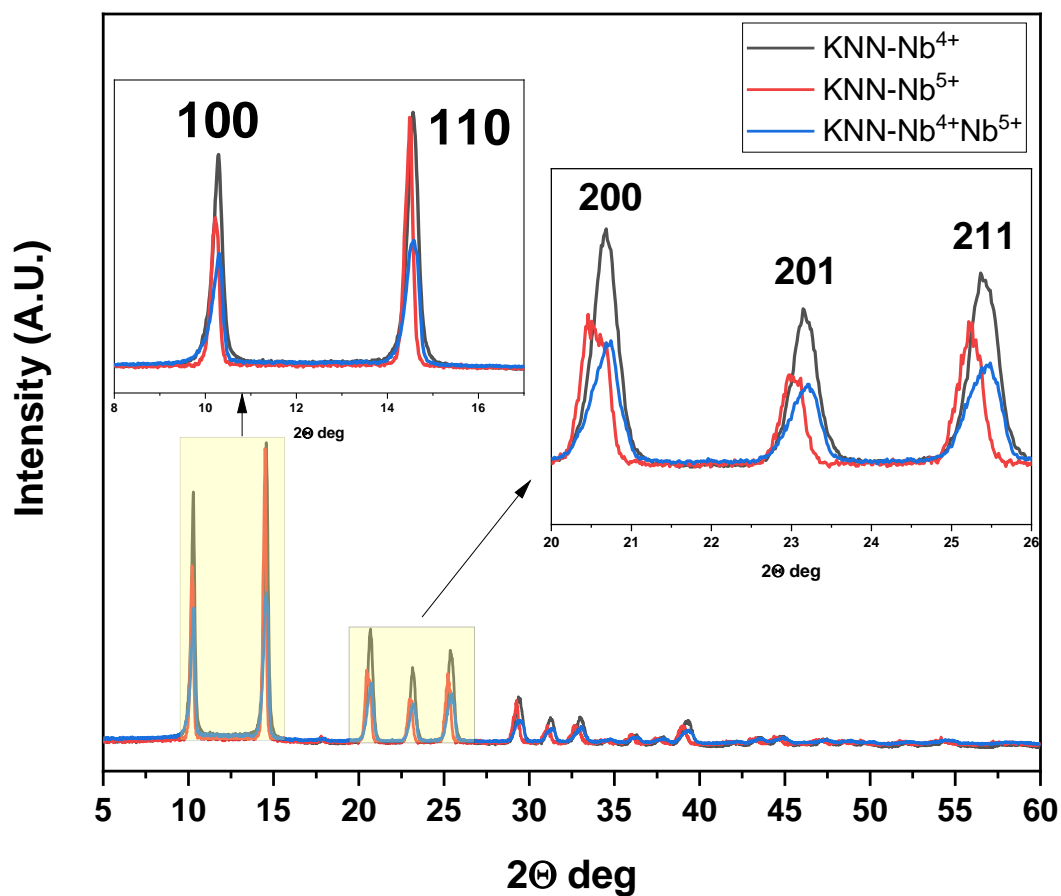


Fig. 6.4. XRD patterns (Mo $K\alpha$) comparing the KNN-powder of the KNN-Nb⁴⁺, KNN-Nb⁵⁺, and KNN-Nb⁴⁺Nb⁵⁺ (Inset: enlarged image of 100, 110, 200, 201, and 211 peaks).

FE-SEM characterization

The microstructure and morphology of KNN thin films have been studied by field emission scanning electron microscopy (FE-SEM). The FE-SEM images of the films deposited on Si(100) for 60 min show a homogeneous surface for all the samples. However, SEM images in fig. 6.5 show different morphologies related to the phase and the precursor used for the deposition with different Nb source. The KNN-Nb⁴⁺ (fig. 6.5a.) film shows very small grains, while KNN-Nb⁵⁺ (fig. 6.5c) shows plate-like structures very smooth and stacked tightly together. KNN-Nb⁴⁺Nb⁵⁺ (fig. 6.5e) shows a uniform surface with crystalline plate grains of about 100 nm. The film thickness is about 70 nm, 210 nm, and 80 nm for the KNN-Nb⁴⁺ (fig. 6.5b.), KNN-Nb⁵⁺ (fig. 6.5d), and KNN-Nb⁴⁺Nb⁵⁺ (fig. 6.5f) films, respectively.

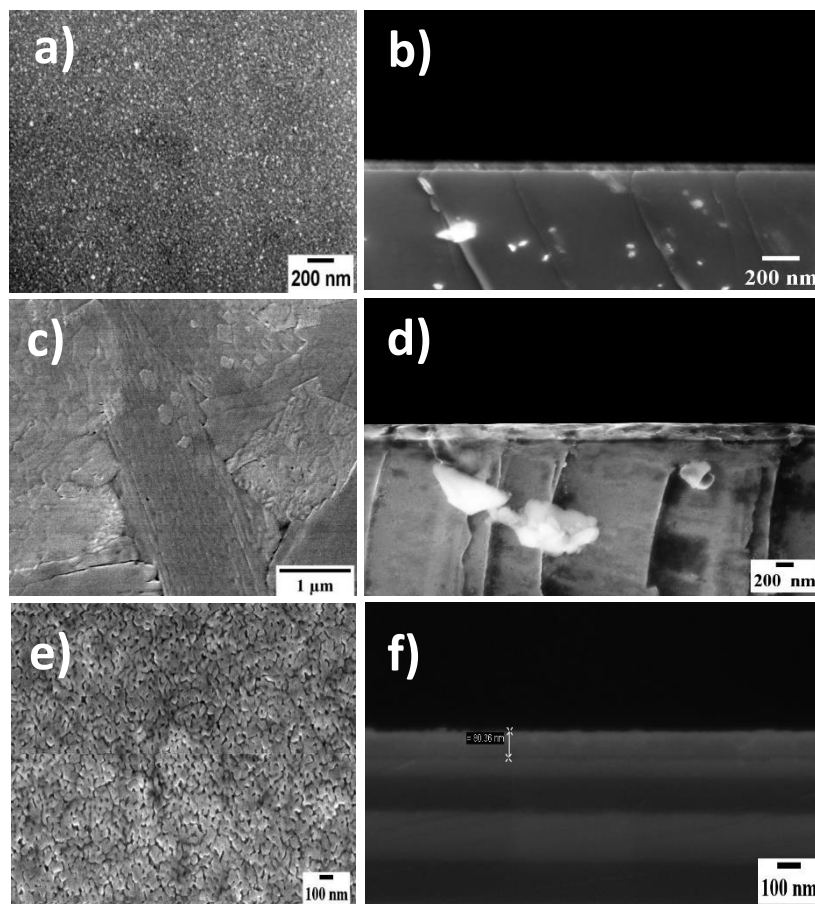


Fig. 6.5. FE-SEM images of the morphology of the thin-film for **a)** plan-view and **b)** cross-section of KNN-Nb⁴⁺; **c)** plan-view and **d)** cross-section of KNN-Nb⁵⁺; **e)** plan-view and **f)** cross-section of KNN-Nb⁴⁺Nb⁵⁺.

The nano fibre's SEM images (fig. 6.6) confirm that the fibers were uniform, cylindrical, and smooth. However, $\text{KNN-Nb}^{4+}\text{Nb}^{5+}$ (fig. 6.6e) shows defects related to the fiber nature that show imperfections, such as bead formations that arise due to the sol-gel. The fiber diameter is about 200 nm before calcination and 150 nm after calcination for the three systems.

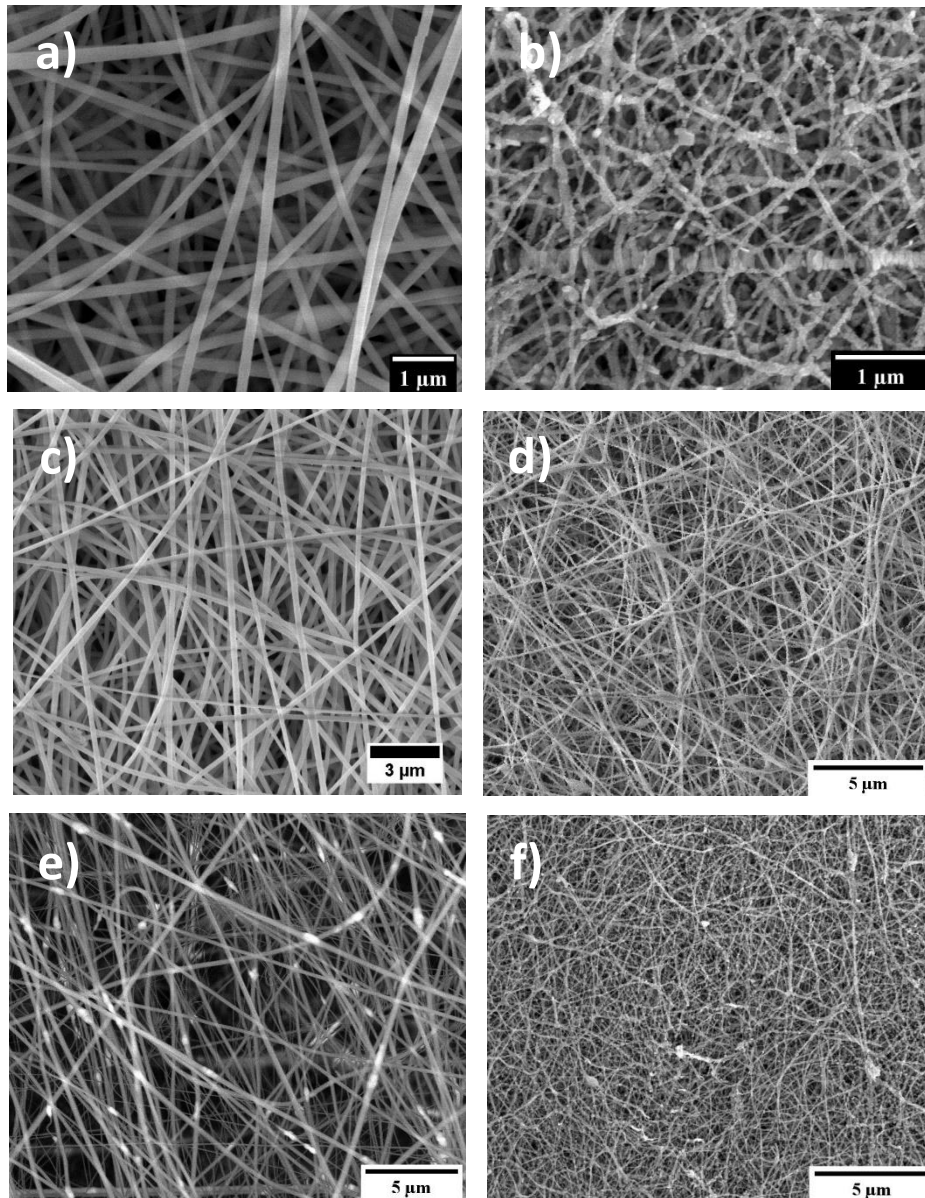


Fig. 6.6. FE-SEM images of nanofibers synthesized as **a)** KNN-Nb^{4+} before calcination; **b)** KNN-Nb^{4+} after calcination; **c)** KNN-Nb^{5+} before calcination; **d)** KNN-Nb^{5+} after calcination; **e)** $\text{KNN-Nb}^{4+}\text{Nb}^{5+}$ before calcination; **f)** $\text{KNN-Nb}^{4+}\text{Nb}^{5+}$ after calcination.

EDX analysis

Regarding composition, energy dispersive X-ray (EDX) analyses have been carried out on thin films. The EDX data (fig. 6.7) established the quantitative film composition in various sites in terms of metal ratio. The EDX spectrum of the KNN-Nb⁴⁺ thin-film shows the typical K α line of the Na, the K α and K β lines of the K, and the L α line of Nb. The peak at 0.520 keV is associated with the O K α . The analysis depicts an average ratio of (K+Na): Nb = 0.59. The atomic % of K and Na corresponds to K_{0.2}Na_{0.39}Nb₁ stoichiometry.

Table 6.1. EDX analysis was done on three different areas of the KNN-Nb⁴⁺ thin film.

Element	Atomic%		
	Area 1	Area 2	Area 3
O K	12.90	13.90	14.40
Na K	0.43	0.66	0.77
Si K	84.81	83.62	82.75
K K	0.31	0.31	0.36
Nb L	1.55	1.51	1.73

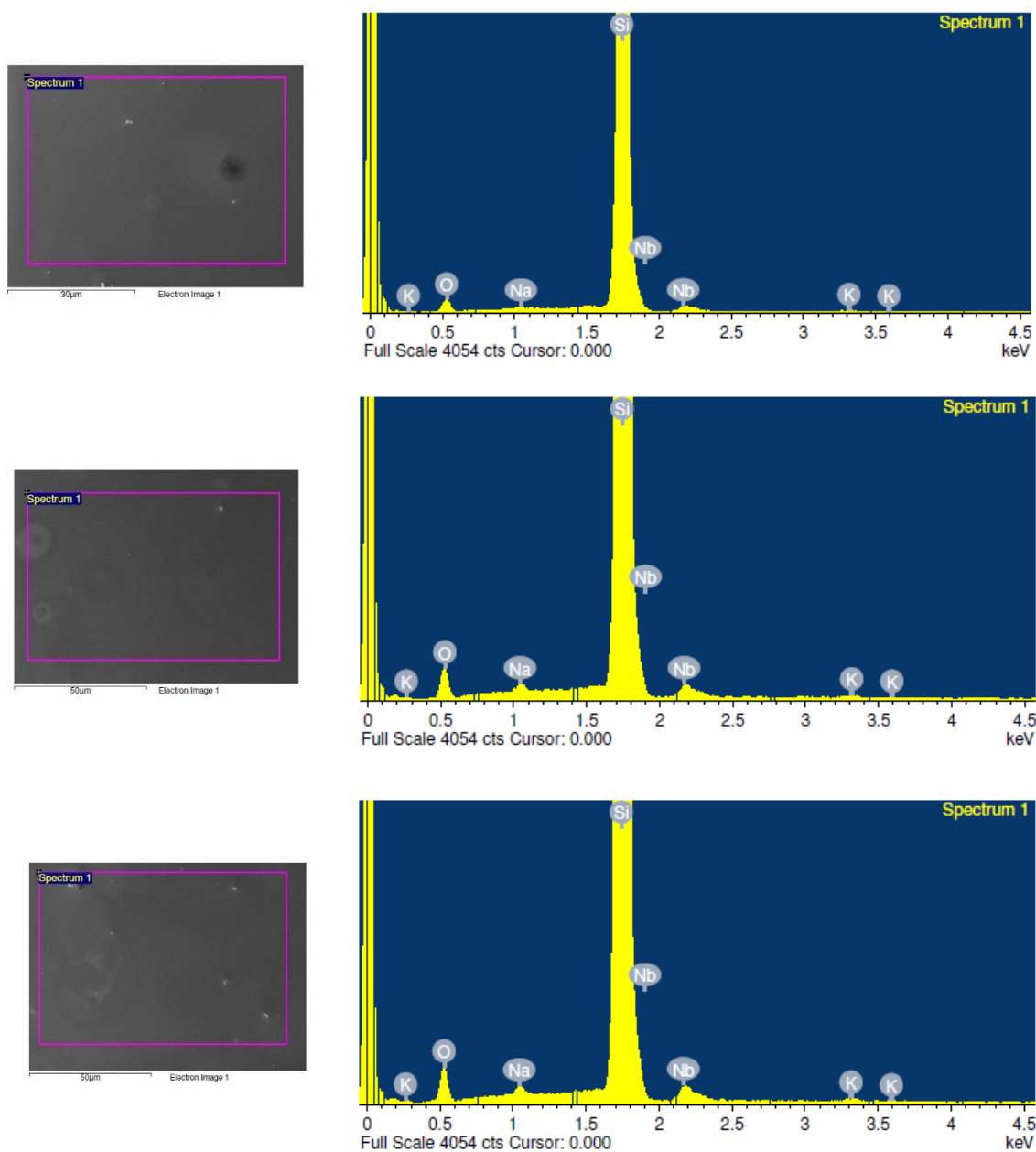


Fig. 6.7. EDX spectra were obtained from area 1 (top), area 2 (middle), and area 3 (bottom) under observation for KNN-Nb⁴⁺.

The EDX spectrum of the KNN-Nb⁵⁺ thin-film (fig. 6.8) shows the typical K α line of the Na, the K α and K β lines of the K and the L α line of Nb. The peak at 0.520 keV is associated with the O K α . The analysis depicts an average ratio of (K+Na): Nb = 0.78. The atomic% of K and Na corresponds to K_{0.29}Na_{0.47}Nb₁ stoichiometry.

Table 6.2. EDX analysis was done on three different areas of the KNN-Nb⁵⁺ thin film.

Element	Atomic%		
	Area 1	Area 2	Area 3
O K	30.65	30.31	31.01
Na K	3.27	3.60	3.13
Si K	56.86	56.77	57.16
K K	2.01	2.11	2.04
Nb L	7.20	7.21	6.67

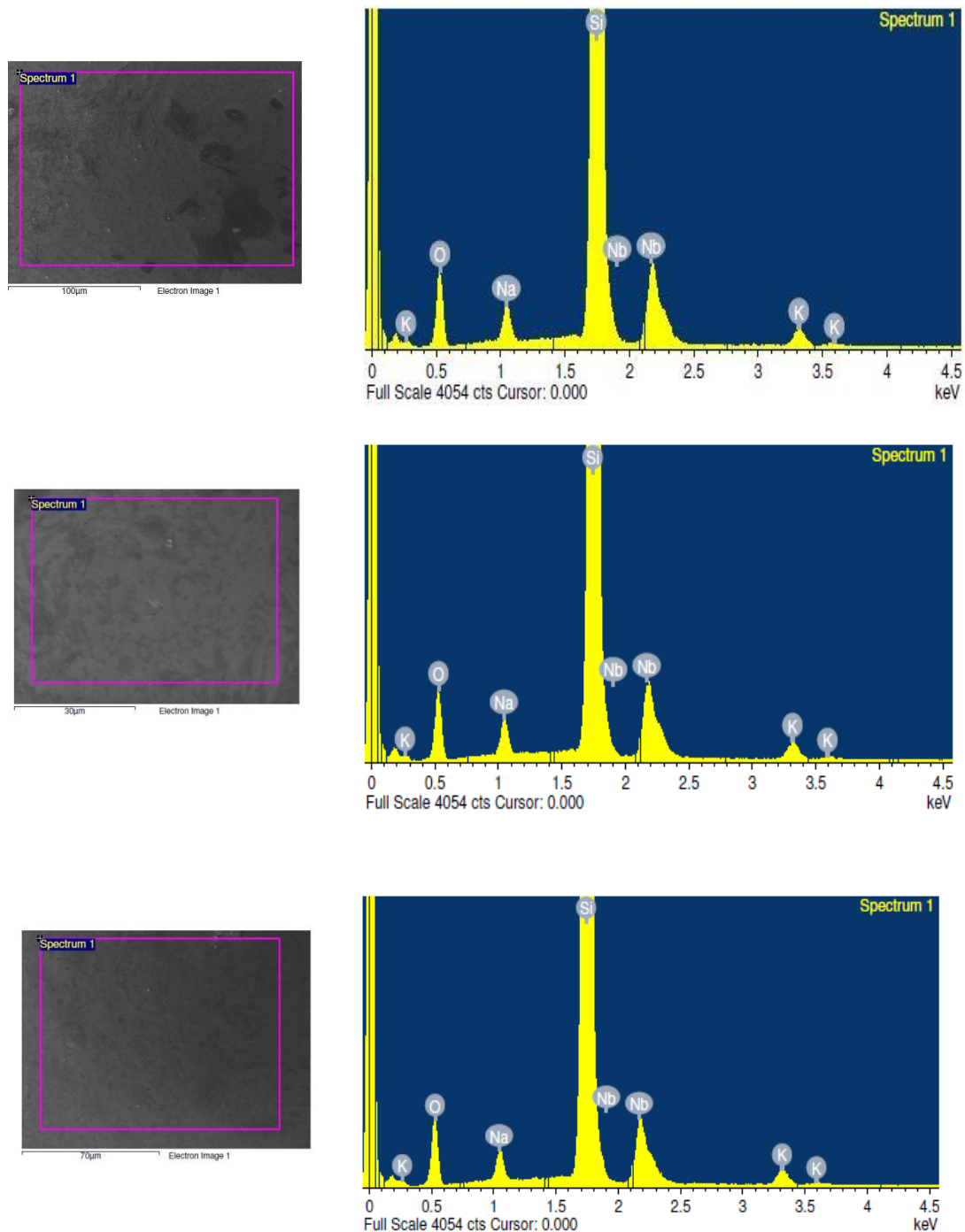


Fig. 6.8. EDX spectra obtained from area 1 (top) area 2 (middle) and area 3 (bottom) under observation for KNN-Nb⁵⁺.

The EDX spectra of the KNN-Nb⁴⁺Nb⁵⁺ thin-film (fig. 6.9) shows the typical K α line of the Na, the K α and K β lines of the K, and the L α line of Nb. The peak at 0.520 keV is associated with

the O K α . The analysis depicts an average ratio of (K+Na): Nb = 0.90. The atomic % of K and Na corresponds to the K_{0.23}Na_{0.67}Nb₁ stoichiometry of the metals.

Table 6.3. EDX analysis was done on three different areas of the KNN- Nb⁴⁺Nb⁵⁺ thin film.

Element	Atomic%		
	Area 1	Area 2	Area 3
O K	13.01	12.61	11.95
Na K	0.62	0.63	0.65
Si K	85.19	85.58	86.22
K K	0.18	0.27	0.21
Nb L	0.99	0.90	0.97

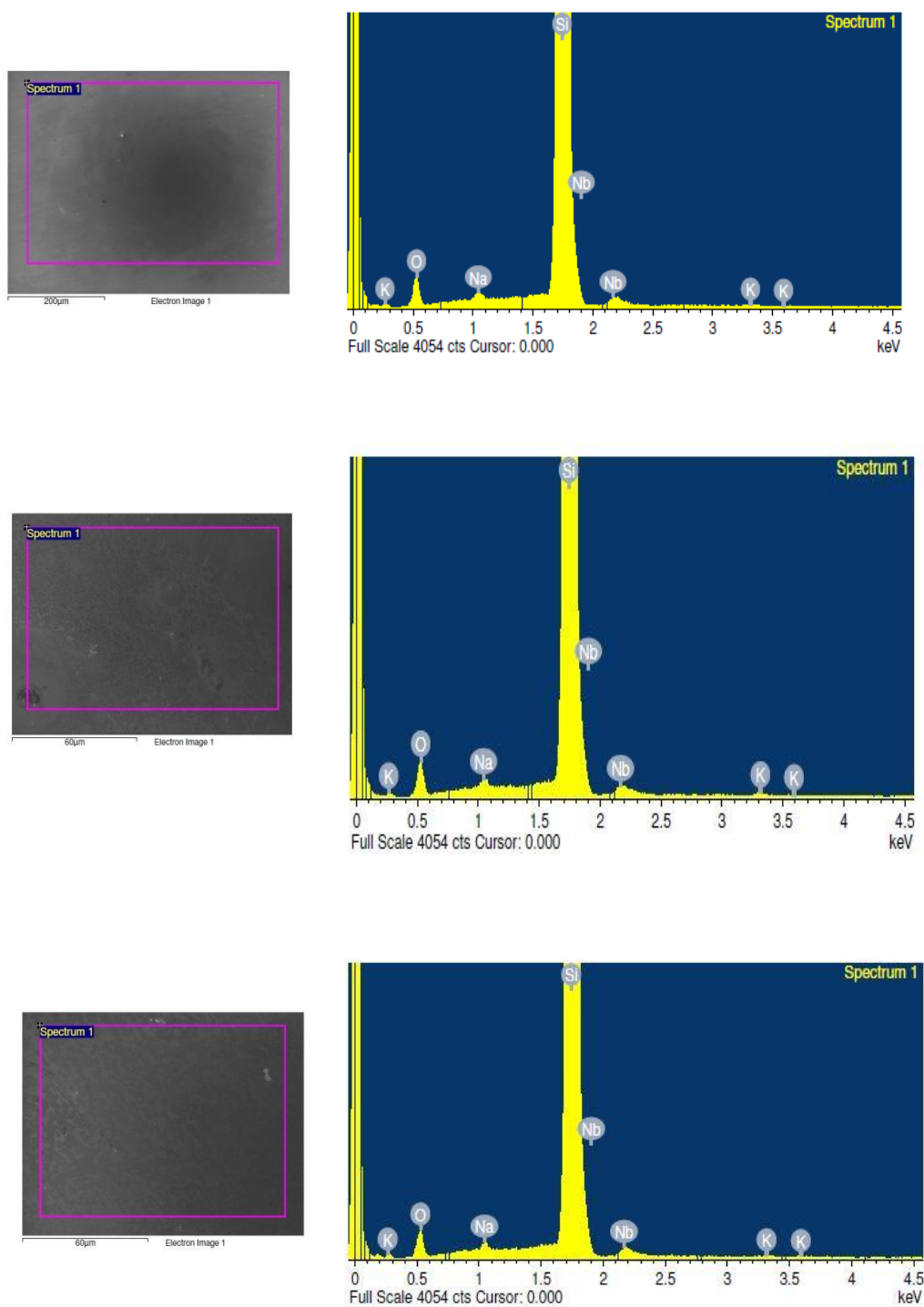


Fig. 6.9. EDX spectra obtained from area 1 (top) area 2 (middle) and area 3 (bottom) under observation for KNN-Nb⁴⁺/Nb⁵⁺ thin films.

6.3 Conclusions

Novel Na(hfa)•tetraglyme and [K(hfa)]₄•tetraglyme complexes, synthesized through a simple one-pot strategy, represent suitable source precursor of Na and K for sol-gel deposition. In particular, this synthetic approach has been successfully applied for the fabrication of K_(1-x)Na_xNbO₃ perovskite structure. Also, cylindrical lead-free, homogeneous KNN nanofibers were successfully produced using the electrospinning process.

The X-ray diffraction (XRD) analysis confirms that the new sol-gel preparation route yields reproducibly orthorhombic and tetragonal phases without any impurity phases or fluoride contamination. Field-emission scanning electron microscopy (FE SEM) images indicate that morphology surfaces, grain dimensions, and thickness are strongly related to the processing parameters. The Nb precursors are utilized as alkoxides β-diketonate show a distinct effect on the crystal lattice because of the Nb⁴⁺ and Nb⁵⁺ in the unit cell. Energy dispersive X-ray (EDX) analyses established the film composition in terms of elemental composition, responsible for the material's piezoelectric nature. Finally, this synthetic strategy paves the way for synthesizing other alkali niobate phases in thin-film forms or nanofibres through these novel alkali metal β-diketonate complexes.

REFERENCES

- [1] D. Maurya, V. Petkov, A. Kumar, S. Priya, Dalton Trans. 41 (2012) 5643–5652.
- [2] J.E. Spanier, A.M. Kolpak, J.J. Urban, I. Grinberg, O.Y. Lian, W.S. Yun, A.M. Rappe, H. Park, Nano Lett. 6 (2006) 735–739.
- [3] Y. Xu, Q. Yu, J.F. Li, J. Mater. Chem. 22 (2012) 23221–23226
- [4] Y. Saito, H. Takao, T. Tani, T. Nonoyama, K. Takatori, T. Homma, T. Nagaya, M. Nakamura, Nature 432 (2004) 84–87.

- [5] Y. Xia, P. Wang, Y. Sun, Y. Wu, B. Mayers, B. Gates, Y. Yin, F. Kim and H. Yan, *Adv Mater.* 2003;15:353-389.
- [6] L. Louis, P. Gemeiner, I. Ponomareva, L. Bellaiche, G. Geneste, W. Ma, N. Setter, B. Dkhil, *Nano Lett.* 10 (2010) 1177–1183.
- [7] B.K. Yun, Y.S. Koo, J.H. Jung, M. Song, S. Yoon, *Mater. Chem. Phys.* 129 (2011) 1071–1074.
- [8] P. Sa, J. Barbosa, I. Bdikin, B. Almeida, A. G. Rolo, E. M. Gomes, M. Belsley, A. L. Kholkin and D. Isakov, *J Phys D: Appl Phys.* 2013;46:105304.
- [9] Gao, D., Kwok, K. W., Lin, D., & Chan, H. L. W., *Journal of Physics D: Applied Physics*, 2009, 42(3), 035411–35416.
- [10] Guo, Y., Kakimoto, K., & Ohsato, H., *Applied Physics Letters*, 2004, 85(18), 4121–4123.
- [11] Hollenstein, E., Davis, M., Damjanovic, D., & Setter, N., *Applied Physics Letters*, 2005, 87(18), 182905–182913.
- [12] Saito, Y., Takao, H., Tani, T., Nonoyama, T., Takatori, K., Homma, T., et al. (2004). Lead-free piezoelectric ceramics. *Nature*, 432, 84–87.
- [13] Du, H., Tang, F., Liu, D., Zhu, D., Zhou, W., & Qu, S., *Materials Science and Engineering B*, 2007, 136(2–3), 165–169.
- [14] Egerton, L., & Dolores, M. D., *Journal of the American Ceramic Society*, 1959, 42(9), 438–442.
- [15] Guo, Y., Kakimoto, K., & Ohsato, H., *Solid State Communications*, 2004, 129(5), 279–284.
- [16] Guo, Y., Kakimoto, K., & Ohsato, H., *Materials Letters*, 2005, 59(2–3), 241–244.
- [17] Kakimoto, K., Hayakawa, Y., & Kagomiya, I., *Journal of the American Ceramic Society*, 2010, 93(9), 2423–2426.

- [18] Kakimoto, K., Ito, T., & Ohsato, H., *Japanese Journal of Applied Physics*, 2008, 47, 7669–7672.
- [19] Chowdhury, A., Bould, J., Zhang, Y., James, C., & Milne, S. J., *Journal of Nanoparticle Research*, 2010, 12(1), 209–215.
- [20] Sumio Sakka, *Handbook of Advanced Ceramics (Second Edition)*, 2013
- [21] R. S.R. Kalidindi, R. Subasri, in *Anti-Abrasive Nanocoatings*, 2015
- [22] L G Hubert-Pfalzgraf, *Applied Organometallic Chemistry*, 1992, 6(8), 627–643.
- [23] K. D. Budd and D. A. Payne, *Inst. Phys. Conf. Ser.* 103 (1), 13 (1989)
- [24] K. D. Budd, S. K. Dey, and D. A. Payne, *Mat. Res. Soc. Symp. Proc.*, D3, 711 (1986).
- [25] R. C. Mehrotra, R. Bohra, and D. P. Gaur, *Academic Press*, 1978.
- [26] D. C. Bradley, R. C. Mehrotra, and G. P. Ganur, *Academic Press*, New York, 1978.
- [27] M. R. Catalano, A. L. Pellegrino, P. Rossi, P. Paoli, P. Cortelletti, M. Pedroni, A. Speghini, and G. Malandrino, *New J. Chem.*, 2017, 41(12), 4771-4775.
- [28] Y. Saito, H. Takao, T. Tani, T. Nonoyama, K. Takatori, T. Homma, T. Nagaya and M. Nakamura, *Nature*, 2004, 432, 84–87 CrossRef PubMed.
- [29] J. Rödel, W. Jo, K. T. P. Seifert, E. M. Anton, T. Granzow and D. Damjanovic, *J. Am. Ceram. Soc.*, 2009, 92, 1153–1177 CrossRef.
- [30] J. Wu, D. Xiao and J. Zhu, *Chem. Rev.*, 2015, 115, 2559–2595 CrossRef PubMed.
- [31] Sushmita Dwivedi, Tanvi Pareek and Sunil Kumar, *RSC Adv.*, 2018, 8, 24286–24296
- [32] T. A. Skidmore and S. J. Milne, *J. Mater. Res.*, 2011, 22, 2265–2272.
- [33] Lee, MK., Yang, SA., Park, JJ. & Gyoung-Ja Lee, *Sci Rep* 9, 4195 (2019).

Conclusion and Future Work

Conclusion

The overall aim of this research work, in alignment with the MSCA-ITN ENHANCE Project, was to design, synthesize and engineer novel alkali metal complexes via a simple one-pot synthesis method to act as alkali-metal source and as viable precursors for the synthesis of lead-free piezoelectric materials, i.e., Lithium Niobate (LiNbO_3) and Potassium Sodium Niobate ($\text{K}_{1-x}\text{Na}_x\text{NbO}_3$). Several novel alkali metal complexes were prepared during this study, which has been extensively studied and characterized for their physical and functional property and discussed earlier in the thesis. The role of β -diketonates and glymes has been the focal point of the strategy developed within this investigation.

To begin with this complex investigation, we collaborated with Dr. Simon Rushworth to understand the industrial constraints of the synthesis of alkali metal precursors and establish an excellent experimental background for the synthesis to facilitate the industrial standards. With the foundation laid down, we worked on Lithium complexes in chapter 2. We had a significant challenge in overcoming the small size of Li^+ to incorporate into an organic structure to act as a precursor. For this, we worked with the fluorinated β -diketonates and glymes, i.e., monoglyme, diglyme, triglyme, and tetraglyme, to synthesize novel Li- β -diketonates complexes. These complexes coordinated as $[\text{Li}_{12}(\text{hfa})_{12}\bullet\text{monoglyme}\bullet 4\text{H}_2\text{O}]_n$, $[\text{Li}_2(\text{hfa})_2\bullet\text{diglyme}\bullet\text{H}_2\text{O}]$, $\text{Li}(\text{hfa})\bullet\text{triglyme}\bullet\text{H}_2\text{O}$ and $\text{Li}(\text{hfa})\bullet\text{tetraglyme}\bullet\text{H}_2\text{O}$. We found some exciting coordination of Li showing its high affinity for water incorporated into the crystal lattice, which does not act as a drawback but instead helps saturate the central metal atom and integrate with the glyme to complete the coordination sphere. $[\text{Li}_{12}(\text{hfa})_{12}\bullet\text{monoglyme}\bullet 4\text{H}_2\text{O}]_n$ shows high degree of polymerization, while $[\text{Li}_2(\text{hfa})_2\bullet\text{diglyme}\bullet\text{H}_2\text{O}]$ is a dimer and held together by hydrogen bonding of the H_2O molecule. We also observed different physical states of the synthesized complexes depending on the length of the polyether used. The synthesized complexes showed remarkable stability in air with good volatility and very low residue. The functional validation of the synthesized precursors was assessed in chapter 5 and carried out in collaboration with Prof. Ausrine Bartasyte at the University of Franche Comte through PI-

MOCVD, wherein we could synthesize pure phase LiNbO_3 with all the novel adducts. The deposition was carried out on C-sapphire, A-sapphire, R-sapphire, and Si. Among all the adducts $[\text{Li}(\text{hfa})]_{12} \bullet \text{monoglyme} \bullet 4\text{H}_2\text{O}$ gave the best results in highly oriented LN-films on C-sapphire with a smooth surface and homogenous morphology.

With this investigation, we started understanding the role of fluorinated β -diketonates and glymes. So, we translated the above work to incorporate Na^+ into the organic structure, which could be released at a relatively low temperature with clean decomposition and no secondary phases. The investigation was taken up in chapter 4. The Na- β -diketonates thus synthesized showed ionic nature depending on the polyether's length, with only tetraglyme complex showing covalent characteristics. The complexes coordinated as $\text{Na}(\text{hfa})$, $[\text{Na}_4(\text{hfa})_6] \bullet [\text{Na} \bullet (\text{diglyme})_2]_2$, $\text{Na}(\text{hfa}) \bullet \text{triglyme} \bullet \text{H}_2\text{O}$ and $\text{Na}(\text{hfa}) \bullet \text{tetraglyme}$. Interestingly, the monoglyme did not coordinate to the metal centre, which further shows the precursor's high ionic nature. Except for the triglyme complex, all the adducts were solid. In the case of $\text{Na}(\text{hfa})$, Na^+ acted as the cationic part and hfa^- the anionic part which saturated together to form $\text{Na}(\text{hfa})$, while in $[\text{Na}_4(\text{hfa})_6] \bullet [\text{Na} \bullet (\text{diglyme})_2]_2$, the charge on $[\text{Na}_4(\text{hfa})_6]^{2-}$ was counterbalanced by $2[\text{Na} \bullet (\text{diglyme})_2^+]$ to form a stable complex. The complexes give a high residue, but this is not an issue for application in liquid-assisted processes, such as the liquid injection MOCVD or the sol-gel route.

Seeing the success of β -diketonates and glymes structure in accommodating alkali metal ions successfully, a similar strategy was devised for K- β -diketonates and glymes. The investigation of the synthesized complexes was taken up in chapter 3. The complexes coordinated as $[\text{K}(\text{hfa})]_3 \bullet \text{monoglyme}$, $[\text{K}(\text{hfa})]_2 \bullet \text{diglyme}$, $\text{K}(\text{hfa}) \bullet \text{triglyme} \bullet \text{H}_2\text{O}$, and $[\text{K}(\text{hfa})]_4 \bullet \text{tetraglyme}$. These complexes show covalent characteristics, making them highly soluble in most organic solvents and stable at room temperature for a longer time. All the complexes favored a high degree of polymerization. Physically all the complexes were solid except for the triglyme derivative, which was liquid.

Finally, with the successful synthesis of K and Na precursors, we tried to utilize these complexes for the synthesis of $\text{K}_{1-x}\text{Na}_x\text{NbO}_3$ type perovskite materials. The investigation about this was taken up in chapter 6, and it was done in collaboration with Prof. Mathur's group from the University of Cologne. We incorporated $[\text{K}(\text{hfa})]_4 \bullet \text{tetraglyme}$ and $\text{Na}(\text{hfa}) \bullet \text{tetraglyme}$ as the source for K and Na metals, and aligning to the complex system,

and we used $\text{Nb}(\text{tmhd})_4$ as the Nb β -diketonate for the source of Nb metal. The focus of this investigation was to study the potential of β -diketonates vs. alkoxides. Thus, we also synthesized KNN by the conventional method, using Sodium isopropoxide (NaO^iPr), Potassium isopropoxide (KO^iPr), and Niobium ethoxide ($\text{Nb}(\text{OEt})_5$). We also tried to synthesize KNN by incorporating both Nb^{4+} and Nb^{5+} together into the crystal lattice. The KNN thus synthesized was in the form of powder, nanofibers, and thin film.

The idea was to understand the role of precursors on the geometry of the crystal lattice or the phase of KNN formed, as $\text{Nb}(\text{tmhd})_4$ provides Nb^{4+} , while $\text{Nb}(\text{OEt})_5$ provides Nb^{5+} ions. To this, in the X-ray diffraction studies, we observed, in the case of powders, with the incorporation of Nb^{4+} and $\text{Nb}^{4+}\text{Nb}^{5+}$, the KNN thus formed was shifted to higher angles in comparison to KNN with Nb^{5+} , signifying shrinkage of the crystal lattice. The powder KNN showed the tetragonal phase of the perovskite-like structure. The KNN fibers, on the other hand, showed orthorhombic phase for KNN-Nb^{5+} , while for KNN-Nb^{4+} and KNN-Nb^{5+} showed tetragonal phases. A similar trend of the unit cell's shrinking can be observed in KNN-fibres with Nb^{4+} and $\text{Nb}^{4+}\text{Nb}^{5+}$. The X-ray diffraction study of the thin films revealed some secondary phases of $\text{K}_4\text{Nb}_6\text{O}_{17}$. These show tungsten bronze-like structures, which may relate to alkali losses, resulting in niobate excess, leading to these alkali niobates' formation. These findings are not straightforward and need to be further analyzed comprehensively to thoroughly understand the phase transformations and the effect on the lattice parameters using β -diketonates as the metal source. On the contrary, these investigations do throw light on Na and K's successful utilization to synthesize KNN as powders and thin films.

Future Work

A successful synthesis and characterization of 11 novel alkali metal complexes with their possible applications in the synthesis of LiNbO_3 and $\text{K}_{1-x}\text{Na}_x\text{NbO}_3$ were discussed in length during this doctoral research work. To complete the story and develop it further, several other investigations could also be performed.

Notably, the impressive coordination of $[\text{Li}_2(\text{hfa})_2 \cdot \text{diglyme} \cdot \text{H}_2\text{O}]$ can be studied further. It coordinates as a dimer with H_2O acting as the bridge linking two lithium units together; it can potentially start material for synthesizing bimetallic complexes. The $\text{Li}(\text{hfa})\text{diglyme}$ units

can be engineered, and the dimerization with H₂O molecule can help in the formation of a bimetallic single-source precursor. This can pave the way towards a more demanding application if Li and Nb can be incorporated in the said fashion, which may be utilized as the precursor for LiNbO₃. Additionally, the liquid complex of Li adducts can be used as the source of Lithium-ion for battery materials.

The Na-β-diketonates can be investigated further in terms of their highly ionic nature as potential electrolyte solutions. Also, since the Na complex was utilized in ceramic material formation, it can further be developed to synthesize alkali niobates as a potential precursor. The presence of fluorine makes them attractive for the synthesis of fluoride-containing phases such as NaF.

The K-β-diketonates have inherently covalent characteristics, which impart all the essential qualities of a suitable precursor. Thus, these complexes can be utilized in many applications, such as synthesizing alkali niobates, fluoride-containing phases, and hybrid materials. Additionally, these precursors can be synthesized as fibers, enhancing their property as a sensor material.

Furthermore, the potassium and sodium complexes synthesized can be utilized for the formation of KNN-piezoelectric energy harvesters. We can investigate the effect of Nb⁴⁺ on the piezo and pyro property of the device. One may hypothesize that incorporating Nb⁴⁺ or Nb⁴⁺Nb⁵⁺ into the crystal lattice may help facilitate the growth of defects that can distort the structure of the KNN and thereby enhance the piezoelectric behavior.

APPENDIX A

Table A.1. Selected bond distances (Å) and angles (°) for $[\text{Li}_{12}(\text{hfa})_{12} \bullet \text{monoglyme} \bullet 4\text{H}_2\text{O}]_n$ (**1**).

Bond distances		Bond angles			
Li(1)-O(1W)	1.991(8)	O(1W)-Li(1)-O(1)	102.0(3)	O(6)-Li(4)-O(8)	86.4(3)
Li(1)-O(1)	2.012(7)	O(1W)-Li(1)-O(2)	102.8(3)	O(6)-Li(4)-O(9)	122(3)
Li(1)-O(2)	2.003(6)	O(1W)-Li(1)-O(3)	97.8(3)	O(6)-Li(4)-O(11)	112.0(3)
Li(1)-O(3)	2.015(6)	O(1W)-Li(1)-O(4)	111.5(3)	O(8)-Li(4)-O(9)	123.6(3)
Li(1)-O(4)	2.012(7)	O(1)-Li(1)-O(2)	88.9(3)	O(8)-Li(4)-O(11)	130.4(3)
Li(2)-O(2)	1.938(7)	O(1)-Li(1)-O(3)	85.6(3)	O(9)-Li(4)-O(11)	86.1(3)
Li(2)-O(4)	1.958(6)	O(1)-Li(1)-O(4)	146.4(4)		
Li(2)-O(5)	1.952(7)	O(2)-Li(1)-O(3)	159.3(4)	O(9)-Li(5)-O(10)	88.3(2)
Li(2)-O(7)	1.946(7)	O(2)-Li(1)-O(4)	84.2(3)	O(9)-Li(5)-O(11)	83.3(2)
Li(3)-O(5)	2.003(7)	O(3)-Li(1)-O(4)	89.6(3)	O(9)-Li(5)-O(12)	145.4(3)
Li(3)-O(2W)	2.010(8)			O(9)-Li(5)-O(1G)	108.0(3)
Li(3)-O(6)	2.011(7)	O(2)-Li(2)-O(4)	87.4(3)	O(10)-Li(5)-O(11)	154.8(3)
Li(3)-O(7)	2.006(7)	O(2)-Li(2)-O(5)	122.6(4)	O(10)-Li(5)-O(12)	84.4(2)
Li(3)-O(7)	2.007(7)	O(2)-Li(2)-O(7)	117.5(3)	O(10)-Li(5)-O(1G)	98.2(3)
Li(4)-O(6)	1.994(6)	O(4)-Li(2)-O(5)	122.2(3)	O(11)-Li(5)-O(12)	89.1(3)
Li(4)-O(8)	1.960(6)	O(4)-Li(2)-O(7)	122.7(3)	O(11)-Li(5)-O(1G)	107.0(3)
Li(4)-O(9)	1.974(6)	O(5)-Li(2)-O(7)	88.3(3)	O(12)-Li(5)-O(1G)	106.6(3)
Li(4)-O(11)	1.978(6)				
Li(5)-O(1G)	2.025(7)	O(2W)-Li(3)-O(5)	107.5(4)	O(1) ⁱ -Li(6)-O(3) ⁱ	84.9(3)
Li(5)-O(9)	2.039(6)	O(2W)-Li(3)-O(6)	99.2(3)	O(1) ⁱ -Li(6)-O(10)	129.5(3)
Li(5)-O(10)	2.031(6)	O(2W)-Li(3)-O(7)	99.8(4)	O(1) ⁱ -Li(6)-O(12)	124.0(3)
Li(5)-O(11)	2.022(6)	O(2W)-Li(3)-O(8)	103.9(3)	O(3) ⁱ -Li(6)-O(10)	97.2(3)
Li(5)-O(12)	2.011(6)	O(5)-Li(3)-O(6)	90.3(3)	O(3) ⁱ -Li(6)-O(12)	136.3(4)
Li(6)-O(1) ⁱ	1.934(6)	O(5)-Li(3)-O(7)	85.2(3)	O(10)-Li(6)-O(12)	88.1(3)
Li(6)-O(3) ⁱ	1.979(7)	O(5)-Li(3)-O(8)	148.6(4)		
Li(6)-O(10)	1.954(7)	O(6)-Li(3)-O(7)	161.0(4)		

Li(6)-O(12)	1.953(6)	O(6)- Li(3)-O(8)	84.7(3)		
		O(7)-Li(3)-O(8)	89.6(3)		

$$i=x-0.5;-y+1.5;z-0.5$$

Table A.2. Selected bond distances (Å) and angles (°) for [Li₂(hfa)₂•(diglyme)•H₂O] (**2**).

Bond distances		Bond angles	
Li(1)-O(1W)	1.96(1)	O(1W)- Li(1)- O(3)	110.5(5)
Li(1)-O(1)	2.03(1)	O(1W)- Li(1) O(1)	101.7(4)
Li(1)-O(2)	2.089(8)	O(1W) -Li(1)- O(4)	101.5(4)
Li(1)-O(3)	2.018(9)	O(1W)- Li(1)- O2	98.5(4)
Li(1)-O(4)	2.073(9)	O(1) -Li(1)- O(4)	91.8(4)
		O(1) -Li(1)- O(2)	86.2(4)
		O(3) -Li(1) -O(2)	85.0(3)
		O(3) -Li(1)- O(4)	86.1(3)
		O(3)- Li(1)- O(1)	147.5(5)
		O(4) -Li(1)- O(2)	159.9(5)
Li(2)-O(2)	1.983(9)	O(2)- Li(2)- O(5)	97.0(5)
Li(2)-O(3)	1.976(9)	O(2)- Li(2)- O(6)	117.9(5)
Li(2)-O(5)	2.09(1)	O(2)- Li(2)- O(7)	108.3(5)
Li(2)-O(6)	2.051(9)	O(3)- Li(2)- O(2)	89.0(3) .
Li(2)-O(7)	2.03 (1)	O(3)- Li(2) O(5)	92.7(4)
		O(3)- Li(2)- O(6)	152.4(5)
		O(3)- Li(2) -O(7)	98.6(5)
		O(6)- Li(2)- O(5)	78.6(4)
		O(7)- Li(2)- O(5)	152.3(5)
		O(7)-Li(2)- O(6)	79.7(3)
Intermolecular Interactions			
X-H...Y	X...Y (Å)	H...Y (Å)	X-H...Y (°)
O(1w)-H(1wa)...O(1) ¹	2.824(6)	1.99(7)	166(6)
O(1w)-H(1wa)...O(4) ¹	2.841(5)	2.14(5)	140(5)

$$^1 = -x, -y+2, -z+2$$

Table A.3. Selected bond lengths (Å) in [K(hfa)]₃•monoglyme (**5**)

5							
K1-O2A	2.697(2)	K2-O1A	2.893(2)	K3-O1A	2.745(2)		
K1-O1B	2.637(2)	K2-O2A	2.797(2)	K3-O2A	2.817(2)		
K1-O2B	2.691(2)	K2-O2B	2.694(2)	K3-O1C	2.729(2)		
K1-O2C	2.762(2)	K2-O1C	2.889(2)	K3-O2C	2.845(2)		
K1-O1B ¹	2.696(2)	K2-O2C	2.838(2)	K3-O3	2.698(2)		
K1-F5A	3.092(3)	K2-O1A ²	2.725(2)	K3-O4	2.767(3)		
K1-F4D ¹	3.033(2)	K2-O1C ²	2.722(2)	K3-F4E ¹	2.955(2)		
K1-F5G ¹	2.918(2)	K2-F5D	2.921(2)				
		K2-F4C ²	3.080(3)				
		K2-F4G ²	3.043(3)				
K1...K2	3.7923(8)	K2...K3	3.7459(9)				
K1...K3	4.1745(9)	K2...K2 ²	3.5642(8)				
K1...K1 ¹	3.871(1)						

Table A.4. Selected bond lengths (Å) in [K(hfa)]₂•diglyme (**6**) .

6							
K1-O1	2.685(2)						
K1-O2	2.666(2)						
K1-O1 ³	2.757(2)						
K1-O2 ⁴	2.787(2)						
K1-O3	2.758(2)						
K1-O4	2.911(2)						
K1-F4A ³	3.131(4)						
K1...K1 ⁴	3.8594(9)						

Table A.5. Selected bond lengths (Å) in [K(hfa)]₄•tetraglyme (**8**)

8							
K1-O1A	2.7380(1)	K2-O1B	2.6926(1)	K3-O2A	2.7226(1)	K4-O1A	2.7301(1)
K1-O1C	2.7037(1)	K2-O2B	2.8340(1)	K3-O1B	2.9836(1)	K4-O2A	2.7535(1)
K1-O3	2.9890(1)	K2-O2C	2.6985(1)	K3-O2B	2.8057(1)	K4-O1B	2.8014(1)
K1-O4	2.7805(1)	K2-O2D	2.8938(1)	K3-O1D	2.6625(1)	K4-O1C	2.6800(1)
K1-O5	2.8423(1)	K2-O2B ⁵	2.6698(1)	K3-O2D	2.7009(1)	K4-O2C	2.7621(1)
K1-O6	2.9074(1)	K2-O1D ⁵	2.7538(1)	K3-F6A	3.0478(1)	K4-O2D	2.8058(1)
K1-O7	2.8042(1)	K2-F4C	2.9011(1)	K3-F6C ⁶	2.9295(1)	K4-F4D	3.0408(1)
K1-F1A	2.8723(1)			K3-F2D	2.8562(1)	K4-O3	2.8929(1)
K1...K4	3.9347(1)	K2...K3	3.9436(1)	K3...K4	3.9770(1)		
		K2...K4	3.8954(1)				
		K2...K2 ⁵	3.8978(1)				

¹ = -x+1,-y,-z+1; ² = -x+1,-y-1,-z+1; ³ = -x+1,-y+1,-z+1; ⁴ = -x+1,+y,-z+1/2; ⁵ = -x,-y,-z; ⁶ = x-1, y, z; ⁷ = -x-1,-y,-z

Table A.6. Selected bond lengths in Na(hfa) (**9**) and [Na₄(hfa)₆]•[Na•(diglyme)₂]₂ (**10**)

	9	10
Na1...Na2	3.422(5)	3.192(5)
Na2...Na3	3.454(5)	3.549(5)
Na3...Na4	3.403(5)	3.174(4)
Na1...Na3 ¹	3.731(5)	
Na1...Na4 ¹	3.027(6)	
Na2...Na4 ³	3.713(5)	
Na1-O1	2.463(8)	2.255(7)
Na1-O2	2.446(8)	2.364(8)
Na1-O3	2.442(8)	2.288(8)
Na1-O4	2.699(8)	2.349(6)
Na1-O5	2.337(8)	2.306(8)

Na1-F15a ³	2.695(8)	
Na1-F20b ⁴	2.782(7)	
Na1-F14a	2.861(8)	2.945(7)
Na1-F10b ²	2.844(8)	
Na2-O2	2.346(8)	2.406(7)
Na2-O4	2.331(8)	2.345(8)
Na2-O5	2.351(8)	2.370(6)
Na2-O6	2.324(8)	2.417(7)
Na2-O7	2.330(8)	2.373(6)
Na2-F5a	2.76(1)	
Na2-F19a	2.864(8)	2.689(6)
Na3-O6	2.335(8)	2.343(6)
Na3-O7	2.346(8)	2.397(7)
Na3-O8	2.330(8)	2.373(6)
Na3-F15a	2.909(8)	2.700(7)
Na3-O9		2.355(7)
Na3-O11		2.342(8)
Na3-O1 ⁵	2.394(8)	
Na3-O3 ⁵	2.392(8)	
Na3-F9a ⁵	2.682(9)	
Na4-O8	2.323(8)	2.310(7)
Na4-O9		2.351(8)
Na4-O10		2.272(7)
Na4-O11		2.346(6)
Na4-O12		2.274(9)
Na4-F20a	2.835(8)	
Na4-O1 ⁵	2.605(8)	
Na4-O2 ⁵	2.444(8)	
Na4-O3 ⁵	2.434(8)	
Na4-O4 ⁵	2.495(8)	

Na4-F19a ⁵	2.661(8)	
Na4-F14b ⁶	2.425(7)	
Na5-O13		2.407(8)
Na5-O14		2.386(7)
Na5-O15		2.393(8)
Na5-O16		2.378(9)
Na5-O17		2.401(8)
Na5-O18		2.382(7)
Na6-O19		2.401(7)
Na6-O20		2.371(8)
Na6-O21		2.377(6)
Na6-O22		2.373(9)
Na6-O23		2.409(7)
Na6-O24		2.357(8)

¹ = x,+y,+z+1; ² = -y+1/2,+x+1/2,-z+3/2; ³ = x,+y,+z+1; ⁴ = y,-x+1,-z+1; ⁵ = x,+y,+z-1; ⁶ = y-1/2,-x+1/2,-z+1/2

Author's Biography

Curriculum vitae

Personal Information

Last name: Peddagopu

First name: Nishant

Nationality: Indian

Date of birth: 18.02.1990

Education

Ph.D. in Material Science & Nanotechnology

March 2021

Marie Curie Scholarship, University of Catania, Italy

- Thesis: *Engineering of Metal-organic precursors from synthesis to mechanistic aspects.*

Masters in Material Science

August 2017

IAESTE trainee & ERASMUS+ scholarship, University of Augsburg, Germany

- Thesis: *Synthesis and Characterization of C-Mo-TiO₂ heterogenous photocatalyst for the decomposition of diacetyl under the influence of blue LED.*

List of Publications

- Nishant Peddagopu, Patrizia Rossi, Carmela Bonaccorso, Ausrine Bartasyte, Paola Paoli, Graziella Malandrino, *Facile synthesis of novel lithium β -diketonate glyme adducts: the effect of molecular engineering on the thermal properties.* Dalton Trans., **2020**,49, 1002-1006

Manuscript in preparation

- Nishant Peddagopu, Salvatore Sanzaro, Patrizia Rossi, Paola Paoli, and Graziella Malandrino, *Engineering the K^+ ion coordination sphere: effect of the polyether length on the “K(hfa)glyme” polymeric network formation.*
- Nishant Peddagopu, Patrizia Rossi, Paola Paoli, Ausrine Bartasyte and Graziella Malandrino, *Synthesis and Deposition of novel Lithium Adducts as Precursors for Lithium Niobates by PI-MOCVD.*
- Nishant Peddagopu, Anna L. Pellegrino, Carmela Bonaccorso, Patrizia Rossi, Paola Paoli, and Graziella Malandrino, *A facile one-pot synthesis of novel Sodium Adducts as Precursors for Fluoride Phases: Effects of Polyether Length on Coordination Spheres and Mass Transport Properties.*
- Nishant Peddagopu, Arun Ichangi, Anjneya Verma, Patrizia Rossi, Paola Paoli, Sanjay Mathur, and Graziella Malandrino, *Application of M(hfa)glyme ($M = Na, K$) adducts to the fabrication of $(K,Na)NbO_3$ phase as nanostructured films and nanofibers.*
- Ishamol Labbaveetti, Nishant Peddagopu, Merieme Oubahaz, Samuel Margueron, Jean-Manuel Decams, Vincent Astié, Graziella Mallandrino, and Ausrine Bartasyte, *Epitaxial $KNbO_3$ films grown by PI-MOCVD.*

Schools Attended

- Multidisciplinary Introductory School to Energy Harvesting Microsystems, UFC, Besancon, France, 16.05.2018 – 18.05.2018; Course: molecular engineering, material science, MEMS, and Energy Harvesting
- International School of Materials for Sustainable Development and Energy, EMFCSC, Erice, Italy, 06.07.2018 – 13.07.2018; Course: Materials for Energy and Sustainability VII

- Career Opportunities, EPFL, Lausanne, Switzerland, 05.08.2018 – 06.08.2018; Course: Career development and opportunities.
- International School and Symposium, UCO, Cologne, Germany, 21.05.2019 – 25.05.2019; Course: From Molecular Engineering to Advance Materials
- The story of the Kilogram, Colloquium, ENSMM, Besancon, 04.07.2019; Guest speaker: Terry Quinn
- Knowledge Transfer, Patenting & Commercialisation, KTN, Online, UK, 13.07.2020 – 16.07.2020; Course: Knowledge Transfer, Patenting & Commercialisation
- Mechatronics and Electronics for Energy Harvesters, Cedrat Technologies, Online, 15.09.2021 – 18.09.2021 & 23.09.2021; Course: Piezoelectricity, Linear magnetic actuators, Random vibrations, and shock analysis, Electronic and control for piezo mechanisms in mechatronics

Conferences Attended

- 2nd International Rhine Ceramic Round table, UCO, Cologne, Germany, 24.09.2018
- “EuroCVD 22 Baltic ALD 16” Conference, Luxembourg, 24.06.2019 - 28.06.2019
Abstract: Synthesis of novel Lithium Adducts as Precursors for Lithium containing phases - Nishant Peddagopu, Carmela Bonaccorso, Patrizia Rossi, Paola Paoli, and Graziella Malandrino (Oral Presentation)
- IWPMA Conference, Lyon, 30.09.2019 – 08.10.2019
Abstract: Synthesis of novel Lithium adducts as precursors for lithium-containing phases - Nishant Peddagopu, Patrizia Rossi, Carmela Bonaccorso, Paola Paoli, and Graziella Malandrino (Poster Presentation)
- MSE2020, Online, Germany, 20.09.2020 – 24.09.2020

Abstract: Synthesis of novel Lithium Adducts as Precursors for Lithium Niobates by DLI-MOCVD - [Nishant Peddagopu](#), Patrizia Rossi, Paola Paoli, Ausrine Bartasyte, and Graziella Malandrino (Oral Presentation)

- 2020 Virtual MRS Spring/Fall Meeting & Exhibit, Online, USA, 28.11.2020-04.12.2020
Abstract: Synthesis of novel Lithium Adducts as Precursors for Lithium Niobate films by DLI-MOCVD - [Nishant Peddagopu](#), Patrizia Rossi, Paola Paoli, Ausrine Bartasyte, and Graziella Malandrino (Poster Presentation & Pitch)

Secondments

- EpiValence, England, 16.04.2018 – 15.05.2018
Area: Metal-organic synthesis
Activity: Understand the industrial constraints for precursor synthesis.
- University of Franche-Comté, France, 15.04.2019 – 02.08.2019
Area: Metalorganic Chemical Vapor Deposition (MOCVD)
Activity: MOCVD application of Li metal precursors.
- University of Cologne, Germany, 21.10.2019 – 29.11.2019 & 06.01.2020 – 28.02.2020
Area: Institute of Inorganic Chemistry
Activity: Deposition of nanofibers and thin film of $K_{1-x}Na_xNbO_3$

Tutoring Activity

- Master thesis: *Nuovi complessi contenenti litio come precursori di fase niobato di litio*, Federica Campione
- Master thesis: *Ottimizzazione del processo di deposizione chimica da fase vapore di film di nichelato di lantanio*, Marco Patané
- Master thesis: *Sintesi di un nuovo precursore bimetallico potassio-ittrio e ottimizzazione del processo MOCVD per l'ottenimento di film KYF_4* , Andrea Annense.